

Design and Utility Assessment of Attitude Control Systems for EVA Task Performance

by

Todd F. Sheerin

A.B., Harvard University (2012)

Submitted to the Department of Aeronautics and Astronautics
in partial fulfillment of the requirements for the degree of

Master of Science

at the

MASSACHUSETTS INSTITUTE OF TECHNOLOGY

September 2015

©2015 DLF Todd Fillmore Sheerin, All rights reserved.

The author hereby grants to MIT and The Charles Stark Draper Laboratory, Inc. permission to reproduce and to distribute publicly paper and electronic copies of this thesis document in whole or in any part medium now known or hereafter created.

Author
Department of Aeronautics and Astronautics
August 20, 2015

Certified by
Jeffrey A. Hoffman
Professor of the Practice of Aeronautics and Astronautics
Thesis Supervisor

Certified by
Michele D. Carpenter
Technical Staff, Charles Stark Draper Laboratory
Thesis Supervisor

Accepted by
Paulo Lozano
Professor of Aeronautics and Astronautics
Chair, Graduate Program Committee

Design and Utility Assessment of Attitude Control Systems for EVA Task Performance

by

Todd F. Sheerin

Submitted to the Department of Aeronautics and Astronautics
on August 20, 2015, in partial fulfillment of the
requirements for the degree of
Master of Science

Abstract

Low gravity astronaut extravehicular activity (EVA) missions using a maneuvering Jetpack and robotic servicing and assembly missions could benefit from spacecraft systems capable of maintaining pointing stability during critical operations. The addition of single-gimbal control moment gyroscopes (CMGs) to the attitude control system of these spacecraft could substantially improve the stability and pointing accuracy of the platform and could also conserve onboard fuel during missions. This thesis contains a description of recent work completed at Draper Laboratory and MIT's Space Systems Laboratory (SSL) and Man Vehicle Laboratory (MVL) that explores the performance and utility of a combined control concept for a Jetpack system using thrusters and CMGs as actuators. Simulation of the Mobility Augmenting Jetpack with Integrated CMGs (MAJIC) at Draper is described as well as the design, integration and physical demonstration of a combined control system with the Synchronized Positoin Hold Engage Reorient Experimental Satellite (SPHERES) facility at the SSL. Primary contributions in simulation for the Jetpack application have focused on implementing a new method for sizing CMG actuators and improving the performance and utility assessment strategies to compare a proposed MAJIC system with a Jetpack that does not include CMGs. Primary contributions with hardware within the context of the SPHERES facility have included the design, simulation, integration and testing of a CMG peripheral actuator package and associated laboratory and reduced-gravity testing with NASA's Flight Opportunity Program.

Thesis Supervisor: Jeffrey A. Hoffman

Title: Professor of the Practice of Aeronautics and Astronautics

Thesis Supervisor: Michele D. Carpenter

Title: Technical Staff, Charles Stark Draper Laboratory

Acknowledgments

I would like to acknowledge first the many advisors and mentors at both MIT and Draper that have seen me transition from an undergraduate physics student to an engineer here at MIT. Most notable among them is Prof. Jeffrey Hoffman who has been an incredibly supportive and patient mentor and advisor since the fall of 2010 when I first knocked on his door. I could not ask for a more enthusiastic and knowledgeable mentor. Bobby Cohan and Phillip Cunio worked with me beginning also in 2010 and to this day continue to be helpful and constructive role-models, teachers and friends that I appreciate dearly. Among my advisors I must also acknowledge Prof. Kerri Cahoy for taking me under her wing and providing me with opportunities and support that I will never forget at the crucial transition between undergraduate and graduate programs. Michele Carpenter at Draper has provided reliable support and has proven to be a patient mentor throughout my graduate program; she has always been enthusiastic and engaged with my work and I owe her many thanks.

Draper Laboratory's most generous support of this program must also be acknowledged: without their institutional support (Michele Carpenter, Bobby Cohan, Kevin Duda) and their financial support (my Draper Laboratory Fellow status, the purchase of Honeybee Robotics CMG actuators and ProtoLabs CMG enclosures) this project would not have been possible. The kindness shown to me by Stacey Goulet at the Contracts Office, Carline Durocher at the Legal Department and Martha Porter and Brenan McCarragher at the Education Office have been most welcome when stress is at a maximum and time availability is at a minimum. In addition I owe my thanks and gratitude to Honeybee Robotics for providing Draper and MIT with control moment gyroscope actuators. They have proven to be a source of support throughout integration and testing and have made the physical realization of a combined control concept at Draper and MIT possible.

I'd also like to acknowledge Danilo Roascio for time and again proving his brilliance and willingness to help throughout the SPHERES integration effort, and Alvar Saenz-Otero for providing insight and direction to the project. I must also acknowledge

Mr. Paul Bauer, resident lab guru and most appreciated mentor without whom so many projects would never leave the drawing board. I also want to thank among my mentors Todd Billings and Dave Robertson in the AeroAstro Gelb machine shop for their insight and patience when helping me with my hardware projects over the years, I don't think anyone has thanked them nearly enough for their tireless contributions to the research and education activities conducted at MIT.

In addition, I'd like to acknowledge the members of the 16.851 Fall 2013 course (Sam Schreiner, Tim Setterfield and Morris Vanegas) who spent so many hours working with me to realize a practical design for the implementation of CMGs on SPHERES, as well as the undergraduates that aided the program's efforts as part of the 16.83X Fall 2013 and Spring 2014 courses. I must also thank the UROPs that helped me complete my research objectives over the past three semester, most notably Jose Gomez for his tireless work. Previous Draper student Celena Dopart provided me with human factors support during my research work that was much-needed; previous Draper student Jared Rize provided me with more insight concerning what might come of a team-based engineering process than I ever could've expected.

The MIT community and the Aero/Astro community in particular have also been pillars of support throughout my experience in this graduate program, and the friends that I've made across all departments constantly surprise and inspire me. Beth Marois and Marie Stuppard in the front office have always looked out for me and the other students like we were their own children and I can't thank them enough. Lastly, the MIT community has provided me with one more gift: an incredibly supportive and loving girlfriend in Whitney. Without her support I may not have made it through this graduate school experience as the complete person I am today.

For my final acknowledgments, I want to thank those closest to me: my family and friends. Sometimes I feel like my parents, my sister, my grandparents, and my aunts, uncles, cousin and friends from home and from college feel the stress and pain of student life on my behalf more acutely than I do myself. My friends Zach, Penyen, Jordan, Juan and Shervin in particular have never stopped reminding me of why life is so precious. I wish to acknowledge the inspiration several family members have

given me: I have been inspired by my mother Nancy's courage, my father Peter's inquisitiveness, my sister Erica's creativity, my grandmother Pearl's togetherness, and my grandfather Merle's imagination. They, along with my grandparents Dotty and Bob, have always been and always will be held close to my heart, providing me strength of will and character when all else fails.

Contents

1	Introduction	29
1.1	Motivation	29
1.2	Thesis Focus	31
1.3	MAJIC System Background	35
1.3.1	Jetpack Heritage	35
1.3.2	Previous Work on MAJIC	36
1.4	MIT SPHERES Background ¹	38
1.5	Dynamics and Attitude Control for a Jetpack and for SPHERES . . .	43
1.5.1	Reaction Control Overview	45
1.5.2	Reaction Control with CMGs for Improved Stability	48
1.6	Thesis Overview	54
2	CMGs for a Jetpack: Concept, Design and Utility Analysis	57
2.1	MAJIC Concept	58
2.1.1	MAJIC's Concept Origins: NASA's SAFER and Advanced Jetpack	59
2.1.2	Control Configurations for MAJIC	61
2.1.3	Mission Concepts	64
2.2	Draper-MIT Simulation	66
2.2.1	Thruster Model	67
2.2.2	CMG Model	69

¹This section includes contributions by Tim Setterfield of the MIT SPHERES team, initially compiled for the Fall 16.851 MIT course on Space Systems Engineering.

2.2.3	6-DoF Suited Astronaut Dynamics Model	71
2.2.4	Sensors and Data Logging	72
2.2.5	Guidance and Navigation	72
2.2.6	Control and CMG Steering with Desaturation	73
2.2.7	EVA Mission Scenario Simulations	75
2.3	MAJIC Design: CMG Actuator Sizing	81
2.3.1	Maximum SWaP for a Practical MAJIC System	81
2.3.2	CMG Actuator Sizing Method	86
2.3.3	CMG Design Parameterization	88
2.3.4	Largest CMG Specification	93
2.3.5	Reducing CMG Size with a Monte Carlo Method	93
2.3.6	Sizing Mission Selection and Sizing Results	95
2.3.7	Monte Carlo Sizing Discussion	97
2.4	MAJIC Utility Analysis	99
2.4.1	Mission Scenario Performance and Mass-Cost	101
2.4.2	Simple Task Performance and Mass-Cost	112
2.4.3	Mass-to-Orbit Cost Projection	126
3	CMGs for SPHERES: CDIO and Utility Analysis²	129
3.1	SPH-Halo-CMG Concept	130
3.1.1	SPH-Halo-CMG System Requirements	132
3.2	SPH-Halo-CMG Design	134
3.2.1	CMG Sizing for SPHERES	134
3.2.2	Structural Design	137
3.2.3	Electrical Design	142
3.2.4	Flight Software Design	150
3.2.5	SPH-Halo-CMG Simulation	156
3.3	SPH-Halo-CMG Integration	165

²This chapter includes contributions by a team of graduate students including the author of this thesis, Sam Schriener, Tim Setterfield and Morris Vanegas; these contributions satisfied partial requirements for the Fall 2013 16.851 MIT course on Space Systems Engineering, advised by Prof. Jeffrey A. Hoffman [1].

3.3.1	Hardware Integration	166
3.3.2	Electrical Integration	171
3.3.3	Software Integration	173
3.4	SPH-Halo-CMG Operations	174
3.5	SPH-Halo-CMG Utility Analysis for the SPHERES Simulation Results	176
3.5.1	Mission Duration Increase	176
3.5.2	Preliminary Mass Trade Analysis	177
4	Conclusion	181
4.1	MAJIC Research Conclusions	181
4.2	SPHERES Research Conclusions	184
4.3	Future Work	185
4.3.1	Future MAJIC Work	185
4.3.2	Future SPHERES Work	187
4.4	Closing Remarks	188

List of Figures

1-1	The Manned Maneuvering Unit and MAJIC. <i>Left: US astronaut Bruce McCandless and the MMU, 1984; courtesy of NASA. Right: Suited astronaut concept with the Mobility Augmenting Jetpack with Integrated CMGs (MAJIC) system considered for this thesis following previous work at Draper and MIT [2, 3, 4].</i>	31
1-2	MAJIC at an asteroid. <i>This screen-shot from a human simulation trial of the MAJIC system conducted at NASA JSC in 2014 depicts the MAJIC system transporting an astronaut near the surface of an asteroid. [3]</i>	33
1-3	MIT’s INSPECT Spacecraft. <i>The Integrated Navigation Sensor Platform for EVA Control and Testing is one of many spacecraft variants that the MIT SPHERES facility has been investigating; CMGs are integrated to improve pointing accuracy of the inspector system. . . .</i>	34
1-4	The Astronaut Maneuvering Research Vehicle (AMRV). <i>The AMRV was flown inside the volume of the Skylab orbiting facility as part of the M509 Experiment on the Skylab 3 Mission, 1973 [5]. The AMRV featured 6 CMGs in three scissor-pair configurations for attitude control testing. Image courtesy of NASA.</i>	36
1-5	SPHERES on the ISS. <i>Astronaut Scott Kelly poses for a photograph with three MIT SPHERES Satellites aboard the International Space Station.</i>	39
1-6	A SPHERES satellite. <i>SPHERES-frame body axes are shown as well as prominent features of the experimental satellite.</i>	40

1-7	SPHERES and the Halo Expansion. <i>Up to six peripherals can be interfaced with Halo and communicate with the central SPHERES satellite.</i>	41
1-8	Two SPHERES Docked. <i>The proposed docked configuration for flight aboard NASA's Reduced Gravity Aircraft in August 2015; the Secondary SPHERES satellite will execute open-loop thruster firings to induced known disturbance torques that the Primary SPHERES satellite will reject either with thruster-only attitude control or CMG attitude control. Closed-loop slew maneuvers will also be completed using this docked configuration as well as with an undocked Primary SPHERES satellite.</i>	42
1-9	Phase plane controller for attitude control with thrusters. <i>Allowable bounds for errors in attitude, θ_{err}, and angular rate, ω_{err}, are selected and thruster firings only occur should the deadband defined by these bounds is exceeded. For a controller with proportional gain K_θ and differential gain K_ω, no controller output is commanded along the dotted line.</i>	46
1-10	Vectors and scalars for a single-gimbal CMG. <i>Definition conventions are borrowed from [6].</i>	50

1-11	CMG pyramid configuration and angular momentum envelope depicting singular surfaces. <i>Left: A 4-CMG pyramid configuration, pyramid angle $\beta = 54.74^\circ$; image modified from [7]. The i^{th} CMG has angular momentum $\mathbf{h}_{\text{cmg},i}$ and a gimbal axis $\hat{\mathbf{g}}_i$. Shaded blue circles on each triangular face indicate available positions for individual CMG angular momentum vectors. Right: The pyramid array's nearly spherically symmetric momentum envelope with singular surfaces pictured; image modified from [8]. When the CMG array's momentum reaches the edge of this envelope when CMG rotors are gimballed such that CMG angular momenta add constructively to a maximum degree, saturation occurs. An external torque provided by thrusters is required to return the CMG array to a fully controllable state.</i>	53
2-1	NASA's SAFER and the Advanced Jetpack / MAJIC Concept. <i>Left: Diagram for the Simplified Aid for EVA Rescue emergency-only astronaut mobility unit currently in use at the ISS for astronaut EVAs. Right: The NASA JSC Advanced Jetpack concept; arrows indicate the location of fuel tanks; for the MAJIC system, half of the fuel tanks would be replaced by the CMG subsystem with minimal impact to Jetpack size and weight.</i>	58
2-2	A 4-CMG pyramid array configuration. <i>This array has a pyramid angle $\beta = 54.74^\circ$. The i^{th} CMG has angular momentum \mathbf{h}_i and a gimbal axis $\hat{\mathbf{g}}_i$. Shaded blue circles on each triangular face indicate available positions for angular momentum vectors \mathbf{h}_i. Image modified from [7].</i>	62
2-3	Control Loop Diagram for MAJIC ACS. <i>In the simplest implementation, all torques are controlled by CMGs and all forces are controlled by thrusters.</i>	64

2-4	Three mission concepts for the CMG-augmented Jetpack. <i>Left: A NASA photograph of an ISS solar array inspection EVA - with a Jetpack, inspection activities would not be limited by the reach of the ISS robotic arm. Middle: A sample recovery mission to near-Earth objects (NEOs) like asteroids and comets would benefit from Jetpack mobility and CMG stability. Right: In the event of an emergency during any low gravity EVA mission, a CMG-augmented Jetpack would enable reliable crew member rescue with stable pointing during transit with a large external mass.</i>	65
2-5	The Draper-MIT Simulink Diagram. <i>A top-level diagram depicting the principle modules of the MATLAB-Simulink simulation used to design and evaluate the utility of MAJIC.</i>	67
2-6	Trajectory profile for the solar array inspection mission. <i>The inspection of one pair of solar arrays at the International Space Station is simulated; the coordinates used in the plot are fixed in the ISS frame.</i>	75
2-7	Asteroid Sampling Mission I: Survey. <i>Flight trajectory for the asteroid sampling mission I. Axes labeled in the ACI frame. An initial approach to the asteroid is followed by a plane change and continued approach for detailed surveying of the asteroid's surface.</i>	76
2-8	Asteroid Sampling Mission II: Sampling Actions. <i>Flight trajectory for the asteroid sampling mission II. A linear translation of 50 meters in the x-axis (ACI) lasting 220 seconds is followed by simulated sampling activities at the asteroid's surface for another 272 seconds. Sampling activities include an overhead reach, hammer blow, and reach to the hip in that order.</i>	77

2-9	Asteroid Mission II Linear Trajectory and Astronaut Torques. <i>(a) Linear trajectory in the x-axis of the asteroid-centered inertial frame. (b) Astronaut torque magnitudes, with a reminder for the MAJIC-body coordinate frame referenced for torque magnitudes; the time scale here is the same as in (a), showing the entire length 492 seconds of the mission. (c) A zoomed perspective of the astronaut torque profiles, as well as labels indicating the individual overhead reach, hammer blow and hip reach actions.</i>	78
2-10	Trajectory profile for the crew member rescue mission. <i>An astronaut departs from the airlock to rescue a fellow crew member; a picture courtesy of NASA is used to visualize the hypothetical mission.</i>	79
2-11	Jetpack Concept Dimensions with CMG Location Options. <i>Regions 1, 2, and 3 illustrate three options for CMG subsystem placement in a MAJIC system based on the JSC Jetpack design.</i>	82
2-12	ISS Solar Array Inspection Mission Performance <i>(a) Full attitude error profile for CMG+Thr combined control (green), the tight deadband thruster-only (red) and loose deadband thruster-only (blue); (b) Attitude error for a 50 degree slew maneuver at mission start. The slightly more negative slope of the tight deadband (red) profile results in an overall lower RMS attitude error for tight deadband thrusters, though CMGs ultimately reach the commanded attitude first; (c) A zoomed-in perspective of the attitude error profile over the whole mission, showing the CMG's superior performance for mission time 49s+.</i>	103
2-13	Asteroid Sampling Mission I Performance <i>(a) Attitude error profile for the newly-sized CMGs (green), the thruster-only 0.5 deadband ACS (full width, corresponding to ± 0.25 degrees) (red) and the thruster-only 2.0 deadband (full width, corresponding to ± 1.0 degrees) (blue); (b) A zoomed-in perspective of the attitude error profile, showing the CMG's superior performance for a majority of the mission; (c) Fuel consumption profile (color scheme same as in attitude error plots).</i>	105

2-14	Asteroid Sampling Mission II Performance	<i>A translation of 85 meters is simulated beginning at mission time 0 s and ending at mission time 245 s; following this, a set of sampling maneuvers between mission time 300 s and 355 s is simulated as disturbance torques on the MAJIC system. (a) The translation profile in time for this mission segment; (b) The disturbance torque profile induced on the MAJIC system as a function of time; (c) Attitude error profile for the combined CMG-thruster MAJIC system (green), the thruster-only 0.5 deadband ACS (full width, corresponding to ± 0.25 degrees) (red) and the thruster-only 2.0 deadband (full width, corresponding to ± 1.0 degrees) (blue).</i> . . .	107
2-15	Asteroid Sampling Mission II Mass-Cost	<i>A translation of 85 meters is simulated beginning at mission time 0 s and ending at mission time 245 s; following this, a set of sampling maneuvers between mission time 300 s and 355 s is simulated as disturbance torques on the MAJIC system. (a) The translation profile in time for this mission segment; (b) The disturbance torque profile induced on the MAJIC system as a function of time; (c) Fuel consumption profile for the combined CMG-thruster MAJIC system (green), the thruster-only 0.5 deadband ACS (red) and the thruster-only 2.0 deadband (blue).</i>	109
2-16	Crew Member Rescue Mission Performance	<i>(a) Trajectory profile; (0,0,0) is taken to be the incapacitated crew member's location in the ISS inertial frame; (b) Attitude error profile for CMGs (green), the thruster-only 0.5 degree deadband ACS (full width, corresponding to ± 0.25 degrees) (red) and the thruster-only 2.0 degree deadband (full width, corresponding to ± 1.0 degrees) (blue); (c) Attitude errors for the last 600 seconds of the mission, showing the CMG's superior performance for the critical mass-offset return phase of the mission.</i> . . .	111

2-17	Crew Member Rescue Mission Fuel Consumption. <i>Fuel mass consumed over the course of the simulated crew member rescue mission is depicted for the tight deadband thrusters (red), loose deadband thrusters (blue) and the combined control Thr+CMGs (green). Note the smaller rate of fuel consumption for the combined control implementation for the majority of the mission as well as the increased fuel consumption for the same implementation during de-saturation procedures.</i>	113
2-18	Attitude error and fuel consumption profiles for a 10 meter translation. <i>Solid lines correspond to translation results with no mass offset and dotted lines correspond to results for translation with mass offset corresponding to the transport of an incapacitated crew member in a rescue scenario; distance traveled is indicated at the top of the figure.</i>	115
2-19	Hammer Blow (strong- 10 Nm scale) Disturbance Torque Profile and Performance. <i>(a) Disturbance torque profile in the MAJIC body reference frame (x, y, z torques represented in magenta, red and blue respectively); (b) Absolute attitude error (CMGs in green, thrusters with 0.5 degree deadband in red, thrusters with 2.0 degree deadband in blue); (c) Fuel consumption (color scheme same as in attitude error plot).</i>	120
2-20	Hammer Blow (weak- 2 Nm scale) Disturbance Torque Profile and Performance. <i>(a) Disturbance torque profile in the MAJIC body reference frame (x, y, z torques represented in magenta, red and blue respectively); (b) Absolute attitude error (CMGs in green, thrusters with 0.5 degree deadband in red, thrusters with 2.0 degree deadband in blue); (c) Fuel consumption (color scheme same as in attitude error plot).</i>	121

2-21	Hip Reach Disturbance Torque Profile and Performance. (a) <i>Disturbance torque profile in the MAJIC body reference frame (x, y, z torques represented in magenta, red and blue respectively); (b) Absolute attitude error (CMGs in green, thrusters with 0.5 degree full width deadband in red, thrusters with 2.0 degree full width deadband in blue); (c) Fuel consumption (color scheme same as in attitude error plot).</i>	123
2-22	Overhead Reach Up Disturbance Torque Profile and Performance. (a) <i>Disturbance torque profile in the MAJIC body reference frame (x, y, z torques represented in magenta, red and blue respectively); (b) Absolute attitude error (CMGs in green, thrusters with 0.5 degree full width deadband in red, thrusters with 2.0 degree full width deadband in blue); (c) Fuel consumption (color scheme same as in attitude error plot).</i>	124
2-23	Mass-to-Orbit Projections for a Jetpack with and without CMGs. <i>Combined control with MAJIC requires thruster fuel, a CMG actuator suite and associated extra battery mass dedicated to CMGs to be sent to orbit; simple thruster-only control with a Jetpack only requires thruster fuel, but with more aggressive cargo delivery given the poorer fuel economy of a thruster-only system.</i>	127
3-1	SPH-Halo-CMG Flight Configurations <i>The SPH-Halo-CMG configuration is used to host two different configurations used for flight testing aboard NASA's Reduced Gravity Aircraft. The INSPECT configuration has an optical range-finder (ORF), stereoscopic cameras (Optics Mount), and a thermographic camera (ThermoCam); the Docked configuration has a Universal Docking Port used to dock to a Secondary SPHERES satellite.</i>	130

3-2	CMG pyramid configuration and angular momentum envelope depicting singular surfaces. <i>Left: A 4-CMG pyramid configuration, pyramid angle $\beta = 54.74^\circ$; a Box-90 configuration is equivalent to a pyramid configuration with a pyramid angle $\beta = 90^\circ$. Right: The pyramid array's nearly spherically symmetric momentum envelope has dimensions $3.15 h_{rotor} \times 3.15 h_{rotor} \times 3.26 h_{rotor}$ (pictured); by comparison, a Box-90 momentum envelope has dimensions $4 h_{rotor} \times 4 h_{rotor} \times 2 h_{rotor}$; images modified from [7] and [8]</i>	137
3-3	Mechanical design for SPH-Halo-CMG. <i>(a) and (b) The CMGs attached to Halo in the Box-90 configuration. (c) The CMGs attached to Halo in the pyramid configuration. (d) An exploded view of the top CMG assembly. (e) An exploded view of the bottom CMG assembly. Image credit: Tim Setterfield [1].</i>	139
3-4	SPHERES keep-out zones. <i>Relevant keep-out zones for the Halo expansion are shown with the CMG system in its Box-90 configuration. (a) Right view of thruster keepout zones. (b) Bottom view of thruster keepout zones. (c) Right view of ultrasonic keepout zones. (d) Bottom view of ultrasonic keepout zones.</i>	141
3-5	A top view of two SPHERES satellites with Halo and on air carriages, attached 0.1 m apart. <i>Two thrusters exert on the active SPHERE a force F_t, creating both an acceleration and an adverse moment τ. Image adapted from [1]</i>	142
3-6	Electrical interface schematic for SPH-Halo-CMG system. <i>The path of information and power from SPHERES to CMGs is depicted. Image credit: Morris Vanegas, [1].</i>	144
3-7	SPHERES expansion port schematic. <i>Expansion port aluminum plate dimensions and the 50-pin connector used to interface to the SPHERES satellite.</i>	145
3-8	Pin layout for the expansion port. <i>SPHERES expansion port electrical interface pin assignments.</i>	146

3-9	VERTIGO expansion port. <i>Expansion side of the VERTIGO avionics stack showing four threaded holes for captive thumbscrews and a 50-pin connector.</i>	147
3-10	VERTIGO expansion port electrical interface pin assignments.	148
3-11	Halo expansion mechanical interface. <i>Diagram of one of two halves of the Halo expansion; each half hosts three total expansion ports to interface external payloads or actuators to the central SPHERES satellite.</i>	149
3-12	USB to serial adapter pin assignments.	149
3-13	SPHERES control loop. <i>A simplified depiction of the control loop on the SPHERES satellite including only key elements. Additionally, the type of data exchanged between each block is shown. The blocks in grey are implemented in the controller software, while the green blocks are hardware components that had to be simulated. Image credit: Sam Schreiner [1].</i>	150
3-14	SPHERES control loop with CMGs <i>The conceptual illustration of the control loop on the SPHERES satellite, extended to command and interface with the CMG payload. This high-level design was used to guide the more detailed software design process. The blocks in grey are implemented in the controller software, while the green blocks are hardware components that had to be simulated. Image credit: Sam Schreiner, [1].</i>	153
3-15	Multithreaded scheduling for SPHERES control <i>The action of a 5 Hz control thread (represented by a solid blue line) is traced; it first accesses data from the metrology thread, then commands the CMG thread (running on the CMG control board). On every fifth control cycle, the main 5 Hz control thread commands thrusters after first commanding the infrared/ultrasound (IR/US) thread to cease global metrology (used to locate the SPHERES within the experiment volume) in preparation for thruster actuation, which would interfere with US sensor operation.</i>	154

3-16	Scissor pair diagram <i>A scissor pair CMG configuration generates torque $\tau_{scissor}$ about a single axis by constraining gimbal angles ϕ of the pair to be equal and opposite at all times, usually by mechanical means. Image modified from [9]</i>	159
3-17	Docked SPHERES configuration <i>The active SPHERES satellite is to the left; when a translation burn is executed, a reaction torque is executed on the system since the system center of mass (CM) is off-set from the active SPHERES' thruster envelope. Force vectors corresponding to the active SPHERES' thruster locations are labeled to highlight this phenomenon. Image adapted from [1].</i>	161
3-18	Performance plots for Docked simulation. <i>Top Left: Linear position (m); Top Right: Attitude error (rad); Mid Left: Linear velocity (m/s); Mid Right: Angular velocity (rad/s); Bottom Left: Fuel consumed (g); Bottom Right: Scissor pair gimbal angle (rad). Graphs from 16.851 final report [1].</i>	163
3-19	Astronaut EVA maneuver with SPHERES <i>A series of screenshots depicting a maneuver designed to imitate an astronaut conducting EVA maintenance activity at two different locations. This animation is quantitatively assessed in Figure 3-20. Images from 16.851 final report [1].</i>	164
3-20	Quantitative results for EVA astronaut maneuver with SPHERES <i>From left to right, top to bottom: Plots of the linear position, angular position, linear velocity, angular velocity, propellant usage, and scissor pair gimbal angle (or CMG Usage) for the combined control system (blue dashed line) and the thrusters-only system (red solid line). Graphs from 16.851 final report [1].</i>	165
3-21	Initial and updated designs for CMG enclosures and electronics housing. <i>Left: The initial CAD model from Fall 2013 [1]; Right: The final, manufactured version.</i>	167

3-22	Final damping solution for CMGs. <i>A double-damping solution was arrived at as the preferred option for reducing vibrations induced on the Halo structure from improperly balanced CMGs. Ring-dampers were used to interface the control electronics box (and Halo) with a base plate; a set of sandwich-style dampers then separate the CMG enclosures from the base plate.</i>	168
3-23	Vibration profile for undamped and damped mechanical assemblies, worst case vibrations. <i>Left: Accelerometer readings for the undamped, worst-case CMG-120. Right: Accelerometer readings for the same CMG-120 actuator stood-off with the damping solution depicted in Figure 3-22.</i>	169
3-24	Schematic of the Halo-to-CMG printed circuit board. <i>Major components have been labeled.</i>	172
3-25	Block diagram of software implementation. <i>SPHERES manages a control algorithm that determines requested forces and torques; forces are passed to thrusters (not shown) and torques are passed to VERTIGO, which converts the SPHERES torque command to a command the CMG electronics can interpret. Telemetry data from CMGs is stored on VERTIGO for post-processing, while key information such as flywheel rates, gimbal angles and gimbal rates are passed to SPHERES for display on the controller's laptop GUI.</i>	174
3-26	The INSPECT configuration at the end of the undergraduate course 16.831 in the spring of 2014. <i>Inspection operations on the MIT SSL's flatfloor facility were demonstrated with this partially-integrated INSPECT system; at the time of this photograph, CMGs are being commanded not by SPHERES but by an external laptop.</i>	175

3-27 Propellant consumption for the SPHERES-simulated astronaut EVA maneuver. *The propellant used to conduct a simulated astronaut EVA maneuver using the SPHERES satellite with thrusters as the only actuator (red solid line) and with the combined thruster and CMG actuators (blue dashed line). This comparison clearly outlines the fuel saved by using CMGs to augment thruster actuation. The green vertical lines indicate the beginning and ending of maneuvers corresponding to Figure 3-19. 178*

List of Tables

2.1	CMG SWaP Constraints	83
2.2	Soft VES Battery Models Applicable to MAJIC	85
2.3	CMG Inertia Bounds for Sizing	89
2.4	Angular momentum bounds for SWaP-compatible MAJIC CMGs <i>A flywheel rate of 30 krpm is assumed as well as inertia bounds listed in Table 2.3 to arrive at the bounds listed here.</i>	90
2.5	Gimbal Rate Bounds to Achieve 2 Nm Torques	91
2.6	Maximum torques achievable by SWaP-compatible CMGs	91
2.7	CMG Parameter Bounds for Sizing	92
2.8	Specifications for the largest-SWaP MAJIC CMG design	93
2.9	Monte Carlo Sizing Performance Metrics	94
2.10	Simulated mission details <i>Mission time, ΔV, RMS attitude errors for a thruster-only (2 degree deadband) Jetpack are listed for each sim- ulated mission</i>	96
2.11	Specifications for MAJIC CMG designs	98
2.12	Specifications for the MAJIC CMG design evaluated for utility	100
2.13	Mission Scenario Performance Results	101
2.14	10m Translation Performance	117
2.15	10m Translation Mass Cost	118
2.16	Astronaut Motions Simulated. <i>Peak torques are listed and are measured in the MAJIC body coordinate frame acting on the MAJIC system's center of mass.</i>	119
2.17	Human Action Mass Cost	125

3.1	Top-Level System Requirements. <i>Table includes requirement statements, implications on project goals for each requirement, and the verification method necessary for each requirement.</i>	133
3.2	Angular momentum and torque specifications for the Honeybee Robotics CMG-120 actuator. <i>Nominal values correspond to a flywheel rate of 6 krpm while the peak values correspond to a flywheel rate of 8 krpm.</i>	135
3.3	SPH-Halo-CMG System Properties with CMG-120 Actuators <i>An outline of the scaling analysis. Performance of the CMG-120 in pyramid and Box-90 configurations are considered. * The maximum pyramid configuration torque is equal to $(4\tau_{cmg} \times \sin(\beta))$ where $\beta = 54.74^\circ$ is the skew angle; † The maximum Box-90 configuration torque is not symmetric; maximums along principal axes ($2h_0$ and $4h_0$) and at 45° ($2\sqrt{2}h_0$) are shown.</i>	136
3.4	Mass budget for SPH-Halo-CMG system. <i>The masses of all major components excluding the electronic components on the connector PCB and the wires connecting the control board to the CMGs.</i>	140
3.5	Details of the SPH-Halo-CMG + SPH scenario (Figure 3-5) <i>Table includes expected performance of both the pyramid and Box-90 CMG arrays using the Honeybee Robotics CMG-120. Analysis credit: Tim Setterfield [1].</i>	143
3.6	Control Frequencies. <i>Initial design values are used in preliminary simulations while the attitude-only design is implemented for the August 2015 Reduced Gravity Re-Flight Opportunity. Values correspond to CMG attitude control; for thruster-only attitude control, thrusters would fire at the frequency listed for CMG Command.</i>	156
3.7	Mass trade-off for simulated SPH-Halo-CMG system <i>A summary of the mass trade-offs involved in adding a CMG payload to the SPHERES satellite testbed. These trade-offs are maneuver-dependent, and are thus presented for both the ‘EVA’ and ‘Docked’ maneuvers.</i>	180

List of Acronyms

ACI - asteroid-centered inertial (frame)
ACS - attitude control system
CAD - Computer-Aided Design
CEV - Crew Exploration Vehicle
CMG - control moment gyroscope
CM - center of mass
DCM - direction cosine matrix
DoF - degree-of-freedom
EMU - Extravehicular Mobility Unit
EPS - electrical power system
EVA - extravehicular activity
GNC - guidance, navigation and control
GUI - graphical user interface
INSPECT - Integrated Navigation Sensor Platform for EVA Control and Testing
IR - infrared
ISS - International Space Station
JSC - Lyndon B. Johnson Space Center
LEO - low-Earth orbit
LVLH - local vertical local horizontal frame
MVL - MIT Man Vehicle Laboratory
MIT - Massachusetts Institute of Technology
MMU - Manned Maneuvering Unit
NASA - National Aeronautics and Space Administration
NEA - near-Earth asteroid
NEO - near-Earth object
ORU - Orbital Replacement Unit
PCB - printed circuit board
PD - proportional-derivative
PID - proportional-integral-derivative
RGA - reduced gravity aircraft
RMS - root mean square
SAFER - Simplified Aid for EVA Rescue
SPHERES - Synchronized Position Hold Engage and Reorient Experimental Satellites
SPH-Halo-CMG - A SPHERES configuration including the Halo expansion and CMGs
SSL - MIT Space Systems Laboratory
UART - Universal Asynchronous Receiver/Transmitter

UDP - SPHERES Universal Docking Port

UROP - MIT Undergraduate Research Opportunity Program

US - ultrasound

USB - Universal Serial Bus

VERTIGO - Visual Estimation for Relative Tracking and Inspection of Generic Objects

Chapter 1

Introduction

A broad range of human space exploration missions could benefit from an astronaut mobility unit capable of providing six-degree-of-freedom (6-DoF) control during extravehicular activities (EVA). At the moment, NASA’s plans for long-term human exploration are uncertain, but several facts have become clear: on-going development of the Space Launch System (SLS) heavy-lift launch vehicle and the Orion Crew Exploration Vehicle (CEV) promise a near-future capability to transport astronauts to destinations like the moon, low gravity objects like asteroids, and ultimately Mars.

1.1 Motivation

The need to develop an operational Jetpack among other technologies has been identified in NASA’s Human Exploration Destination Systems Roadmap [10] and is motivated not by a particular mission architecture or proposed mission but instead by the long-term goals of NASA’s human exploration program. NASA is currently conducting research for an Advanced Jetpack at the Johnson Space Center (JSC) that might fill this technology gap, though the need for off-surface EVA mobility will become more pronounced when operations with the Orion CEV begin¹. The reason is that unlike the previously-proposed Multi-Mission Space Exploration Vehicle

¹The term “Advanced Jetpack” is the current name for NASA’s next back-mounted thruster mobility unit; future references in this thesis will refer to the device simply as the Jetpack

(MMSEV), a pressurized crew vehicle designed for low gravity exploration of near-Earth objects (NEO) and near-Earth asteroids (NEA), the Orion CEV design does not include plans for a robotic arm. This implies that EVAs around the Orion CEV are to be restricted to the mobility afforded by the few hand-holds on the vehicle's external surface. This restriction would limit the potential value that could be gained from EVAs conducted in the vicinity of the CEV, especially when visiting low gravity bodies of scientific interest.

While an Advanced Jetpack promises to enhance the utility of deep space human exploration missions when the Orion CEV enters operation in the near future, benefits of an Advanced Jetpack could be realized now at the International Space Station (ISS). A picture of the Manned Maneuvering Unit (MMU), NASA's previous back-mounted thruster mobility unit, as well as the Advanced Jetpack variant described further in this thesis are shown in Figure 1-1. The ISS solar arrays are bombarded by radiation and micrometeorites that degrade the arrays' performance over time. Periodically, EVAs are conducted in which astronauts use the ISS robotic arm to visually inspect the arrays, but the robotic arm does not extend far enough to allow for complete inspection. An Advanced Jetpack would enable a full inspection of the ISS solar arrays. The expanded mobility afforded by a Jetpack would also enable more complex maintenance scenarios than are currently possible for consideration in EVA missions, including installation of Orbital Replacement Units (ORU). In addition, more direct travel routes and reduced tethering requirements for routine EVAs at the ISS would reduce crew fatigue and improve efficiency of EVA operations. The simplification of EVA translation paths has the added benefit of potentially saving mass and cost needed to support EVA operations. Finally, an Advanced Jetpack would enable astronauts to conduct emergency rescue operations for crew members that have become untethered or otherwise incapacitated beyond the reach of a robotic arm, much like the Shuttle was able to maneuver to rescue endangered crew members in pre-ISS missions.

With potential mission applications that include ISS solar array and ORU inspection and maintenance, as well as crew member rescue and in the future Near-Earth

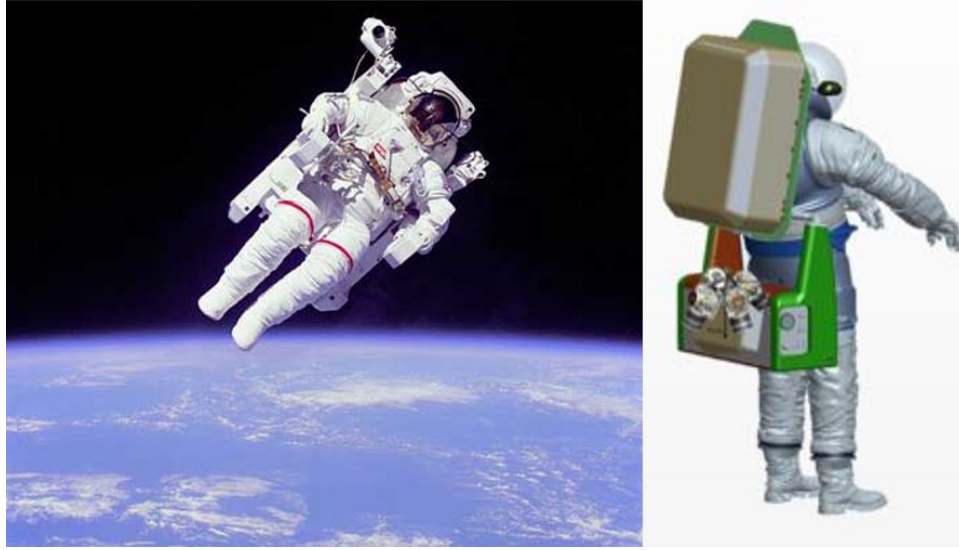


Figure 1-1: **The Manned Maneuvering Unit and MAJIC.** *Left: US astronaut Bruce McCandless and the MMU, 1984; courtesy of NASA. Right: Suited astronaut concept with the Mobility Augmenting Jetpack with Integrated CMGs (MAJIC) system considered for this thesis following previous work at Draper and MIT [2, 3, 4].*

Object (NEO) exploration and sample recovery, the Jetpack will be required to provide 6-DoF control to astronauts or robotic configurations conducting a broad range of tasks, often without the aid of hand-holds. This means that an equally broad range of reaction torques are expected to be induced on the Jetpack system that must be counteracted to maintain platform stability throughout any given mission. The stability of the platform becomes especially important for precise EVA tasks including sample recovery activities at a low gravity astronomical body and experimental payload installation and maintenance.

1.2 Thesis Focus

This thesis describes the design exploration of introducing CMGs in the attitude control system (ACS) of the Jetpack as well as in the SPHERES facility. Primary contributions described fall into two broad categories:

1. First, a Draper-MIT simulation of the Jetpack system in a MATLAB-Simulink environment corresponding to various system configurations operating in the

vicinity of the ISS or a low-gravity Near-Earth Asteroid (NEA); and

2. Second, a hardware demonstration of combined thruster and CMG control of the Synchronized Position Hold, Engage, Re-Orient Experimental Satellite (SPHERES) facility at the MIT Space Systems Laboratory (SSL).

The Draper-MIT Jetpack simulation provides the capability to explore the design for CMG actuators to include in the MAJIC system for specific mission profiles and to evaluate the performance of combined CMG-thruster and thruster-only implementations for a broad range of missions. Figure 1-2 depicts a graphical representation of an astronaut using MAJIC to operate near an asteroid's surface. The addition of small control moment gyroscopes (CMGs) to the Jetpack could improve the attitude stability of the EVA platform beyond what is possible with an all-thrusters attitude control system (ACS). In addition to the extra stability, CMGs might also conserve on-board fuel and extend the length of EVA missions since thrusters would only be used for translation and CMG desaturation when necessary. Preliminary studies conducted by the Charles Stark Draper Laboratory (Draper) and the Massachusetts Institute of Technology (MIT) for a Mobility-Augmenting Jetpack with Integrated CMGs (MAJIC) system provides an indication that such a system might provide stability and fuel economy benefits for a new Jetpack system [2]. A notional representation of the MAJIC system is depicted to the right of the MMU in Figure 1-1.

The MAJIC system is conceived to be a human-piloted EVA spacecraft, but it shares several key characteristics with autonomous vehicles proposed for on-orbit assembly, robotic servicing of satellites, reconfigurable robotic inspection and maintenance EVA spacecraft outside the ISS and astronaut assistant spacecraft inside the ISS. First, all of these spacecraft must operate in the vicinity of highly valued assets; second, all these spacecraft must conduct precision tasks; and finally, all of these spacecraft must control the orientation and position of variable-size and variable-mass systems to accomplish their objectives.

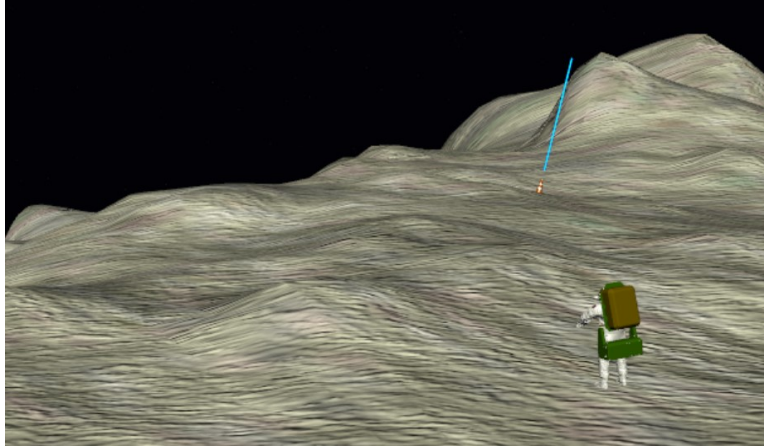


Figure 1-2: **MAJIC at an asteroid.** *This screen-shot from a human simulation trial of the MAJIC system conducted at NASA JSC in 2014 depicts the MAJIC system transporting an astronaut near the surface of an asteroid. [3]*

The hardware demonstration effort involving SPHERES enables the capability to immediately compare performance of the two types of systems (i.e. thruster ACS vs. CMG ACS) on a physical satellite system representative of the MAJIC system or small robotic systems such as autonomous robotic service and assembly or robotic EVA inspection and maintenance that would similarly benefit from precise pointing and high torque capabilities. The fact that the SPHERES satellites already have the capacity to be programmed for control modes such as attitude hold only strengthens the parallelism between SPHERES and MAJIC.

The SPHERES facility is composed of three satellites on orbit inside the ISS and several matching satellites in MIT's Space Systems Laboratory (SSL) and NASA Ames Research Center. SPHERES acts as a reconfigurable controls research program with over 15 years of development history and with nearly 10 years experience aboard the ISS as a microgravity experimental testbed. In the past few years, the SPHERES facility has seen the introduction of Halo, an expansion port enabling up to six payloads to interface with a central SPHERES satellite, and the universal docking port (UDP) enabling multiple SPHERES to remotely sense and dock to one another. Together, these new technologies allow the SPHERES facility to be used to investigate research topics in autonomous on-orbit assembly, robotic servicing of satellites, reconfigurable robotic inspection and maintenance EVA spacecraft and astronaut assistant

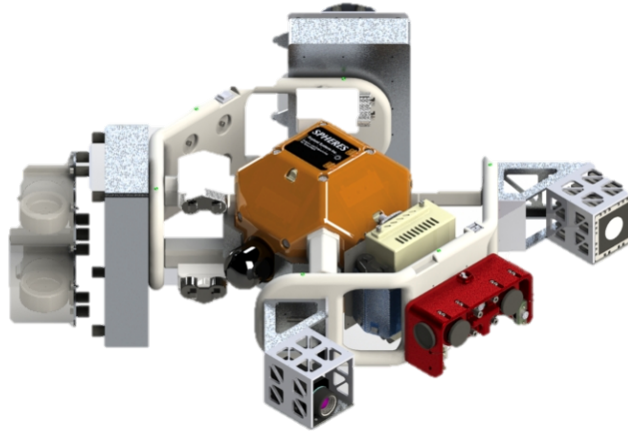


Figure 1-3: **MIT's INSPECT Spacecraft.** *The Integrated Navigation Sensor Platform for EVA Control and Testing is one of many spacecraft variants that the MIT SPHERES facility has been investigating; CMGs are integrated to improve pointing accuracy of the inspector system.*

spacecraft. That is, the latest state of the SPHERES facility provides a mature platform to evaluate the utility of adding CMGs for enhanced attitude control. Figure 1-3 depicts a computer-aided design model for a prototype reconfigurable inspection spacecraft with integrated CMGs named the Integrated Navigation Sensor Platform for EVA Control and Testing (INSPECT) built at MIT's Space Systems Laboratory as part of this thesis and the MIT senior undergraduate space systems design course 16.83.

What follows is a description of the background for both Jetpack and SPHERES satellite technologies as well as the previous work completed that serves as a foundation for the work presented in this thesis. Next, introductory concepts of attitude control with and without CMGs is presented. Finally, this introductory chapter concludes with an overview of the thesis contained herein.

1.3 MAJIC System Background

1.3.1 Jetpack Heritage

Astronaut mobility units have several notable historical precedents that have been tested and operated in low-Earth orbit (LEO) over the years. Following the Apollo program, NASA developed the MMU pictured on the left in Figure 1-1, a back-mounted thruster mobility unit designed to enable astronauts to aid with satellite capture operations [11]. The MMU successfully met its operational goals on a handful of missions in the early 1980s. On STS-51A, for instance, astronauts Joseph Allen and Dale Gardner retrieved malfunctioning satellites Palapa-B2 and Westar-VI with the aid of the MMU [12]. After the Challenger disaster in 1986, though, the decision was made to retire the MMU. Apart from cost considerations, the decision was motivated by a lesson learned from a failed attempt at grappling the Solar Maximum Mission spacecraft with the MMU on STS-41C in 1984: during this mission it was found that the use of a robotic arm alone was a safe and effective alternative for satellite capture [13]. It wasn't until 1994 that another 6-DoF capable mobility unit, the Simplified Aid for EVA Rescue (SAFER), was tested on-orbit during the STS-64 mission. Unlike the MMU, SAFER was never intended to be used during nominal operations but is instead an emergency-only option for astronauts to self-rescue in the event of tether separation [14]. The SAFER has since become a trusted default contingency for maintaining crew safety during EVAs, especially during the construction of the International Space Station (ISS).

Interestingly enough, the concept of using CMGs in an astronaut mobility unit to achieve performance gains over a thruster-only system is not entirely new. In the initial design studies for the MMU, a unit that included CMGs was built and flown inside the Skylab orbiting facility as part of the M509 Experiment in 1973 pictured in Figure 1-4 [5]. Despite the greater stability afforded by CMGs, the final MMU design did not include CMGs and instead relied only on thrusters for both position and attitude control. The decision to exclude CMGs from the MMU's design was driven by the fact that the target satellite capture system design for the MMU did



Figure 1-4: **The Astronaut Maneuvering Research Vehicle (AMRV).** *The AMRV was flown inside the volume of the Skylab orbiting facility as part of the M509 Experiment on the Skylab 3 Mission, 1973 [5]. The AMRV featured 6 CMGs in three scissor-pair configurations for attitude control testing. Image courtesy of NASA.*

not require a high degree of astronaut movement precision or platform stiffness, and because CMG options at the time were too large and required too much power to justify for the MMU given the system’s objectives. The miniaturization of CMGs in recent years as well as the evolving human exploration goals of the near future together motivate a serious reconsideration of the combined control of a Jetpack with thrusters and CMGs, a topic which features prominently in this thesis.

1.3.2 Previous Work on MAJIC

Previous MAJIC system design and operator evaluation studies at Draper and MIT have focused on developing a simulation environment and performing Monte Carlo CMG actuator sizing and operator evaluation studies. Following the initial system concept study documented in [2], a detailed model-based simulation was implemented in MATLAB and Simulink that allowed for the evaluation of Jetpack system performance in the context of particular missions [15, 16]. Suited astronaut 6-DoF dynamics are modeled that include realistic disturbance torque profiles for operator-directed simulations corresponding to limb articulation and tool wielding

activities such as using hammers and reaching up or out with a suited arm. This 6-DoF astronaut dynamics model utilized human body parameters from the Generator of Body Data (GEBOD) program [17] and relied on the astronaut dynamics model developed in [18]. Candidate mission profiles for both the sizing study and the operator evaluations were constructed as well as corresponding concepts of operation (CONOPS) for MAJIC use.

The actuator sizing approach initially adopted by the MAJIC program sought to identify a CMG design that effectively paid for its weight over the course of a single EVA mission. The idea was that a low-mass CMG ACS might provide improved stability and control authority of the Jetpack without incurring a mass penalty at any point during operations. After finding a candidate CMG design with this constraint, though, operator evaluations using NASA's VR Lab at the Johnson Space Center revealed that such a small CMG did not have the capability to improve performance beyond the control authority of a thruster ACS [3]. The reason was that the total angular momentum capacity of the small CMGs was too small to effectively counter astronaut motion-induced disturbance torques and frequently required desaturation with thrusters. In short, the goal of achieving immediate mass savings was shown to be at odds with the objective of providing a stiff and responsive work platform for astronauts during EVAs.

To address the limitations of this initial study, the sizing approach that is presented in this thesis and that is also documented in [4] seeks to identify high-performance CMGs that improve the platform stability over that achievable by a thruster-only system as measured by total attitude error throughout a mission profile. A modified, methodical approach to identifying CMG parameter constraints corresponding to Jetpack mass, volume and power budgets is presented in this thesis. Coupled with improved physics-based simulations for CMG kinematics as well as the addition of 6-DoF astronaut motion disturbance torques to simulated mission profiles, the revised sizing methodology results in the identification of an ideal CMG design based on Jetpack size, weight and power (SWaP) restrictions as well as a smaller CMG design optimized for a particular mission profile representative of a wide variety of

potential missions. Performance comparisons of a Jetpack with and without these newly-sized CMGs provide insight into the gains in stability and multiple-mission fuel economy that could be expected with a CMG ACS as opposed to that which might be achievable with a traditional thruster ACS.

1.4 MIT SPHERES Background²

In addition to the theoretical investigation of the MAJIC system, a hardware demonstration effort also figures prominently in the MAJIC program at Draper and MIT. A peripheral CMG actuator suite relying on commercially-acquired CMGs was designed, built, integrated and tested to function as part of the Synchronized Position Hold, Engage, Re-orient Experimental Satellite facility at the International Space Station and MIT's Space Systems Laboratory. A physical realization of combined thruster and CMG control for SPHERES would provide the most convincing simulation environment for MAJIC system development, but it would also serve the objectives of parallel research conducted at the SSL for reconfigurable autonomous control of distributed structures for on-orbit assembly, robotic servicing or autonomous EVA inspection and maintenance and intra-vehicular activity (IVA) astronaut assistance. A photograph taken at the ISS shows astronaut Scott Kelly with the three SPHERES satellites on-board the ISS in Figure 1-6.

Since their launch to the ISS in 2006, the SPHERES on orbit have proven to be a versatile controls testbed, a fact that has been repeatedly reinforced throughout the program's 15+ year history of research and development both on the ground and in reduced-gravity aircraft. Not only are the SPHERES a well-established, low-cost and low-risk option for controls testing, but there is also a strong precedent for using the SPHERES satellites for testing of peripheral payloads in a reconfigurable manner; in fact, the SPHERES satellites were initially designed for this purpose [19]. For instance, fluid behavior in micro-gravity has been investigated with the SPHERES

²This section includes contributions by Tim Setterfield of the MIT SPHERES team, initially compiled for the Fall 16.851 MIT course on Space Systems Engineering.



Figure 1-5: **SPHERES on the ISS.** *Astronaut Scott Kelly poses for a photograph with three MIT SPHERES Satellites aboard the International Space Station.*

satellites on-orbit as part of the fluid slosh experiments [20]. Visual navigation algorithms have also been developed on-orbit with an augmentation to the SPHERES facility that included the addition of two Visual Estimation for Relative Tracking and Inspection of Generic Objects (VERTIGO) units along with a pair of stereoscopic cameras that fasten directly to the SPHERES-VERTIGO stack [21]. Also, a set of Universal Docking Ports (UDPs) have recently been shipped to the ISS and will soon enable two SPHERES to autonomously dock rigidly to one-another in the micro-gravity environment. Soon after, the Halo expansion that extends the number of available expansion slots on each SPHERES satellite from one to six will follow the UDPs to allow all three SPHERES to dock to one another, but also to enable more ambitious hardware configurations and control algorithm development with the SPHERES facility on-orbit.

A SPHERES satellite can be seen in Figure 1-6. Each SPHERES satellite has a mass of 4.2 kg, a CO₂ tank and micro-machined nozzles for propulsion, an ultrasound ranging system with infrared triggers, a small on-board processor, an Inertial Measurement Unit (IMU) containing three rate gyros and three accelerometers, an internal replaceable battery pack, and has both SPHERE-To-SPHERE and SPHERE-To-Laptop wireless communication channels. The SPHERES satellites use twelve

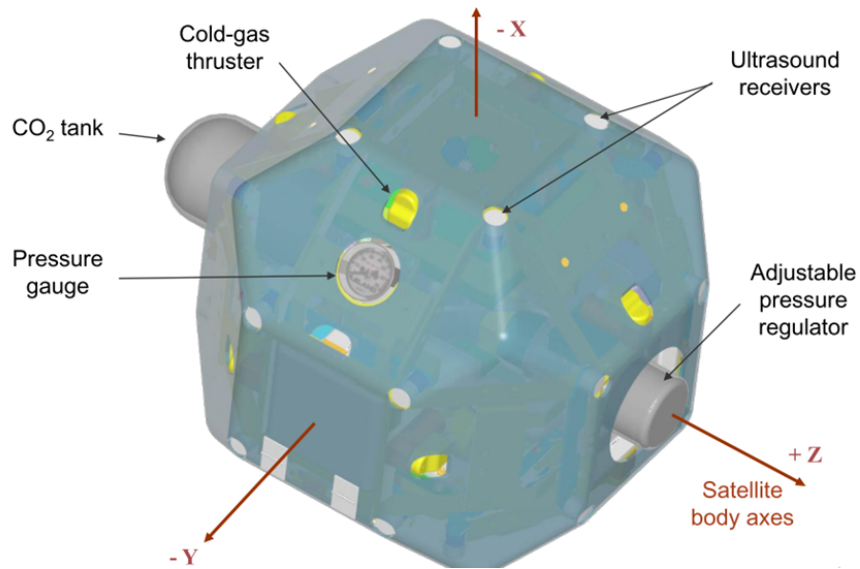


Figure 1-6: **A SPHERES satellite.** *SPHERES-frame body axes are shown as well as prominent features of the experimental satellite.*

cold-gas thrusters for both translation and rotational control to attain a specified attitude and position inside a test volume that is dependent upon test location (the SSL air-bearing table, a microgravity aircraft, or the ISS). Infrared (IR) pulses from SPHERES trigger static, external ultrasound (US) beacons surrounding the test volume to determine the satellite’s distance from each beacon, and the SPHERES on-board computer uses this information to determine its position and orientation in space.

Each SPHERES satellite is equipped with an expansion port used to interface with additional hardware. The expansion port allows the addition of another SPHERES satellite, payload, sensors, or actuators. In 2010, the MIT Space Systems Lab and Aurora Flight Sciences began the DARPA sponsored Visual Estimation and Relative Tracking for Inspection of Generic Objects (VERTIGO) program [?]. VERTIGO hardware is composed of a Linux computer (avionics stack) and stereo camera pair (goggles). The physical demonstration effort described in this thesis takes advantage of the VERTIGO avionics stack’s USB output to create a pass-through for information from SPHERES to the CMG control board.

Halo is an add-on for SPHERES that will increase the number of available expan-



Figure 1-7: **SPHERES and the Halo Expansion.** *Up to six peripherals can be interfaced with Halo and communicate with the central SPHERES satellite.*

sion ports on SPHERES from one to six. As shown in Figure 1-8, the Halo structure surrounds a central SPHERES satellite, providing a mechanical interface, a data connection, and power to a maximum of six peripherals. All communication with Halo peripherals will pass through the VERTIGO avionics stack, which is a single-board Linux computer. An electrical port will provide USB and Ethernet data connections to the VERTIGO avionics stack, as well as power from $4 \times$ NikonE N-EL4a 11.1 V, 2500 mAh batteries. Halo will support a suite of instruments and actuators currently under development and expand the possible research activities that can be conducted on SPHERES.

Halo provides the most useful avenue for combined control research with thrusters and control moment gyroscopes for two reasons: first, Halo would enable CMGs to operate in conjunction with multiple other payloads including (but not limited to) optical payloads, docking ports and robotic arms for a broad range of robotic spacecraft operations envisioned for the future; and second, because the use of Halo allows for increased power availability for CMG operations. For these reason, the concept described in more depth in Section 3.1 assumes a configuration of a central SPHERES satellite, a VERTIGO avionics stack and a Halo expansion, along with an

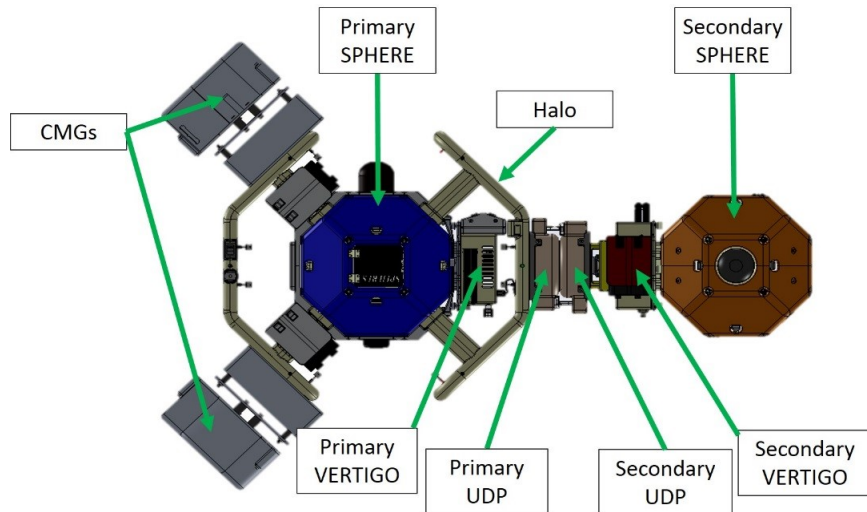


Figure 1-8: **Two SPHERES Docked.** *The proposed docked configuration for flight aboard NASA’s Reduced Gravity Aircraft in August 2015; the Secondary SPHERES satellite will execute open-loop thruster firings to induced known disturbance torques that the Primary SPHERES satellite will reject either with thruster-only attitude control or CMG attitude control. Closed-loop slew maneuvers will also be completed using this docked configuration as well as with an undocked Primary SPHERES satellite.*

actuator suite of CMGs (henceforth referred to as the SPH-Halo-CMG configuration).

The addition of commercial CMGs acquired from Honeybee Robotics for attitude control will enable stable and responsive control of a broad range of potential SPHERES configurations. Options for configurations include those useful in advanced imaging and inspection missions such as in [22], in novel robotic arm or robotic servicer operations, or in larger-still docked configurations of multiple SPHERES satellites applicable to autonomous in-orbit structure assembly as well as robotic servicing and maintenance missions. The development of a CMG subsystem that is Halo- and SPHERES-compatible paves the way for on-orbit demonstrations of a combined thruster-CMG control concept in the next few years.

Already, the CMG subsystem for SPHERES has been designed for flight, and an implementation of the system flew on NASA’s reduced gravity aircraft in August 2014 [22] further strengthening a future argument for extended flight operations. On this flight, the integration of CMGs in the INSPECT SPHERES configuration were shown to successfully apply torques to the system in a manner consistent with

quick response times and slew rates for the INSPECT system for efficient inspection operations. Unfortunately, closed-loop control of the system necessary to investigate precision pointing performance could not be demonstrated aboard the reduced gravity aircraft at the time.

A follow-up flight opportunity scheduled for August 2015 aims to investigate closed-loop control algorithms with the ultimate goal of comparing pointing capabilities of a thruster-only attitude control system on SPHERES as compared to a CMG attitude control system with both a single SPHERES configuration and a two-SPHERES docked configuration. These new tests will hopefully distinguish thruster and CMG performance more readily as compared with what was possible with the INSPECT configuration. Since inspection sensor fusion objectives and mass moment of inertia identification of the INSPECT system were successfully carried out on the August 2014 flight opportunity, the focus of the 2015 opportunity will focus solely on attitude control system comparison for application to spacecraft applications introduced in this thesis.

1.5 Dynamics and Attitude Control for a Jetpack and for SPHERES

Attitude or reaction control of a Jetpack or SPHERES is analogous to attitude control for any other spacecraft in the sense that torques must be delivered to the system in order to achieve desired angular rates $\Delta\omega$ for pointing or slewing throughout a mission. The magnitude and direction of required spacecraft torque $\boldsymbol{\tau}_{body}$ depends on the mass moment of inertia tensor of the spacecraft to be controlled, \mathbf{I} and the desired angular rate vector $\boldsymbol{\omega}$ by the familiar equation

$$\boldsymbol{\tau}_{body}^{B/N} = \mathbf{I}_{body} \cdot \dot{\boldsymbol{\omega}}^{B/N} + \boldsymbol{\omega}^{B/N} \cdot (\mathbf{I}_{body} \times \boldsymbol{\omega}^{B/N}) \quad (1.1)$$

In the equation 1.1, the moment of inertia tensor is referenced to axes defined by the spacecraft's body frame B , with an origin at the spacecraft's center of mass.

The angular acceleration and resulting torque on the spacecraft body frame B is expressed with respect to the inertial frame N using the superscript B/N . Usually, pointing requirements are driven by a spacecraft's payload and orbit in addition to the power (in the case of solar powered spacecraft) and thermal subsystem requirements. For example, a geostationary communication satellite (GEO comsat) must point its antennas to the Earth, its solar arrays to the sun and its radiators to deep space. In the case of GEO comsats and most other spacecraft, pointing and slewing tasks are well defined by angular rates stipulated by payload specifications and the spacecraft's orbit. Torque requirements of the ACS are readily derived with accurate knowledge of the spacecraft's mass properties and expected disturbance torques induced by solar radiation pressure, gravity gradients, atmospheric drag or Earth's magnetic field. A time-varying profile for spacecraft mass properties can be calculated from expected fuel consumption in order to better inform attitude control commands as a mission progresses.

A Jetpack or a robotic servicer or on-orbit assembly spacecraft as represented by the reconfigurable SPHERES facility differ from the usual spacecraft in two important ways that affect ACS design: the first pertains to disturbance torques and the second pertains to spacecraft mass properties. First, disturbance torques acting on the Jetpack or SPHERES systems are not restricted to solar radiation pressure, gravity gradients, atmospheric drag, Earth's magnetic field or even fuel slosh in micro-gravity. Instead, disturbance torque profiles for the Jetpack application are dominated by torques caused by astronaut motions corresponding to using tools and interacting with the spacecraft vehicle, experimental payloads, or other low gravity bodies as part of normal EVA operations. For the SPHERES application, disturbance torque profiles are dominated by the specific configuration type and the characteristics thereof corresponding to robotic arm actuation or docked peripheral dynamics. Second, the mass properties of the Jetpack and SPHERES systems vary over the course of a mission beyond the usual mass loss associated with fuel consumption. This change in the Jetpack mass properties reflects the movement of an astronaut pilot's arms and legs during an EVA, as well as the extra mass that must be accounted for by the atti-

tude control system when an astronaut pilot uses heavy tools or grips massive objects such as an ORU or experimental payload at the ISS, a hammer or drill at a NEA to be sampled, or another crew member in a rescue scenario. The change in SPHERES mass properties may reflect docking among multiple SPHERES or grappling activities that may be conducted with a robotic arm.

Finally, a necessary capability of any Jetpack or successful SPHERES implementation would be to enable an astronaut user or mission planner to plot any number of different trajectories. In practice, translation with thrusters³ will induce rotations arising from imperfect thrust vector control with a real system. Different trajectories will induce different angular rates to be corrected by the attitude control system depending on the specific distribution of mass at the time of thruster firings. These considerations introduce the challenges associated with attitude control system design for an Advanced Jetpack or the reconfigurable SPHERES facility; the following subsections describe options for attitude control solutions.

1.5.1 Reaction Control Overview

The most straightforward solution to the problem of Jetpack or SPHERES attitude control is to use thrusters for attitude control, since they are already necessary for position control. This was the solution implemented in NASA's MMU and SAFER astronaut mobility units. Thrusters in the MMU, SAFER and proposed Jetpack are discrete on-off actuators with attitude control defined by a phase plane controller like the one in Figure 1-9. In phase plane control, allowable bounds for attitude error and sometimes angular rate error are selected; thruster firings for attitude control only occur if those error bounds are exceeded. What results is a deadband around the desired attitude (and angular rate if angular rate errors are selected). Inside this deadband, the system is allowed to drift until a large enough attitude (or angular rate) error accumulates. In this type of control implementation, propellant use is

³A solar sail or other non-rocket alternative to propulsion for translation and position control is far from being practical at this time, especially since high thrust (as compared with solar radiation pressure) is required for quick translation times in human EVAs or SPHERES testing aboard the ISS

traded with pointing accuracy since more thruster firings are necessary to maintain a tighter deadband. In the MMU, the attitude deadband corresponds to attitude error alone and is adjustable between 0.5 and 2.0 degrees [11]. This deadband selection corresponds to attitude errors of 0.25 and 1.0 degree, respectively, since the total allowable error is equivalent to half of the selected deadband. The SAFER is designed along the same principles and has a fixed deadband of 2.0 degrees [14] corresponding to an allowable attitude error of 1.0 degree. The SPHERES system is designed specifically to allow for any conceivable control implementation and so a variety of thruster attitude control deadbands might be implemented for future applications.

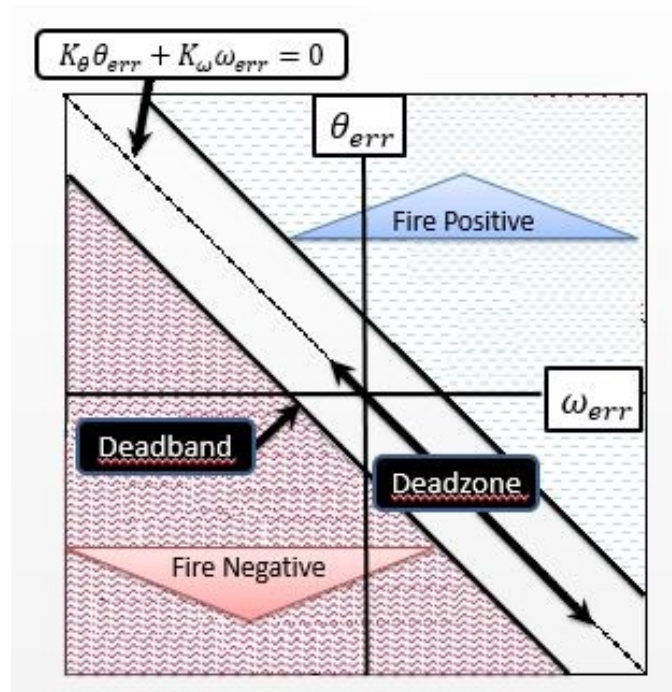


Figure 1-9: **Phase plane controller for attitude control with thrusters.** Allowable bounds for errors in attitude, θ_{err} , and angular rate, ω_{err} , are selected and thruster firings only occur should the deadband defined by these bounds is exceeded. For a controller with proportional gain K_{θ} and differential gain K_{ω} , no controller output is commanded along the dotted line.

The problem of a deadband cannot be completely avoided by using an internal torquing mechanism like CMGs for attitude control. There will always be a limit to the minimum torque deliverable by an attitude actuator suite, as there will always be a limit to the sensitivity and time-resolution of inertial sensor measurements that

are used in a control law for attitude.⁴ The advantage of using CMGs is that the deadband can be significantly reduced without fear of eliminating control authority as in the case of on-off thrusters. One reason is that CMGs provide a range of torques as opposed to the fixed torque delivered provide a minimum torque to the system that is less than the torque deliverable by a thruster pair (even with fast-acting solenoids to actuate thrusters, the torque delivered is not throttled, but instead delivered in discrete increments as defined by minimum on-times).

As is the case for any phase plane control implementation, drift resulting from a deadband practically defines the platform stiffness an astronaut pilot or a researcher of the SPHERES program might expect. Narrowing the deadband would increase the system's stability, but at the expense of increased actuation; for thrusters, this results in increased fuel consumption, and for CMGs this results in increased battery energy consumption. Because on-off gas thrusters are not throttleable, tuning of control inputs can only be achieved by altering thruster on-times. CMGs, by contrast, can provide a range of torques to the system as defined by the minimum and maximum gimbal rates.

Practically, lower torque control inputs allow for narrower deadbands without fear of runaway consumable use. Of course, the capability to provide large torque control inputs is desired for impulse disturbance rejection and to achieve slews for extended mass configurations. Ideally, then, a tunable torque magnitude is desirable, which can be accomplished with CMGs and which cannot be accomplished with thrusters. In addition, a CMG array's collective angular momentum provides a gyroscopic stiffness to the system that reduces the effect of external torques, thereby decreasing the control demands of the attitude control system to achieve precise pointing. Gyroscopic stiffness can be understood simply as the conservation of angular momentum. A disturbance torque applied for a given amount of time is nothing more than a con-

⁴The selection of an inertial measurement unit (IMU) for a Jetpack or for SPHERES should take into account the attitude control demands reflecting deadband objectives as well as those demands defined by translation control demands as well as payload demands that are as-yet undefined. The selection of sensors for MAJIC or the SPHERES system is outside the scope of this thesis; instead, the focus of this thesis is on the selection and evaluation of CMG actuators that might be used in conjunction with sensors that already exist (as in the case of SPHERES) or that are to be selected in future design studies (as in the case for MAJIC).

tribution of angular momentum to the system \mathbf{H}_{dist} ; for a CMG array that already has a collective, non-zero CMG angular momentum \mathbf{H}_{cmg} ⁵, the overall change in the system’s angular rate ω corresponds not to just the disturbance angular momentum \mathbf{H}_{dist} , but rather to the *difference* in angular momenta $\mathbf{H}_{cmg} - \mathbf{H}_{dist}$. With these points considered, deadbands considerably tighter than those achievable with fixed, on-off thrusters are possible for CMGs.

Aside from the inherent limit to deadband size with fixed on-off thrusters, a second major drawback of using thrusters for reaction control of a Jetpack is the potential for thruster plume contamination of scientific samples or instruments during an EVA. In an asteroid sampling mission, for instance, a priority of the EVA would be to limit the sources of contamination on recovered samples. If reaction control with thrusters were used to maintain astronaut stability during proximity sampling activities, then there would be a large probability that thruster plumes would be introduced to the asteroid sample population. If an internal torquing actuator such as CMGs were used to maintain attitude stability during sampling operations, collected samples have a higher probability of remaining clean, enhancing the potential scientific yield from collected specimens. Similarly, if an astronaut conducting an EVA must inspect or repair an optical instrument that must remain clean, then it might be difficult to avoid depositing plume particles on the optics with the use of traditional thruster-mediated attitude control as opposed to using internal torquers.

An equivalent argument applies to a SPHERES configuration that must operate in close proximity to sensitive scientific instruments or other items that must be protected from thruster plumes, though with current ISS practices in conducting SPHERES experiments, thruster plumes do not pose these dangers.

1.5.2 Reaction Control with CMGs for Improved Stability

Control moment gyroscopes provide an attractive alternative to thrusters for an astronaut EVA Jetpack’s attitude control as alluded to above, as well as to SPHERES configurations aimed at exploring the performance attainable by future autonomous

⁵For a formal definition of \mathbf{H}_{cmg} , see Equation 1.4 in Section 1.5.2.

on-orbit assembly, robotic servicer or other reconfigurable spacecraft. CMGs are continuous actuators that can accommodate narrower deadbands than thrusters and can thus provide greater stability than thrusters. Greater stability for a Jetpack or for extended SPHERES configurations would correspond to an enhanced capacity to support precision tasks that align with future space exploration objectives including asteroid sampling missions or scientific instrument maintenance tasks. MAJIC as well as CMG-augmented SPHERES configurations would have the added potential to decrease the total amount of fuel required for a given mission since fuel consumption would be limited to translation tasks and CMG de-saturation. Depending on the nature and length of the MAJIC system's operational lifetime as well as the SPHERES' operational lifetime, there is also the potential to save on overall mass required to be transported to orbit. What follows is a description of how CMGs generate torques that can be used for attitude control, and what options exist in designing such a CMG subsystem.

Control moment gyroscopes store angular momentum in the form of a spinning flywheel. A single CMG unit generates torque by gimbaling the axis about which the flywheel spins. Relevant torques and scalars for an individual single-gimbal CMG (henceforth referred to simply as a CMG) are depicted in Figure 1-10, following the naming convention of [6]. The gimbal axis unit vector $\hat{\mathbf{g}}$ is the axis about which the flywheel is rotated during operations. The gimbal angle ϕ describes the amount by which the flywheel is rotated about the gimbal axis. The angular momentum vector of the flywheel rotor is labeled as \mathbf{h}_{rotor} , and the torque generated by the CMG, a torque that is equal and opposite to the torque induced on the spacecraft structure, is labeled as $\boldsymbol{\tau}_{rotor}$.

While there are different types of CMGs including those with multiple gimbals or variable speed flywheels, only single-gimbal CMGs with fixed flywheel rates are considered for this study since this type of CMG applies most readily to the Jetpack application. The reason is that single-gimbal CMGs have large torque-to-power ratios owing to the fact that torques are produced in an axis orthogonal to the gimbal motor and flywheel motor axes (which are themselves perpendicular) and thus put strain on

the spacecraft structure instead of a motor [6].

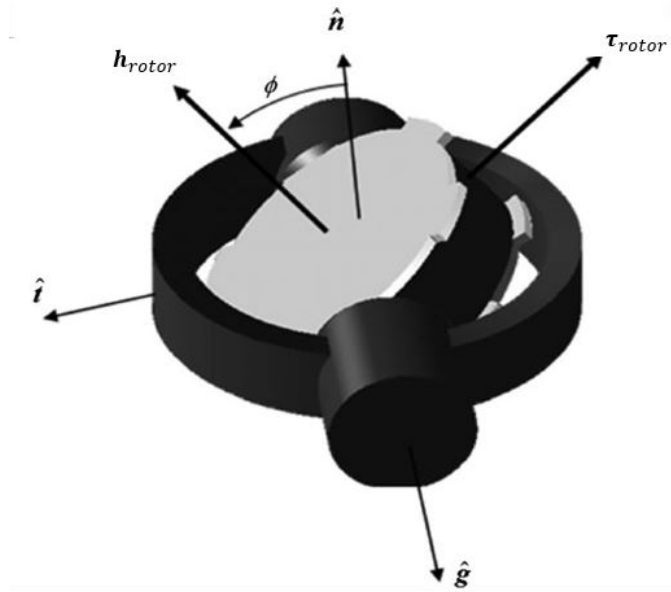


Figure 1-10: **Vectors and scalars for a single-gimbal CMG.** *Definition conventions are borrowed from [6].*

Angular momentum of the flywheel rotor is equal to the product of the flywheel rotor's mass moment of inertia tensor, I_{rotor} and the angular rate of the flywheel rotor $\boldsymbol{\omega}_{rotor}^{R/G}$ measured from a fixed-gimbal reference frame G with respect to a fixed-rotor reference frame R . That is,

$$\mathbf{h}_{rotor} = \mathbf{I}_{rotor} \cdot \boldsymbol{\omega}_{rotor}^{R/G} \quad (1.2)$$

The gyroscopic torque in the spacecraft body frame B produced by a CMG actuator is expressed as:

$$\boldsymbol{\tau}_{rotor} = -\dot{\phi} \hat{\mathbf{g}} \times \mathbf{h}_{rotor} \quad (1.3)$$

In Equation 1.3, $\dot{\phi}$ is the time derivative of the gimbal angle ϕ of the CMG, and \mathbf{h}_{rotor} is the angular momentum vector of the CMG rotor. This representation is a simplification of the true physical situation since the gimbal structure has an angular momentum associated with its motion during a torquing maneuver. Since this contribution to CMG torque is small compared with the change in angular momentum associated with the CMG rotor, only the latter is included here.

Because each CMG provides torques that are constrained to a plane, at least three CMGs are required to provide full three-axis control. Usually, a fourth actuator is included for redundancy and also to ensure singularity avoidance depending on the specific array implementation. Several configurations of CMGs including the scissor pair, Box-90, pyramid, roof-top, and more have been proposed and implemented for other spacecraft systems [23, 24, 25]. Ideally, the CMG array should be capable of tolerating the failure of at least one unit (singly-redundant), but should also be implemented with as few CMGs as possible to reduce mass and power requirements. Depending on the application, a CMG array should also provide a roughly uniform control authority to the CMGs as defined by the shape of the angular momentum envelope achievable. An angular momentum envelope is specific to a particular CMG array configuration and is a representation of the possible vector sums for individual CMG actuator angular momenta measured at different gimbal angle combinations. Since the pyramid configuration minimizes the mass and power requirements of the array by requiring only four CMGs for a singly-redundant system, and since the pyramid configuration has a roughly spherically symmetric momentum envelope, its application to the Jetpack is considered in more depth in this thesis.

The total angular momentum of the MAJIC system including CMGs \mathbf{H}_{sys} in the inertial frame N is equal to the collective angular momentum of the CMG array \mathbf{H}_{cmg} and the MAJIC structure \mathbf{H}_{body} :

$$\mathbf{H}_{sys} = \mathbf{H}_{cmg} + \mathbf{H}_{body} = \sum_{i=1}^n \mathbf{h}_{cmg,i} + \mathbf{I}_{body} \cdot \boldsymbol{\omega}^{B/N} \quad (1.4)$$

In equation 1.4, \mathbf{I}_{body} is the mass moment of inertia tensor of the MAJIC structure with respect to the center of mass of the system and $\boldsymbol{\omega}^{B/N}$ is the angular rate of the MAJIC structure body frame B with respect to the inertial frame N . It should be noted that \mathbf{H}_{cmg} is composed of the sum of the individual angular momenta from all n CMGs in an array where $\mathbf{h}_{cmg,i}$ is the angular momentum vector of the i^{th} CMG, including both the dominant flywheel rotor momentum term and minor terms associated with gimbal structure momentum. Taking the time derivative of Equation

1.4 yields the total torque on the system:

$$\boldsymbol{\tau}_{sys} = -\boldsymbol{\tau}_{cmg} + \boldsymbol{\tau}_{body} = \frac{d}{dt} \mathbf{H}_{cmg} + \mathbf{I}_{body} \cdot \frac{d}{dt} \boldsymbol{\omega}^{B/N} + \boldsymbol{\omega}^{B/N} \times (\mathbf{I}_{body} \cdot \boldsymbol{\omega}^{B/N} + \mathbf{H}_{cmg}) \quad (1.5)$$

The negative sign in front of $\boldsymbol{\tau}_{cmg}$ in Equation 1.5 represents the fact that torques produced by CMGs generate a reaction torque in the system that is equal in magnitude but opposite in direction to the CMG torque. Producing a desired torque with the CMG array to effect a given $\Delta\omega$ of the system depends on the instantaneous gimbal angle of each CMG as well as the relative orientation of the individual units by the following relation:

$$-\boldsymbol{\tau}_{cmg} = \frac{d\mathbf{H}_{cmg}}{dt} = \frac{\partial \mathbf{H}_{cmg}}{\partial t} \frac{\partial \phi}{\partial t} = \mathbf{J}(\phi) \dot{\phi} \quad (1.6)$$

The performance of an individual CMG is usually defined by the CMG's angular momentum storage capacity and individual torque described by Equations 1.2 and 1.3 respectively. The control authority of a CMG array, however, is usually characterized by the angular momentum envelope that represents all possible angular momentum states of the collective system found by summing the instantaneous three-vector angular momenta of individual CMGs that make up the array. Torques are generated with transitions within the momentum envelope of the array's collective angular momentum according to the left-most equality in Equation 1.6.

The momentum envelope of a pyramid configuration CMG array with four CMGs described in [7] and [8] is depicted in Figure 1-11. When the CMGs of the array are all oriented such that the maximum collective angular momentum \mathbf{H}_{cmg} in a given direction is reached, a degree of freedom is lost and the array can no longer generate torques in that direction. When this situation arises, the array is said to saturate or encounter an external singularity. In order to return control authority to the CMG array, the array must be desaturated by using an external torquer. For the Jetpack application, thrusters can be readily applied as external torquers to desaturate CMGs. For these occasions, thrusters would fire in order to hold attitude, for instance, while CMGs are gimballed back to a state of full controllability. In addition to external

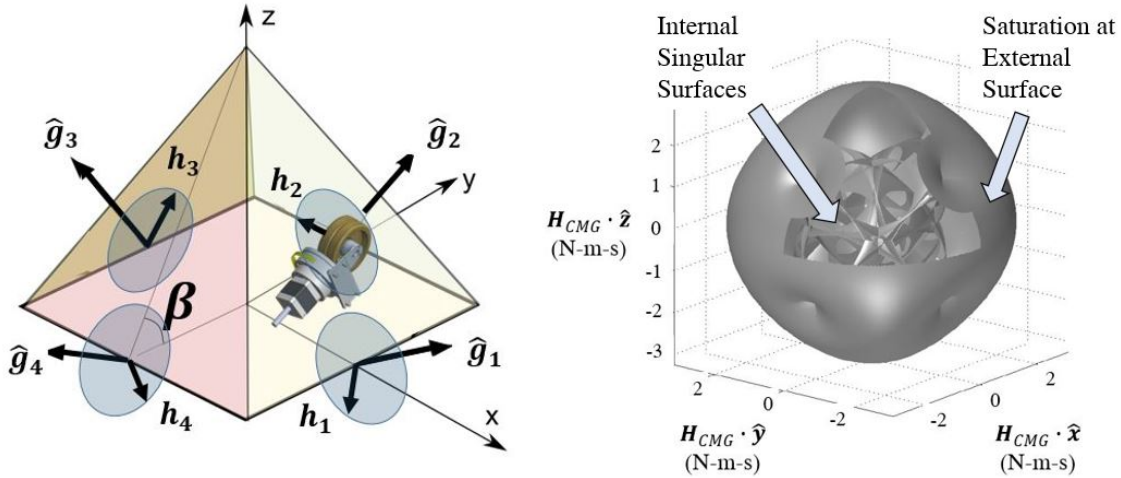


Figure 1-11: **CMG pyramid configuration and angular momentum envelope depicting singular surfaces.** *Left: A 4-CMG pyramid configuration, pyramid angle $\beta = 54.74^\circ$; image modified from [7]. The i^{th} CMG has angular momentum $\mathbf{h}_{\text{cmg},i}$ and a gimbal axis $\hat{\mathbf{g}}_i$. Shaded blue circles on each triangular face indicate available positions for individual CMG angular momentum vectors. Right: The pyramid array's nearly spherically symmetric momentum envelope with singular surfaces pictured; image modified from [8]. When the CMG array's momentum reaches the edge of this envelope when CMG rotors are gimballed such that CMG angular momenta add constructively to a maximum degree, saturation occurs. An external torque provided by thrusters is required to return the CMG array to a fully controllable state.*

singularities, CMG arrays may also encounter internal singularities in which a degree of control freedom is lost while the collective CMG momentum still resides inside the momentum envelope, i.e. when there are momentum cancellations. External torques are required to librate a CMG array from these internal singularities just as in the case of saturation.

For systems with more than three CMGs (that is, for effectively all practical CMG arrays), the Jacobian matrix $\mathbf{J}(\phi)$ from Equation 1.6 is not a square matrix and therefore cannot be directly inverted to solve for gimbal rates that should be commanded to effect a desired torque. For this reason, a pseudoinverse steering law is required. The task of identifying a proper steering law is complicated by the existence of internal singular states of a particular CMG array configuration. The topic of identifying and avoiding singular states of CMG arrays with a real-time, computationally-practical pseudoinverse steering law is the subject of on-going

research and lies outside the scope of this thesis. For a comprehensive survey of theory and steering law designs for single-gimbal CMGs, see Kurokawa’s survey [26].

1.6 Thesis Overview

This thesis contains a performance and utility analysis of a combined control concept of thrusters and CMGs for precision pointing and high-stability spacecraft applications. This goal has been addressed both in simulation and with physical demonstration. Primary contributions in simulation have focused on implementing a new method for sizing CMG actuators and improving the performance and utility assessment strategies to compare a proposed MAJIC system with a Jetpack that does not include CMGs. Primary contributions with hardware have included the design, simulation, testing and integration of a CMG peripheral actuator package for the MIT SPHERES facility in the MIT SSL.

This thesis has a two-fold objective: first to describe the simulation efforts that have resulted in CMG actuator sizing and a system performance and utility assessment as compared with thruster-only Jetpack implementations; and second to detail the hardware demonstration efforts that have utilized commercial, miniature CMGs and the SPHERES facility in the MIT SSL.

- **Chapter 1: Introduction** The first chapter of this thesis serves as an introduction to the thesis and has summarized the motivation behind simulation, design, hardware demonstration and utility analysis for a combined control CMG+thruster concept of operations for a low gravity astronaut EVA jetpack and for the SPHERES facility. After providing background information concerning Jetpack heritage, the MAJIC program and the SPHERES facility, spacecraft dynamics and attitude control concepts were introduced that apply to the rest of this thesis.
- **Chapter 2: CMGs for a Jetpack** The second chapter of this thesis contains a comprehensive description of the concept, design and utility analysis for the

Draper-MIT Mobility Augmenting Jetpack with Integrated CMGs. Figuring prominently in the description of the MAJIC concept are the mission concepts and the Draper-MIT simulation built for design activities and utility analysis purposes. Design efforts for the MAJIC system focus on the definition of the CMG subsystem properties that would be most appropriate for a low gravity EVA Jetpack and a Monte Carlo approach to reducing the overall mass, size and power requirements of the actuator suite for a particular application. Finally, a utility analysis is conducted that evaluates the performance and consumable use for the combined control MAJIC system as compared with that of a thruster-only Jetpack over various mission profiles.

- **Chapter 3: CMGs for SPHERES** The third chapter of this thesis concerns hardware demonstration efforts of a combined thruster+CMG control system for the MIT SPHERES facility. A majority of the chapter is devoted to a description of the concept, design, integration and operations of a CMG-augmented SPHERES facility. Following a description of the combined control concept and research objectives for CMG-augmented SPHERES configurations, the design and simulation of the new system are described. Next, integration activities including the implementation of mechanical and electrical interfaces as well as software development and integration testing are described. Finally, functionality testing and operations of the augmented SPHERES facility in the laboratory and in micro-gravity experimentation on-board NASA's reduced gravity aircraft are presented. The chapter concludes with a utility analysis of the SPH-Halo-CMG system and a discussion of research implications of this hardware demonstration of a combined control concept.
- **Chapter 4: Conclusion** This thesis concludes with a summary of the Jetpack simulation and hardware demonstration achievements on the path toward further research and development of the MAJIC system and an augmented SPHERES facility. Recommendations for future work corresponding to further simulation and hardware development in both the near- and mid-term are pre-

sented. Near-term future work includes further development of the Draper-MIT simulation environment and controls development for the CMG subsystem of SPHERES in the SSL at MIT. Mid-term future work includes proposed on-orbit demonstrations of the combined control concept with the SPHERES facility inside the volume of the ISS as well as with a modified SAFER unit to serve as a prototype for NASA JSC's Advanced Jetpack both inside and outside the habitable volume of the ISS.

Chapter 2

CMGs for a Jetpack: Concept, Design and Utility Analysis

The Mobility Augmenting Jetpack with Integrated CMGs system is first and foremost a spacecraft. Of course, MAJIC is special in the sense that it hosts a human astronaut pilot that can also be considered a payload. As a spacecraft, MAJIC features propulsion, power, attitude control, avionics and thermal subsystems as well as inertial measurement and navigation sensors. Environment control and life support systems (ECLSS) and communications are provided by the Extravehicular Mobility Unit (EMU) spacesuit; in the event that the MAJIC system design is updated in the future to have tele-operated or autonomous operating modes, a communications subsystem among other additional subsystems will also be included. A notional design for the NASA JSC Advanced Jetpack is pictured in Figure 2-1 to the right of a diagram of the NASA SAFER unit currently in operation.

Usually spacecraft are designed around their payloads, and MAJIC is no different. A successful design would facilitate a variety of EVA tasks including ISS solar array and Orbital Replacement Unit (ORU) equipment inspection and replacement, asteroid exploration and sampling, and in the event of an emergency, crew member rescue operations. The Jetpack must be capable of stabilizing an astronaut user throughout an EVA to enable direct translation and precision tasks involved with instrument installation or asteroid sampling despite disturbances arising from tool use, astronaut

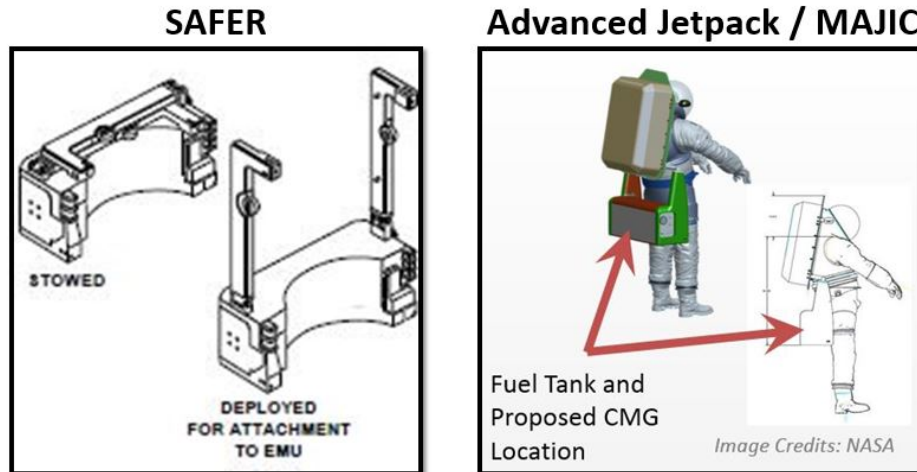


Figure 2-1: NASA’s SAFER and the Advanced Jetpack / MAJIC Concept. *Left: Diagram for the Simplified Aid for EVA Rescue emergency-only astronaut mobility unit currently in use at the ISS for astronaut EVAs. Right: The NASA JSC Advanced Jetpack concept; arrows indicate the location of fuel tanks; for the MAJIC system, half of the fuel tanks would be replaced by the CMG subsystem with minimal impact to Jetpack size and weight.*

motions, or mass-offsets in the case of large object manipulation in low gravity.

Section 2.1 describes the combined control concept and several missions conceived for a low gravity astronaut EVA Jetpack. The Draper-MIT simulation utilized to design and evaluate MAJIC as a Jetpack is then described in Section 2.2 and serves as a bridge between descriptions for concept and design of MAJIC. Section 2.3 details the design efforts conducted as part of this thesis to determine the size, weight and power (SWaP) values most appropriate¹ for CMGs in a MAJIC system. Finally, Section 2.4 describes the utility of MAJIC as a low gravity astronaut EVA Jetpack as compared with the utility that might be afforded by a thruster-only Jetpack.

2.1 MAJIC Concept

To better understand the design decisions endorsed by the Draper-MIT MAJIC program, the vision of the MAJIC system’s application as well as other Jetpack

¹Most appropriate here refers to the smallest SWaP that still satisfies the control needs of a Jetpack to meet NASA’s objectives for human space exploration.

and CMG array precedents are introduced in this chapter. First, design features of NASA's SAFER unit and NASA JSC's Advanced Jetpack that apply to MAJIC are introduced in Section 2.1.1. Next, CMG array control configurations are presented in Section 2.1.2 that are considered to be most practical for the MAJIC system. Finally, mission concepts for a low gravity astronaut EVA Jetpack are introduced in Section 2.1.3.

2.1.1 MAJIC's Concept Origins: NASA's SAFER and Advanced Jetpack

The MAJIC program was initiated at Draper and MIT in 2012 as a means to explore the impact on the performance and utility of NASA JSC's Advanced Jetpack when CMGs are integrated as attitude control actuators. As such, the design of the MAJIC system essentially reduces to the integration of CMGs into the design proposed for the JSC Jetpack. The NASA JSC Advanced Jetpack, in turn, is an adaptation of the emergency-use-only SAFER. Figure 2-1 depicts a diagram of the SAFER unit next to the notional design for NASA's Advanced Jetpack; the MAJIC system is assumed to be the Advanced Jetpack with integrated CMGs.

The SAFER unit is worn in conjunction with an astronaut's Extravehicular Mobility Unit (EMU) spacesuit and features an Automatic Attitude Hold (AAH) mode and a Hand Controller Mode (HCM). The AAH is activated with a pushbutton to activate an automated process by which an unwanted spin with respect to the LVLH coordinate frame of the ISS is halted. The HCM mode must then be used by an astronaut pilot to navigate back to the airlock and safety. The SAFER unit has a total of 24 thrusters, four thrusters pointing in each of the $\pm x$, $\pm y$, and $\pm z$ axes of the SAFER body coordinate frame. Each thruster is capable of providing 0.8+/- 0.08 lbf of thrust for a maximum SAFER ΔV of 10 ft/s and a minimum specific impulse of 70 s corresponding to the use of gaseous nitrogen as a propellant. The SAFER's inertial measurement unit (a Litton LN-200 Inertial Measurement Unit) is equipped with gyroscopes that are capable of sensing +/- 1000 deg/s. Control logic hosted

on the SAFER's avionics calculate thruster on-times based on sensor input and user input. A replaceable 36 V DC primary lithium manganese dioxide (LiMnO_2) battery pack powers SAFER avionics, with a shelf life of one year, and is capable of supporting one self-rescue mission scenario. SAFER does not provide environmental control and life support to the astronaut since the EMU satisfies this function.²

NASA's Advanced Jetpack will build off the SAFER's design but, like NASA's Manned Maneuvering Unit before SAFER, the Jetpack will be capable of continuous operation for translation, rotation and attitude hold throughout an EVA. For this reason, several changes need to be made to SAFER. Changes include (but are not limited to) the replacement of the primary LiMnO_2 battery with a rechargeable, most likely Lithium ion battery, additional thruster fuel mass and volume allowance, and improved avionics to take advantage of the improvement in electronics since the SAFER was built in the 1990s. New human interfaces for Jetpack control are being actively investigated, including the research conducted toward hands-free interfaces as described in [27]. Additional sensors or communication equipment may also be necessary if the Advanced Jetpack is to act as an autonomous or tele-operated spacecraft for redundant control or expanded EVA capabilities such as pilot-less inspection or equipment maintenance.

The addition of CMGs to the Advanced Jetpack would require a change to the Jetpack's electrical power source (EPS) as well as the addition of CMG-related avionics. If the overall mass and size of MAJIC is to remain close to that of the Jetpack, then the mass and volume budgets for other Jetpack subsystems must be reduced according to the size of a CMG subsystem included. More detailed information about SWaP considerations allocations for the MAJIC system are described along with CMG actuator sizing details in Section 2.3.1.

Another change that may be warranted for the MAJIC system that hasn't yet been mentioned is a change to the number, placement, and orientation of thrusters. This change would be effected to more efficiently make use of fuel in a combined control configuration; since translation is the primary objective for the thruster sub-

²Technical specifications for the SAFER included in this paragraph can be found in [14]

system of MAJIC, there may be a benefit to be gained from placing several thrusters closer to the expected center of mass of the system. By only using these thrusters during translation, the inevitable thrust vector error that arises from practical system operations would induce smaller disturbance torques that are to be rejected by a CMG attitude control system. For the purposes of this thesis, the thruster number, placement and orientation of the MAJIC system are unchanged from the SAFER unit.

2.1.2 Control Configurations for MAJIC

Just like any spacecraft's attitude control system, MAJIC's ACS must process sensor inputs as well as position and attitude commands in order to actuate thrusters and CMGs in an appropriate manner to achieve a desired state. Torques are generated in CMGs by array-specific steering laws, though even with the best steering laws available CMGs are still susceptible to singularities. This subsection describes the motivation for the CMG array selection for MAJIC and the various control options available for combined control with thrusters and CMGs.

CMG Actuator Array Selection

Several configurations of CMGs have been proposed and implemented in previous space systems [24, 25, 23]. Ideally, the CMG array should be capable of tolerating the failure of at least one unit (singly-redundant), but should also be implemented with as few CMGs as possible to reduce mass and power requirements. At the very least four CMGs are required for 3-DoF control with a single level of redundancy. Depending on the application, a CMG array should also provide a roughly uniform control authority to the CMGs as indicated by the shape of the angular momentum envelope of the array. One configuration that only requires four CMGs and that affords a roughly symmetric momentum envelope is the pyramid configuration seen in Figure 2-2.

The pyramid configuration consists of four CMGs that are oriented such that the

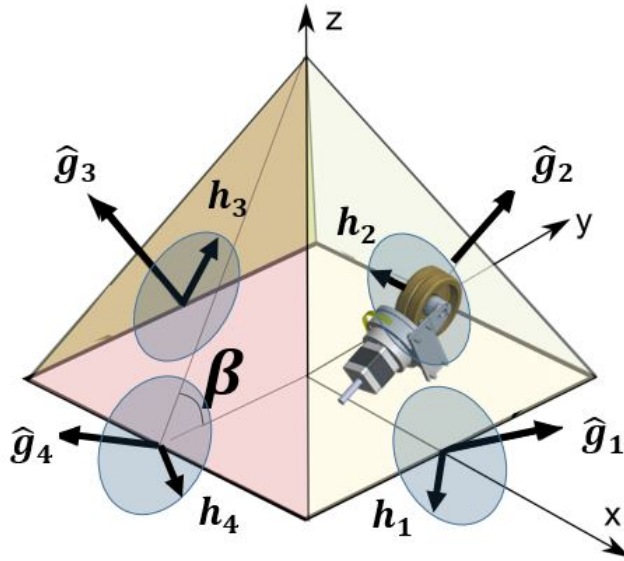


Figure 2-2: **A 4-CMG pyramid array configuration.** This array has a pyramid angle $\beta = 54.74^\circ$. The i^{th} CMG has angular momentum \mathbf{h}_i and a gimbal axis $\hat{\mathbf{g}}_i$. Shaded blue circles on each triangular face indicate available positions for angular momentum vectors \mathbf{h}_i . Image modified from [7].

angular momentum vector of each CMG is constrained to one of the triangular faces of a right pyramid. When the pyramid angle $\beta = 54.74^\circ$ the angular momentum envelope is nearly spherical: the space in the body-fixed frame B that the angular momentum of the array, H_{cmg} , spans is has maximum values in (x, y, z) equal to $(3.15 h_{rotor} \times 3.15 h_{rotor} \times 3.26 h_{rotor})$ respectively, where h_{rotor} is equal to the angular momentum stored in a single CMG flywheel rotor [7]. As in Equation 1.4 in Section 1.5.2, the array's momentum H_{cmg} is the sum of flywheel momenta and gimbal structure momenta. The maximum torque that can be provided by this configuration, τ_{max} is equal to:

$$\tau_{max} = 4 \cdot \tau_{rotor} \cdot \sin(\beta) \quad (2.1)$$

In Equation 2.1, τ_{rotor} is defined by Equation 1.3 and β is once again the pyramid angle of the array. For the pyramid configuration with $\beta = 54.74^\circ$, the maximum torque is equal to $\tau_{max} = 3.27\tau_{rotor}$. The pyramid configuration offers the least massive, lowest-power, and most uniform control authority option of known CMG ar-

rays, but avoiding internal singularities can be complicated. Perhaps for this reason, published research efforts for CMG control in the past couple decades have focused almost exclusively on this type of configuration geometry. A reason for this academic focus may be the geometric complexity of internal singular surfaces and the correspondingly complex steering algorithms that might be capable of optimally traversing momentum space in real-time.

MAJIC is a primary example of a spacecraft system that could benefit from a redundant CMG system that is minimally massive and minimally power-hungry while providing a large and spherically symmetric momentum envelope. With this in mind, the pyramid configuration has been selected as MAJIC's CMG array configuration for the purposes of this study. More information about the steering logic implemented to simulate MAJIC's pyramid array of CMGs can be found below, in Section 2.2.6.

Combined Control Options

The attitude control loop of the MAJIC system is depicted in Figure 2-3. There are two practical types of combined thruster and CMG control options that are available. First, all $\Delta\omega$ commands can be sent to CMGs while all ΔV commands are sent to thrusters. Since CMGs may encounter internal singularities or may become saturated, thrusters are also needed to maintain an attitude hold while CMGs are gimbaled out of their singular state. In this implementation, thrusters provide control forces while CMGs provide control torques.

The second type of combined control can be described as limited hybridization of thruster and CMG ACS. In this implementation, small $\Delta\omega$ commands are sent to CMGs while larger commands are handled by both CMGs and thrusters or only thrusters. This hybrid approach would be useful in reducing the probability of CMG saturation but would still maintain the precise pointing and robust rejection of small disturbances with CMG actuation. This type of control could also be used in the event that a torque magnitude exceeding CMG array capacity is requested by the ACS during large disturbance events.

Hybrid control is an exciting area to be pursued in future work. The simulation

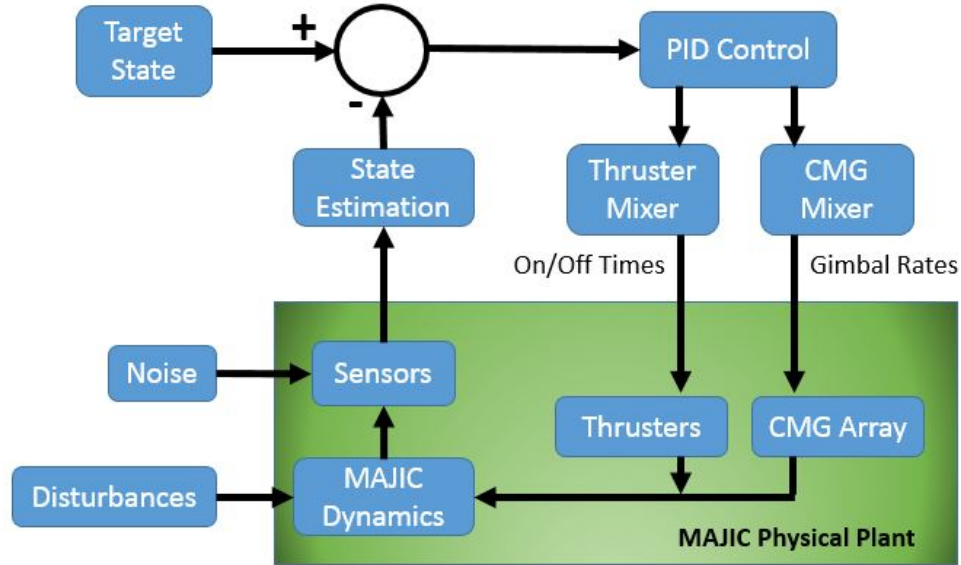


Figure 2-3: **Control Loop Diagram for MAJIC ACS.** *In the simplest implementation, all torques are controlled by CMGs and all forces are controlled by thrusters.*

implemented for the current design study utilizes the first type of combined control, i.e. all $\Delta\omega$ commands are sent to CMGs while all ΔV commands are sent to thrusters.

2.1.3 Mission Concepts

Three basic mission types pictured in Figure 2-4 are simulated for this research effort: solar array inspection at the International Space Station, sampling activities at a low gravity near-Earth asteroid, and emergency crew member rescue of an incapacitated crew member during an EVA. Together, the three missions span a spectrum of EVA operations that would be enabled by the MAJIC system and so provide a mechanism to evaluate the performance of different attitude control system designs given an uncertain future of mission objectives.

ISS Solar Array Mission Concept

The International Space Station’s solar arrays are exposed to the radiation and micrometeorite environment of low-Earth orbit and suffer degradation over time. Although monitoring of individual proxy solar cells on the array are used to indicate the overall health of the solar array, periodic EVAs are also conducted to allow astro-



Figure 2-4: **Three mission concepts for the CMG-augmented Jetpack.** *Left: A NASA photograph of an ISS solar array inspection EVA - with a Jetpack, inspection activities would not be limited by the reach of the ISS robotic arm. Middle: A sample recovery mission to near-Earth objects (NEOs) like asteroids and comets would benefit from Jetpack mobility and CMG stability. Right: In the event of an emergency during any low gravity EVA mission, a CMG-augmented Jetpack would enable reliable crew member rescue with stable pointing during transit with a large external mass.*

nauts to visually inspect the arrays. Currently, visual inspections are limited by the reach of the ISS robotic arm as seen in the photograph included in the left panel of figure 2-4. These EVAs can be improved with the use of a Jetpack that would enable complete solar array inspection and more freedom in motion for follow-up inspection of components with questionable integrity. The implementation of a mission profile corresponding to this concept can be found in Section 2.2.7.

Asteroid Sampling Mission Concept

Another mission scenario considered for the Jetpack application is near-Earth asteroid (NEA) and comet surveying and sampling. Asteroid 25143 Itokawa is a near-Earth asteroid that was the subject of a joint Japanese Aerospace Exploration Agency (JAXA)-NASA-Australia asteroid sampling mission launched in 2003 and which returned to Earth in 2010. Thanks to this mission, there are detailed topological and gravity maps of the asteroid from [28] that can be readily applied to the purposes of the MIT-Draper simulation as described further in Section 2.2.7.

A CMG-augmented Jetpack would provide astronauts conducting EVAs a mobile and stiff platform from which to observe and interact with the low gravity object.

But the use of CMGs for attitude control during sampling activities would provide an extra advantage over added stability. By using only CMGs to maintain attitude, there would be no thruster plumes to impinge on and potentially reduce the scientific value of asteroid specimens at the asteroid's surface during sampling operations. Simulations for asteroid surveying and asteroid sampling activities are described further in Section 2.2.7.

Crew Member Rescue

Finally, an emergency crew member rescue mission scenario is considered in the event that the MAJIC system is needed to transport a second astronaut to the location of an incapacitated crew member in order to bring the compromised astronaut back to safety. This scenario involves a large change in mass properties that must be handled by the control system of the rescuing astronaut's MAJIC apparatus. If the use of CMGs in this context could improve the pointing accuracy of the tandem pair and the efficiency of the transfer maneuver, this would be useful information for mission planners of future human exploration missions at the ISS and beyond. Further information about the simulation of this emergency scenario is included in Section 2.2.7.

2.2 Draper-MIT Simulation

Draper and MIT have built a MATLAB-Simulink model for MAJIC operations that includes guidance, navigation and control blocks as well as a module for 6-degree of freedom (6-DoF) human dynamics and re-configurable task planning. The environment is built for the assessment of the MAJIC attitude control system in proposed mission settings. At the highest level of abstraction, the simulation is a control loop featuring guidance, navigation and control (GNC) logic that processes desired Jet-pack states and actual states as measured by inertial sensors in order to command thrusters and CMGs to effect the desired state. In addition to commanding actuation to accomplish a given trajectory in simulation defined by a pre-determined task plan

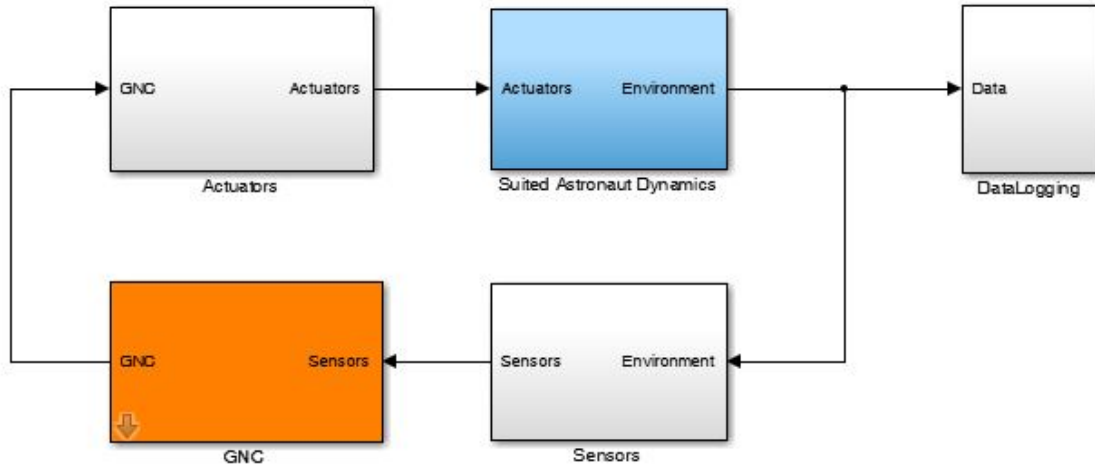


Figure 2-5: **The Draper-MIT Simulink Diagram.** *A top-level diagram depicting the principle modules of the MATLAB-Simulink simulation used to design and evaluate the utility of MAJIC.*

or by a human user, the control loop also accounts for disturbance torques induced by center of mass offsets, astronaut limb articulation or tool use, and astronaut interaction with external objects such as experimental payloads or crew members that need rescuing in the event of an emergency. Figure 2-5 shows the top-level block diagram of the simulation.

2.2.1 Thruster Model

Thrusters respond to translation demands of the system by firing in a manner to produce desired forces. Depending on the control mode settings, either thrusters or CMGs respond to attitude demands of the system with torque actuation. The primary consumable logged for thrusters is the total fuel consumed, while the primary consumable logged for CMGs is the energy consumed during gimbal rate maneuvers.

Thrusters are modeled after the NASA SAFER design [14] for the simple reason that NASA’s initial Jetpack studies were focused on upgrading the emergency-only SAFER unit into a full-mission thruster Jetpack. There are 24 thrusters placed to match the location and orientation of the thrusters on the SAFER system. Each thruster has a nominal thrust of 0.8 lbf (3.6 N) and a nominal flow rate of 0.006 lb/s (0.003 kg/s). For the modeled Jetpack, just like the actual SAFER unit, four thrusters

are used for translation maneuvers in each axis and two thrusters are used for roll, pitch or yaw maneuvers. Jetpack thruster impulses are simulated with minimum on-times and step function profiles which approximate the on-off nature of fixed, solenoid-actuated thrusters. Thruster selection and pulse width modulation is performed to produce thruster on-time commands from velocity and angular rate commands (ΔV and $\Delta\omega$ commands, respectively).

The only significant difference between the simulated Jetpack thruster system design and SAFER thruster design is the fuel selection. The SAFER utilizes compressed nitrogen corresponding to a thruster specific impulse I_{sp} of 72 s, while the simulation model assumes the use of a TridyneTM gas mixture that can achieve an I_{sp} of 135 s. In the simulation, a value of 133.29 s is used for TridyneTM I_{sp} corresponding to NASA's preliminary design studies for Jetpack using this fuel. TridyneTM is a dilute mixture of hydrogen and oxygen in a helium or other inert gaseous base. Passage of this gas mixture over a catalyst bed induces a reaction between the hydrogen and oxygen that heats the propellant before it is expelled through thruster nozzles [29, 30].

Using TridyneTM in a warm gas implementation for Jetpack thrusters is attractive primarily for the large improvement to specific impulse over a cold gas nitrogen implementation. For a set of maneuvers with a prescribed ΔV , the ideal Tsiolkovsky rocket equation 2.2 is used to find an estimate for the necessary propellant mass fraction given a thruster's specific impulse.

$$\frac{m_{prop}}{m_{dry}} = e^{\frac{\Delta V}{I_{sp}g}} - 1 \quad (2.2)$$

In this form of the rocket equation, the propellant mass fraction is expressed as the total propellant mass m_{prop} consumed during the ΔV maneuver divided by the dry mass of the spacecraft m_{dry} . As usual, g in equation 2.2 is the gravitational constant 9.8 m/s². For a set of maneuvers in a low-gravity environment with negligible atmospheric drag or other external forces, the ideal rocket equation 2.2 is a close approximation to reality. For a set of maneuvers that collectively require a change of velocity of 5 m/s, a Jetpack using cold nitrogen gas ($I_{sp} = 72$ s) would require a mass

fraction of 0.71%, while the use of TridyneTM ($I_{sp} = 133.29$ s assumed for simulation) only requires a mass fraction of 0.38%. For a Jetpack and astronaut that collectively weigh 609 lbs (the value used for large astronauts in the simulation), this means that 4.3 lbs of nitrogen gas would be required for the collective 5 m/s velocity change as opposed to only 2.3 lbs of TridyneTM that would be required for the same maneuvers.

2.2.2 CMG Model

Control moment gyroscopes have been modeled [15] as uniform disks with a moment of inertia about the spin axis, $I_{rotor,zz}$ (written as I_{rotor} for simplicity) given by:

$$I_{rotor} = \frac{1}{2}mr^2 \quad (2.3)$$

Where radius r and height $r/2$ define the geometrical dimensions of the disk. The density and mass of the disk are described by ρ and m respectively. CMG angular momentum is calculated by using Equation 1.4, with the simplifying assumption that gimbal structure angular momentum is negligible and that CMG flywheel angular momentum and MAJIC system body angular momentum dominate.

Although power is consumed in an array of CMGs by avionics, flywheel and gimbal motors as well as flywheel and gimbal rate, current and temperature sensors, only gimbal motor power is modeled in the simulation. The power consumption of flywheel and gimbal sensors are assumed to be negligible with respect to the power consumed by the gimbal motor and are therefore neglected in simulation. The consumption of power by CMG avionics is highly dependent on specific implementation and so for the current simulation, avionics power consumption is neglected. The reason for neglecting flywheel motor power consumption in simulation is slightly more involved, but also involves the variability of flywheel motor power consumption as a function of specific implementation as opposed to attitude control demands.

The power consumption profile of the flywheel motor is largest during CMG spin-

up, which occurs before or at the beginning of EVA operations³ and remains relatively low and constant during nominal operations. The low, constant power consumption profile of the flywheel motor owes to the fact that maintaining a CMG unit’s flywheel rate only requires overcoming friction; torquing maneuvers apply torques in an axis orthogonal to the flywheel (and gimbal) motor and therefore do not require increased power consumption directly. The specific nature of flywheel motor consumption is therefore largely dependent on friction losses and the speed at which spin-up is programmed to occur, both of which depend entirely on specific physical implementation. Because flywheel motor use is so highly dependent on specific implementation and has little to do with control torque magnitudes, flywheel motor power consumption is neglected from the simulation.

Unlike flywheel motor actuation, gimbal motor actuation corresponds to CMG-induced torque maneuvers. By only modeling this source of power consumption, a minimum value for CMG peak power and energy use can be modeled and utilized as a limit for MAJIC design. Power is calculated according to gimbal rate activity described further below and energy is calculated as an integration over time of power use.

The power required of a gimbal motor for a single CMG during a maneuver is the dot product of gimbal torque τ_{gim} and gimbal rate $\dot{\phi}$ of the unit as measured in the MAJIC system’s body frame of reference B . Since gimbal torque and gimbal rate vectors are necessarily orthogonal for a single gimbal CMG, the gimbal motor power for the i^{th} CMG of a given array can be expressed as:

$$P_{gim,i} = |\tau_{gim,i}\dot{\phi}_i| \tag{2.4}$$

The absolute value is taken assuming there is not a regenerative motor, since in that case both positive and negative work contribute to the total power consumed at the gimbal motor [6]. The total CMG power from the array is then found by summing

³Mission planners may desire to spin-up CMGs while the astronaut pilot is still inside the airlock to more efficiently make use of EVA time

the power contributions from each gimbal motor:

$$P_{gim} = \sum_{i=1}^n |\tau_{gim,i} \dot{\phi}_i| \quad (2.5)$$

For the case of a four-CMG array, $n = 4$ and the i^{th} CMG has gimbal torque $\tau_{gim,i}$ and gimbal rate $\dot{\phi}_i$. This calculation of CMG power, equation 2.5, should be distinguished from the power of the body rotation rate of the full MAJIC system, equation 2.6⁴.

$$P_{base} = |\tau_{cmg} \cdot \omega_b| \quad (2.6)$$

In this body-rate power equation, τ_{cmg} is the collective torque of the CMG array and ω_b is the rotation rate of the Jetpack body with respect to the inertial LVLH frame. The main reason equation 2.6 is not preferable to use for power budget formulation is that it does not account for CMG power consumption directly, but the kinematic power of the MAJIC system as a rigid body. CMG arrays achieve a desired torque by adding individual, non-parallel CMG torques that often cancel each other out along given axes. Thus the work done by individual gimbal motors is obscured by looking only at system-level dynamics. Torques associated with astronaut motions or interactions with objects must be canceled by the CMG array to achieve a commanded attitude, and so a successful ACS implementation would result in limited body rotation. In this way, using equation 2.6 for an estimate of CMG power would result in an unrealistic, nearly zero power consumption. For these reasons, equation 2.5 is used instead.

2.2.3 6-DoF Suited Astronaut Dynamics Model

Previous human factors work at MIT and Draper developed a set of models corresponding to the dynamics of an astronaut's motions during an EVA mission. Three types of astronauts can be modeled: a 4 ft 10.5 in, 100 lb female astronaut (a small option), a 6 ft 0 in, 180 lb male astronaut (the JSC model astronaut and medium option) and finally a 6 ft 4 in, 210 lb male astronaut (a large option). In this model,

⁴This was the method adopted by the initial kinematics model of the MAJIC simulation [15]

arm and leg motions with and without tools are individually modeled as well as the use of a hammer and power tool, details of which are found in [2] and [16]. As mentioned in Section 1.3.2, these models have utilized human body parameters from the Generator of Body Data (GEBOD) program [17] and have been built with use of the astronaut dynamics model developed in [18].

In addition to having the capacity to implement any custom set of astronaut maneuvers, a switch-case was implemented by the author of this thesis that enables a simulation to model large mass property changes at specified simulation times. In practice, a change to the center of mass of the system and an enlargement of the mass moment of inertia matrix of the MAJIC system part-way through a mission represents the acquisition and transport of an external mass during an EVA such as an incapacitated crew-member or experimental payload.

2.2.4 Sensors and Data Logging

At the moment, sensor estimation based on a realistic system is not modeled. Instead, a perfect sensor suite is implemented in which forces and torques induced by the actuator suite as well as torques induced by astronaut motions and mass property changes are directly passed back to the GNC block. Before doing so, however, all forces and torques as well as all actuator commands, environmental data and other information of interest is logged in the Data Logging Block for future reference after the simulation ends. Important data for post-processing primarily concerns data relating to system design and performance: CMG size, mass, angular momentum and torque characteristics, control mode implementation, fuel and energy consumed, peak power required and root-mean squared attitude error measured to name several.

2.2.5 Guidance and Navigation

The GNC block of the Draper-MIT simulation is broken up into four modules: mission management, navigation, guidance and control. The mission management block contains the trajectory profiles as well as attitude and position control settings

for the Jetpack. It is in this block that the control mode and desired trajectory are set for each mission.

Next, the guidance module processes desired trajectory and control mode settings as well as current estimates for system state and time obtained from the navigation module to output a 3-axis ΔV vector. It should be noted here that the navigation module is a simple block that passes sensor information for position, velocity, attitude, angular rate, CMG actuator state, and thruster fuel mass as well as target position and target velocity information to the other modules including the guidance module. Finally, the control block processes information at 25 Hz from all three other modules of the GNC block (mission manager, guidance and navigation) and implements proportional-integral-derivative (PID) control to output commands to thrusters and CMGs. Physical models for thruster and CMG actuators convert thruster on-times and CMG gimbal rate commands into forces and torques induced on the system.

2.2.6 Control and CMG Steering with Desaturation

Steering laws for an arbitrary array of n CMGs are designed to solve for the gimbal rates $\dot{\phi}$ required to produce a given spacecraft torque. This calculation requires knowledge of the $3 \times n$ Jacobian matrix $\mathbf{J}(\phi)$. For the pyramid configuration with $n = 4$ CMGs and skew angle $\beta = 54.7$ degrees, the array Jacobian can be expressed as:

$$\mathbf{J}(\phi) = h_{rotor} \begin{bmatrix} -\cos \beta \cos \phi_1 & \sin \phi_2 & \cos \beta \cos \phi_3 & -\sin \phi_4 \\ -\sin \phi_1 & -\cos \beta \cos \phi_2 & \sin \phi_3 & \cos \beta \cos \phi_4 \\ \sin \beta \cos \phi_1 & \sin \beta \cos \phi_2 & \sin \beta \cos \phi_3 & \sin \beta \cos \phi_4 \end{bmatrix} \quad (2.7)$$

CMG steering for MAJIC's pyramid configuration is accomplished with a singularity-robust (SR) implementation modeled after Bedrossian [31]. The SR inverse \mathbf{J}^* with respect to the Jacobian for the pyramid configuration defined by Equation 2.7 can be expressed as:

$$\mathbf{J}^* = \mathbf{J}^T(\mathbf{J}\mathbf{J}^T + k\mathbf{I})^{-1} \quad (2.8)$$

where k is a weighting factor that is a function of the singularity measure: k has a large value near singularities, and a small or zero value far from singularities. The major drawback of the SR inverse method is that if the system enters a singularity and a torque is commanded in the singular direction, the SR inverse will lock the CMG array into the singular state. As long as the commanded torque is in a direction that differs from a singularity-pointing direction the SR inverse formulation will produce non-zero torques to aid in singularity escape.

While the SR steering law enables avoidance of internal singularities, the CMG array is still prone to external singularities, or saturation, in which the maximum angular momentum of the array in one direction is reached. If the CMG array reaches 90% saturation along any axis, the originally commanded torque is disregarded and instead gimbal rates ϕ are commanded to reduce the angular momentum vector of the system along that axis. Usually, a CMG torque $\boldsymbol{\tau}_{cmg}$ is controlled according to:

$$\boldsymbol{\tau}_{cmg} = -[\mathbf{I}^B u + (\boldsymbol{\omega}^{B/N} \times \mathbf{h}_{cmg}^B)] \quad (2.9)$$

$$u = K[(\mathbf{I}^B)^{-1} \cdot \mathbf{H}_{cmg}] \quad (2.10)$$

The superscripts in Equation 2.9 represent the fact that terms are expressed in fixed-body frame B coordinates. When the system is not in desaturation mode, u is the angular acceleration command from the PID attitude controller. When in desaturation mode, however, thrusters are given a command to hold attitude while the angular acceleration command to CMGs is modified such that the magnitude of the angular momentum vector \mathbf{H}_{cmg} is reduced in a manner described by Equation 2.10. The result is that CMG array is returned to a state of full control authority once again. At this point, thrusters are commanded to relinquish attitude control back to CMGs

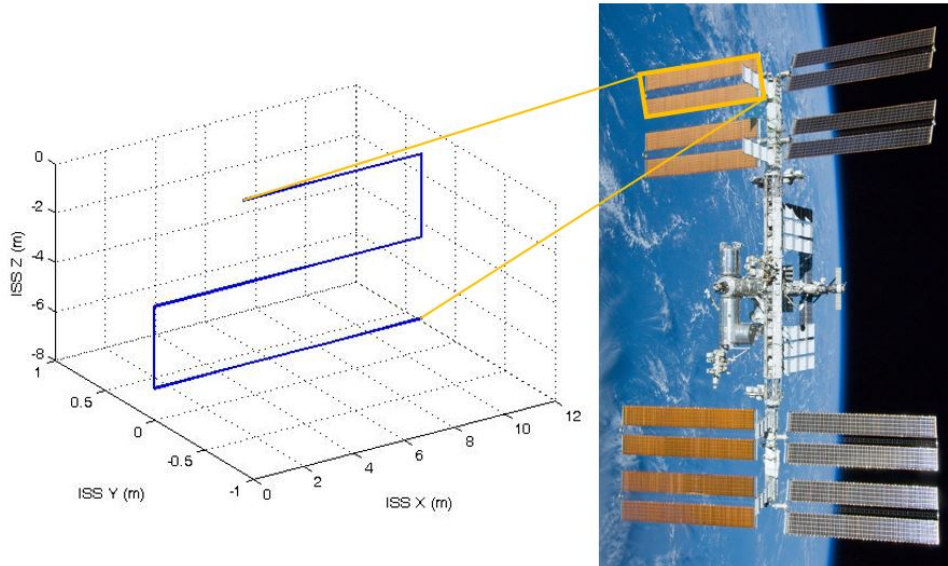


Figure 2-6: **Trajectory profile for the solar array inspection mission.** *The inspection of one pair of solar arrays at the International Space Station is simulated; the coordinates used in the plot are fixed in the ISS frame.*

2.2.7 EVA Mission Scenario Simulations

The following sections describe the specific implementation adopted in simulation for the mission concepts described in Section 2.1.3. For all missions simulated, a large astronaut (male, 210 lbs, 6 ft 4 in) with mass properties defined by the 6-DoF suited astronaut model introduced in Section 1.3.2 is used as the simulated MAJIC operator.

ISS Solar Array Inspection Mission

The trajectory of a hypothetical solar array mission that has been simulated is pictured in Figure 2-6. In this simulated EVA, one large double-panel array⁵ is inspected over the course of 50 min. The trajectory begins with a 50 degree slew followed by translations following the trajectory of Figure 2-6. The simulation ends before the astronaut returns to the airlock, since this study evaluates only a combination of mission actions that represent attitude control demands in an ISS solar array inspection EVA rather than a full 6+ mission.

⁵A single solar panel is assumed to measure 10.67 m × 3.35 m.

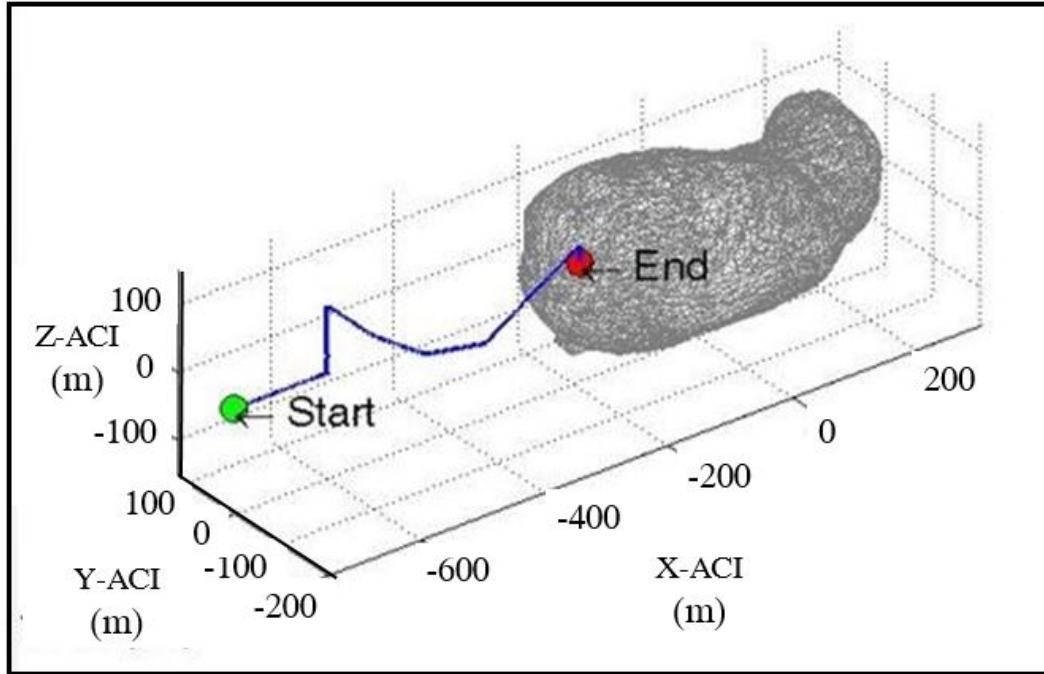


Figure 2-7: **Asteroid Sampling Mission I: Survey.** *Flight trajectory for the asteroid sampling mission I. Axes labeled in the ACI frame. An initial approach to the asteroid is followed by a plane change and continued approach for detailed surveying of the asteroid's surface.*

Asteroid Sampling Missions I and II: Survey and Sample Actions

The asteroid sampling mission considered in this study has been broken down into two segments (I and II) that can be simulated individually to serve as representative components of a full-length EVA at the surface of a near-Earth asteroid. The first segment is pictured in Figure 2-7 with an asteroid-centered inertial (ACI) coordinate frame. In this segment, the pilot astronaut approaches and surveys the asteroid from a distance before a final approach. This part of the mission does not include disturbance torques associated with human motions, but does involve translation and plane changes as well as slewing that puts stress on the attitude control system to maintain pointing. This mission segment is referred to as Asteroid Sampling Mission I.

The second segment of an asteroid sampling mission that has been simulated, Asteroid Sampling Mission II: Sample Actions, is a final approach and asteroid encounter followed by a series of human motions corresponding to an overhead reach, hammer

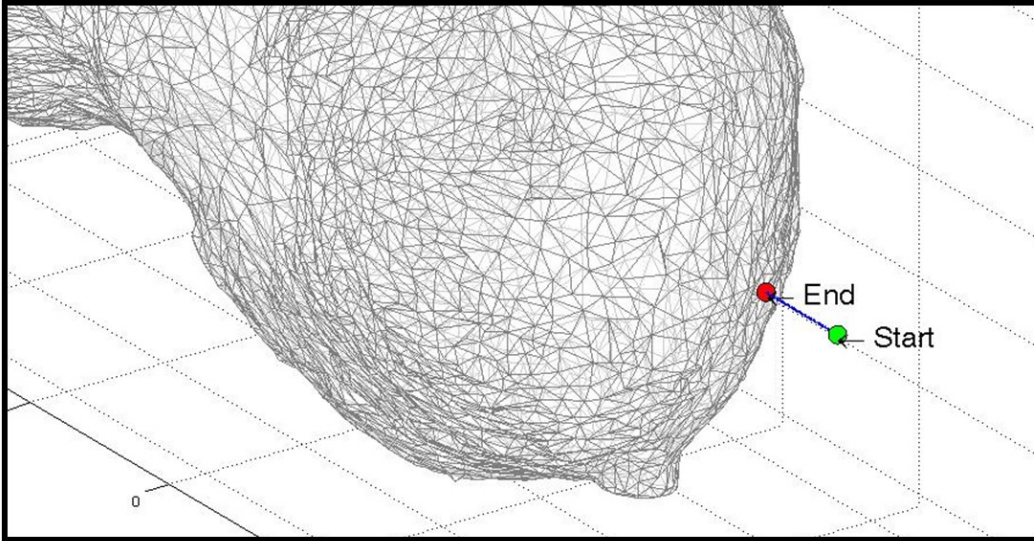
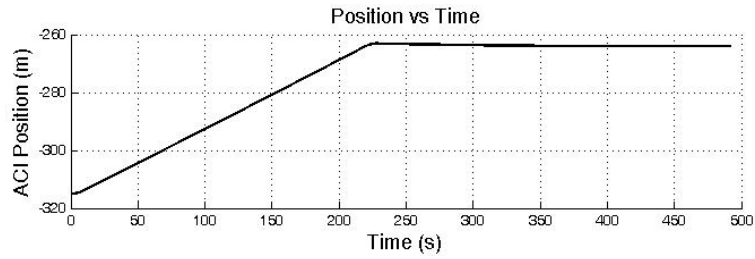


Figure 2-8: **Asteroid Sampling Mission II: Sampling Actions.** *Flight trajectory for the asteroid sampling mission II. A linear translation of 50 meters in the x-axis (ACI) lasting 220 seconds is followed by simulated sampling activities at the asteroid's surface for another 272 seconds. Sampling activities include an overhead reach, hammer blow, and reach to the hip in that order.*

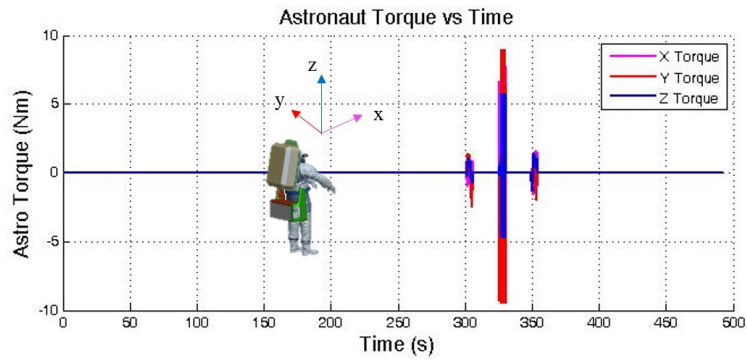
blow and reach to the hip; this sequence of motions represents an astronaut preparing for a sampling strike, making contact with the low gravity body and finally arresting and storing a loosened specimen from the asteroid surface. This mission segment is graphically represented in relation to the asteroid Itokawa in Figure 2-8. Translation in this mission segment is limited to the x-axis of the asteroid-centered inertial frame, depicted in Figure 2-15a. Astronaut torque profiles corresponding to sampling motions that are executed after arriving at the asteroid's surface are depicted in Figures 2-15b and 2-9c.

Crew Member Rescue

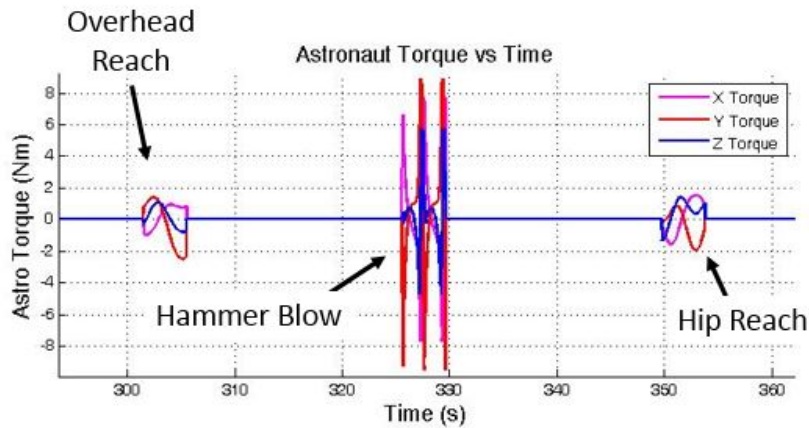
Finally, an emergency crew member rescue mission scenario has been simulated that begins at the ISS airlock, curves down around the rounded structure of the airlock and proceeds to a location of the incapacitated crew member near a different module of the ISS. Once reaching this location, the mass properties of the MAJIC system are changed to reflect the situation in which the astronaut operator of MAJIC grabs hold



(a)



(b)



(c)

Figure 2-9: Asteroid Mission II Linear Trajectory and Astronaut Torques. (a) Linear trajectory in the x -axis of the asteroid-centered inertial frame. (b) Astronaut torque magnitudes, with a reminder for the MAJIC-body coordinate frame referenced for torque magnitudes; the time scale here is the same as in (a), showing the entire length 492 seconds of the mission. (c) A zoomed perspective of the astronaut torque profiles, as well as labels indicating the individual overhead reach, hammer blow and hip reach actions.

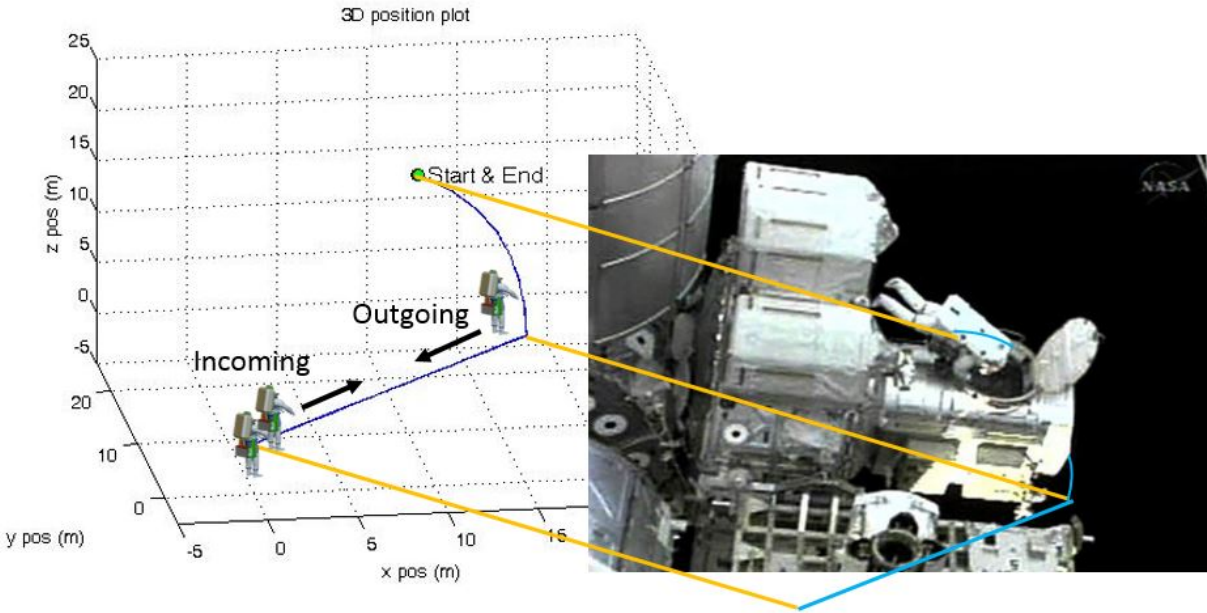


Figure 2-10: **Trajectory profile for the crew member rescue mission.** *An astronaut departs from the airlock to rescue a fellow crew member; a picture courtesy of NASA is used to visualize the hypothetical mission.*

of the incapacitated crew member for transport back to safety. The second half of the mission profile follows the initial pathway in reverse, bringing both astronauts back to the airlock after first a straight translation followed by a curved profile around the airlock. The trajectory profile for this mission is depicted in Figure 2-10.

In order to physically simulate the changes to the MAJIC system’s mass properties for the crew member rescue mission, the mass properties of the MAJIC system are altered to simulate a situation in which the incapacitated crew member is gripped, tethered and shouldered for transport by the rescuing astronaut.⁶ To physically represent this transport scenario, the center of mass (CM) is off-set by 50 centimeters in the MAJIC body frame’s x, y and z axes.

The incapacitated crew member is assumed to have the same mass properties of the rescuing astronaut. That is, the rescuing and incapacitated crew member are assumed to have a mass of 276 kg with moments of inertia (MoI) defined for each astronaut’s respective body frames as $I_{solo,0}$ and $I_{solo,1}$ given by Equations 2.11 and ???. The “0”

⁶This transport configuration is not optimal but is instead representative of an emergency situation in which the rescuing astronaut does not have time to assume the best orientation and simply tethers and shoulders the incapacitated crew member.

and “1” subscripts correspond to the rescuing and incapacitated crew member’s body frames, respectively. Likewise, $B-0$ represents the rescuing astronaut’s MAJIC body frame, while a superscript of $B-1$ represents the incapacitated astronaut’s MAJIC body frame.

The parallel axis theorem (shown in Equation 2.12) is employed to calculate the new moment of inertia matrix I_{pair}^{B-P} for the two-astronaut pair in a reference frame centered at the new combined system’s center of mass. Equation 2.11 shows the moment of inertia matrix for the rescuing astronaut, $I_{solo,0}^{B-0}$. The superscript $B-0$ indicates that the moment of inertia is referenced to the rescuing astronaut’s center of mass. The incapacitated crew member is assumed to have identical mass properties, that is, $I_{solo,0}^{B-0} = I_{solo,1}^{B-1}$.

$$I_{solo,0}^{B-0} = \begin{bmatrix} 44.7432 & 0 & 0 \\ 0 & 48.2387 & 0 \\ 0 & 0 & 17.2689 \end{bmatrix}^{B-0} \quad kg \cdot m^2 \quad (2.11)$$

$$I_{pair}^{B-P} = I_{solo,0}^{B-0} - m_0 \cdot r_0^x r_0^x + I_{solo,1}^{B-1} - m_1 \cdot r_1^x r_1^x \quad (2.12)$$

The new moment of inertia matrix I_{pair}^{B-P} is calculated in Equation 2.12. In this equation, m_0 and m_1 correspond to the mass of the rescuing and incapacitated crew member, respectively, which are both equal to 276 kg. The vector distance from the new system center of mass to the rescuing astronaut’s center of mass is represented by r_0 , with a skew-symmetric matrix cross product representation given by r_0^x . Corresponding values for the incapacitated crew member are shown with a subscript of “1”. More explicitly, for a vector distance separating the two astronauts’ centers of mass $r = [r_x, r_y, r_z]'$, the skew-symmetric matrix cross product r^x is given by:

$$r^x = \begin{bmatrix} 0 & -r_z & r_y \\ r_z & 0 & -r_x \\ -r_y & r_x & 0 \end{bmatrix} \quad (2.13)$$

Using $r_0 = [0.5, 0.5, 0.5]'$ and $r_1 = [-0.5, -0.5, -0.5]'$ and MoI values given by Equa-

tions 2.11 and ??, Equation 2.12 is solved to find the joint moment of inertia I_{pair}^{B-P} given by:

$$I_{pair}^{B-P} = \begin{bmatrix} 365.4864 & -138 & -138 \\ -138 & 372.4774 & -138 \\ -138 & -138 & 310.5378 \end{bmatrix}^{B-P} \quad kg \cdot m^2 \quad (2.14)$$

2.3 MAJIC Design: CMG Actuator Sizing

Design activities for MAJIC described in this thesis focus on CMG actuator sizing as well as CMG subsystem requirements considerations to effectively integrate the attitude control actuator suite to the Jetpack concept.

2.3.1 Maximum SWaP for a Practical MAJIC System

In order to determine the size, weight and power available for CMGs, the design of the larger MAJIC system must be taken into account. As mentioned in the introductory chapter, a previous sizing study conducted at Draper and MIT concluded that when constrained to have a mass equal to the mass of fuel expected to be saved in a single EVA, the CMG subsystem of MAJIC would have degraded performance with respect to a thruster-only reaction control system implementation. The latest sizing study instead begins with the limiting case of the largest SWaP CMG subsystem design that might be practically integrated into NASA’s Advanced Jetpack concept as of 2013 [27]. A reduction in CMG size, mass and power consumption from this maximum limit then follows to explore the capability of smaller CMG subsystem designs to maintain performance throughout various EVA tasks and mission profiles.

The dimensions of the NASA JSC Advanced Jetpack concept are indicated in Figure 2-11. The large, upper compartment pictured in the diagram is reserved for avionics, inertial measurement, remote sensing, and communication payloads. At the bottom of the diagram in Figure 2-11, there is a compartment that houses thruster fuel tanks. If fewer tanks were placed in this location and instead a CMG suite could

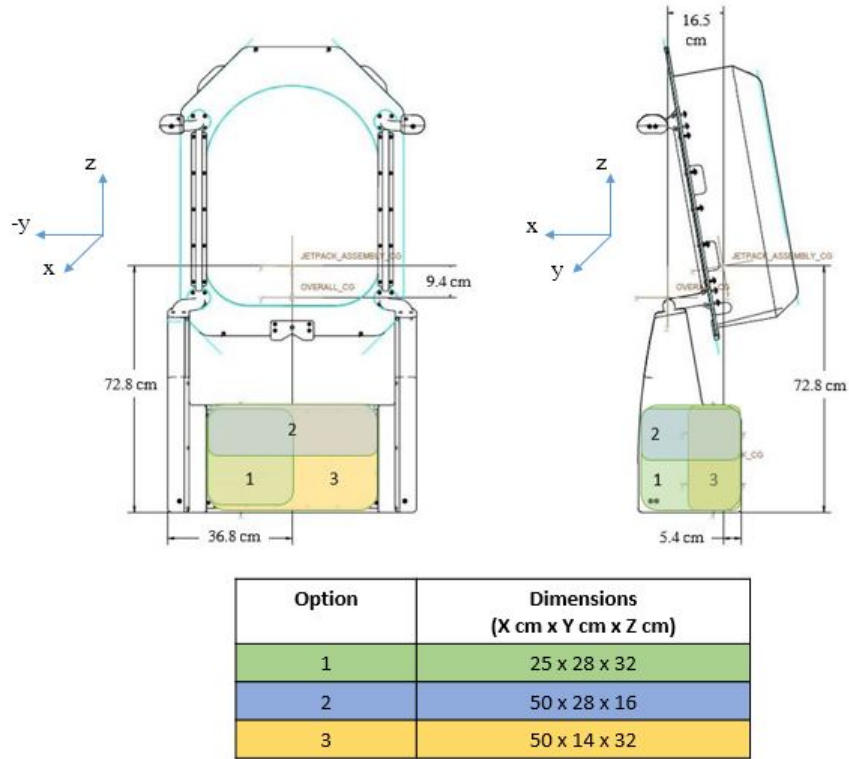


Figure 2-11: **Jetpack Concept Dimensions with CMG Location Options.** *Regions 1, 2, and 3 illustrate three options for CMG subsystem placement in a MAJIC system based on the JSC Jetpack design.*

be integrated, then few changes would be needed in the overall system design. Of course, the placement of all payloads and actuators would ultimately be decided based on overall mass properties and with the efficiency of operations in mind. For now, though, the assumption that CMGs are to be placed in the fuel compartment of the Jetpack is taken as a constraint for the size of CMG actuators. The three different colored regions in Figure 2-11 represent three different options for CMG subsystem placement that each occupy half the fuel tank compartment.

CMGs in a pyramid configuration do not necessarily need to be spatially separated as depicted in Figure 1-11; rather, all that matters is the relative orientation of CMGs with respect to one another and with respect to the MAJIC body frame. Ideally, CMGs should be placed such that during operations, the overall system's center of mass remains relatively close to the geometric center of the space spanned by thruster locations. CMGs do not need to be placed at the center of rotation of the Jetpack

system since they provide pure moments that do not depend on lever arms. CMG placement does affect the overall system mass moment of inertia and center of mass, though, which affect the MAJIC body rates in the LVLH frame resulting from CMG torque applied. Thrusters generate linear forces and so their placement relative the system's mass distribution is of critical importance to their efficient operation. If CMGs were placed in such a manner that the center of mass moved significantly, then thruster efficiency will invariably decrease.

The SWaP constraints for MAJIC can be defined with only the information considered in Figure 2-11 as well as a reasonable target for the mass of the CMG subsystem including the CMG units, the dedicated electronics, cabling, and dedicated structures for CMGs, and the battery mass necessary to support CMG use during operations. Table 2.1 indicates the SWaP allotted to the CMG subsystem for one implementation scenario.

Table 2.1: **CMG SWaP Constraints**

Volume Allowance	50 cm x 28 cm x 16 cm
Max CMG Rotor Radius	5 cm
Mass Allowance	20 kg
Max CMG Unit Mass	4 kg
Max Battery Mass	2 kg

The volume allowance corresponds to a selection of Option 2 in Figure 2-11. This selection allows for CMG hardware to be placed as close to the initial center of mass of the Advanced Jetpack design so as to limit the change in center of mass location that will arise from the addition of a CMG actuator suite. The total mass allowance of 20 kg has been chosen as an estimate; the motivation behind this figure is the following: the mass of the astronaut pilot and Jetpack system without CMGs has been assumed in simulation to be 276 kg. A reasonable restriction to the mass of the CMG actuator suite could be to limit the design target size to less than 10% of the total system mass before its addition. A round number of 20 kg is selected to make the addition of CMGs even more palatable.⁷

⁷Since SWaP values are assumed before simulations are conducted, limits are assumed that may

A Note on MAJIC Electrical Power

Although the total power that may be required from CMGs is uncertain before simulations to determine a reasonable torque value for CMGs, properties of the EPS system that are informative for a SWaP description can be introduced. The objective would be to determine a reasonable battery specific energy (Wh/kg or J/kg), that can be used later to determine battery mass required for MAJIC operations in a given mission context.

The change to the Jetpack's electrical power source to accommodate CMGs involves the addition of a CMG-dedicated EPS or a re-sized central EPS that can accommodate the CMG subsystem's power budget. In either case, MAJIC's batteries must have the capacity sufficient for continuous CMG actuation in addition to normal Jetpack modes of operation for the duration of an EVA (up to 8 hours), and a discharge current high enough to meet peak power demands for high-torque maneuvers with the CMG suite.

Human-rated rechargeable batteries with high specific energy (Wh/kg) and high energy density (Wh/m³) are most desirable. These batteries would need to be capable of providing constant power to avionics for CMG-dedicated processing and CMG sensors for flywheel rate, gimbal position, gimbal rate, as well as flywheel and gimbal motor temperature and current. There are many options for high specific energy (J/kg or Wh/kg), high energy density (J/L or Wh/L) batteries, though Li-ion chemistries outperform the rest in these metrics. For the purposes of this design study, several Li-ion batteries produced by Saft are considered, with specifications from [32] listed in Table 2.2.⁸ The reason these batteries are considered is that Saft has 50 years experience in space battery applications, and their catalog features a range of batteries.

One or more of a single type of battery can be used in series to increase the

later be shown to be impractical. Thus, the values listed in Table 2.1 should be understood as values set rigidly for this study, but that would be flexible in the larger MAJIC design program.

⁸It should be noted that the human-rating of these batteries has not been verified for EVA use; the consideration of these batteries is used as a baseline from which future, more in-depth studies can be carried out.

Table 2.2: **Soft VES Battery Models Applicable to MAJIC**

Battery Model	VES 16	VES 140	VES 180
Nominal Capacity (Ah)	4.5	39	50
Mean Voltage (V)	3.6	3.6	3.6
End of Charge Voltage (V)	4.1	4.1	4.1
Energy (Wh)	16	140	180
Specific Energy (Wh/kg)	155	126	165
Height (mm)	60	250	250
Diameter (mm)	33	53	53
Mass (kg)	0.155	1.13	1.11
Main Application	GEO, MEO	GEO, MEO	LEO, GEO

output voltage or in parallel in order to increase the output current available. For the purposes of this design, a central EPS is assumed that utilizes the largest, most energy-dense Soft battery listed, the VES 180. The specific energy of this battery is 165 Wh/kg, or 594 kJ/kg; because the output voltage and current can be selected by the circuit implemented, this design study only considers the specific energy value for SWaP considerations.

Combined Li-ion, Ultra-cap EPS

A serious drawback of using only Li-ion batteries is the limited discharge current afforded by this type of battery chemistry. While it is possible to connect many Li-ion batteries in parallel to achieve high discharge currents, this may require more batteries than are necessary for the application. One way to circumvent this problem is to have a combined system that utilizes Li-ion batteries for their high energy density and ultra-capacitors (Ultra-caps) such as those described in [33] for their high power density (large discharge capability). With this combined EPS concept, constant, low-power demands would be satisfied by Li-ion batteries (that would also charge up ultra-caps while those are not in use), while high-power, temporary demands from high CMG torques would be satisfied by a bank of ultra-caps.

2.3.2 CMG Actuator Sizing Method

Utility assessment of CMGs as attitude actuators for a low-gravity astronaut EVA Jetpack begins with a sizing study to find appropriate CMGs using simulations for MAJIC operations. But what is appropriate or necessary for the MAJIC system? Traditionally, optimality in attitude control systems refers to accomplishing a given control task with minimized system mass, volume, power, or some combination thereof. But tasks for an astronaut Jetpack are not well defined mainly because there are few well-defined missions or campaigns that will constitute the next generation of human space exploration. Because of this, analytically deriving CMG properties is not straightforward.

Other CMG sizing studies for small spacecraft [7, 8, 34, 35] begin with well-defined satellite mission operations concepts and associated design requirements for slew rates. These studies also usually assume static spacecraft mass properties throughout a mission, with an assumption of periodic and known disturbance torques arising from atmospheric drag, solar radiation pressure or gravity gradients. With these assumptions, standard optimization practices can be used to find an appropriate CMG design that minimizes mass, volume and power requirements while meeting the minimum torque requirements.

This general approach cannot be directly applied to MAJIC since torque requirements are not known *a priori*. In this case, control requirements are not dominated by slew rate profiles and desired pointing accuracy but instead by the nature of disturbance torques that must be rejected. A strategy to address this problem is to model representative types of disturbance torques that might be expected for a range of missions and then perform a statistical analysis of the performance of potential CMG designs for these representative missions. This can be done either with a series of isolated mission action simulations that could collectively make up a range of mission types, or with mission simulations that include a specific combination of the isolated mission actions to represent a specific EVA scenario.

The previous sizing study and human operator evaluation for MAJIC documented

in [3] sought to identify a CMG design that effectively paid for its weight over the course of a single EVA mission. The idea was that a low-mass CMG ACS might provide improved stability and control authority of the Jetpack without incurring a mass penalty at any point during operations. After finding a candidate CMG design with this constraint, though, operator evaluations using NASA's VR Lab at the Johnson Space Center revealed that such a small CMG did not have the capability to improve performance beyond the control authority of a thruster ACS [3]. The latest sizing effort seeks to relax the mass constraint for candidate CMG designs in order to identify a MAJIC system that exhibits the benefits of precision pointing CMG ACS in a manner that is physically realizable.

Sizing Method Summary

Sizing begins with the parametrization of CMG properties. Upper bounds for size and mass of the CMG units are derived by referencing SWaP values listed in Table 2.1. Bound selection for CMG properties pertaining to flywheel and gimbal capabilities then follows with practical considerations for implementation with commercial, off-the-shelf (COTS) components. A detailed description of this process is found in Section 2.3.3.

Next, a Jetpack equipped with CMGs that have the maximum allowable angular momentum and torque are tested with EVA mission profiles described in 2.2.7. The most taxing of these missions on the attitude control system as defined by performance metrics described in Section 2.3.5 is then identified as the sizing mission to be used for Monte Carlo statistical analysis of CMG designs that meet the criteria identified in variable parameterization. The optimal design that minimizes a selected cost function can be identified.

In this way a smaller CMG SWaP can be identified that is appropriate for the sizing mission. The task of sizing CMGs in the current context is equivalent to finding what the minimum angular momentum and torque capacity for CMGs that might satisfy the control needs of a specific mission profile.

2.3.3 CMG Design Parameterization

Performance drivers for a CMG design are the angular momentum, h_{rotor} (Equation 1.2) and torque, τ_{rotor} (Equation 1.3) achievable with a single unit. For clarity, Equations 2.15 and 2.16 show these equations as they appear in Chapter 1. Maximum angular momentum determines the size of the momentum envelope within which three-axis rotation control is afforded by the CMG array; maximum torque determines the types of disturbance torques that can be rejected, but also determines the speed with which the CMG array state traverses the momentum envelope.

$$\mathbf{h}_{rotor} = I_{rotor} \cdot \boldsymbol{\omega}_{rotor}^{R/G} \quad (2.15)$$

$$\boldsymbol{\tau}_{rotor} = -\dot{\phi} \hat{\mathbf{g}} \times \mathbf{h}_{rotor} \quad (2.16)$$

Clearly, rotor geometry as reflected by I_{rotor} and flywheel spin rate vector $\boldsymbol{\omega}_{rotor}^{R/G}$ determine a CMG unit's angular momentum, and the maximum allowed gimbal rate $\dot{\phi}$ then dictates the torque capacity of the CMG unit. Rotor inertia may be parameterized as a function of rotor radius and rotor material density since the geometry, i.e. the volume of the CMG flywheel is a function of rotor radius according to the assumptions taken in Section 2.2.2. Materials and densities ρ considered for the rotor are aluminum ($\rho = 2700 \text{ kg m}^{-3}$), steel ($\rho = 7850 \text{ kg m}^{-3}$), brass ($\rho = 8520 \text{ kg m}^{-3}$) and tungsten ($\rho = 19600 \text{ kg m}^{-3}$).

The first task for CMG parameter bound definition is to find the maximum rotor radius that can be accommodated in MAJIC. Three options for placement of the CMG array and control electronics are pictured in Figure 2-11. In order to accommodate all three options to allow for maximum applicability of the CMG subsystem to future design iterations, an upper limit on the rotor radius of the CMG actuators is selected to be 5 cm. The SWaP requirement that CMG actuators remain under 4 kg (see table 2.1), combined with this upper bound for rotor radius and a selection of rotor material together determine the maximum allowable angular momentum for CMG unit designs. A lower rotor radius bound of 3 cm is selected to limit variability in statistical studies. Resulting inertia bounds for aluminum, steel, brass and tungsten

designs are listed in Table 2.3.

Table 2.3: **CMG Inertia Bounds for Sizing**

Material	Lower Bound for I_{rotor} (kg m²)	Upper Bound for I_{rotor} (kg m²)
Aluminum	5.15×10^{-5}	6.63×10^{-4}
Steel	1.50×10^{-4}	1.51×10^{-3}
Brass	1.63×10^{-4}	1.43×10^{-3}
Tungsten	3.74×10^{-4}	8.22×10^{-4}

From Table 2.3 it can be seen, at least for the rotor geometry and materials considered for this study, that steel allows for the largest mass moment of inertia. Even though both brass and tungsten are denser materials, the limit of 4 kg in CMG unit mass (assumed to be 3x the mass of the rotor mass) limits allowable inertias for these materials to a lower maximum than the inertia allowable for steel.

The next task is to identify the performance capability as determined by flywheel and maximum gimbal rates. Because the angular momentum that can be stored in a single actuator determines the size of the momentum envelope and hence the control space that is afforded to the array, a maximum angular momentum, h_{rotor} , is desired. After consulting with professional miniature CMG providers including Honeybee Robotics, the provider of CMGs for a Draper-MIT hardware demonstration described further in Chapter 3 and in [22], a maximum of 30 krpm is identified as the upper limit for standard flywheel motor technology.

In order to reduce the required SWaP for a CMG, the most straightforward means to do so is to reduce the size and weight of the flywheel and to increase the flywheel rate and maximum gimbal rates to achieve large angular momentum and torque capacities. Reducing the flywheel rate would do nothing to reduce SWaP requirements directly; rather, this would simply relax the requirements levied on the flywheel motor and electronics technology. For this reason, the sizing study in this thesis assumes the largest possible flywheel rate, here taken to be 30 krpm. Table 2.4.

The selection of gimbal rate bounds is more complicated. Since individual CMG torque is equal to the product of stored flywheel angular momentum and gimbal rate

Table 2.4: **Angular momentum bounds for SWaP-compatible MAJIC CMGs**
A flywheel rate of 30 krpm is assumed as well as inertia bounds listed in Table 2.3 to arrive at the bounds listed here.

Material	Lower Bound for h_{cmg} (N m s)	Upper Bound for h_{cmg} (N m s)
Aluminum	0.16	2.08
Steel	0.47	4.75
Brass	0.51	4.50
Tungsten	1.18	2.58

(see Equation 1.3), larger gimbal rates enable larger torques that might be delivered from a CMG array. But, since the power consumed by a CMG scales with gimbal rate squared (see Equation 2.4), a desire to limit the power requirements and associated system battery size and mass corresponds to a reduction in maximum allowable gimbal rate. In addition there is another reason to limit gimbal rates to lower values: a CMG array is more likely to encounter a singular state with increased gimbal rates, since the control space afforded inside the momentum envelope is traversed more quickly than with slower gimbal rates (see Figure 1-11), effectively causing saturation more often.

Instead of defining a maximum gimbal rate immediately, torque bounds corresponding to human factors research from [16] are selected to identify what magnitudes for gimbal rate are desirable. A minimum torque target for a CMG unit is thus set to be 2 Nm. Of course, higher torques would be preferable in order to handle larger disturbance torques and provide a higher level of stiffness for the platform, but at the cost of increased battery energy consumed and a higher probability of saturation with increased gimbal rates (really, with an increased torque-to-angular momentum ratio). At the same time, there are real-world limitations to the development of small gimbal motors to be integrated in the MAJIC system as defined up to this point. After consulting with professional miniature CMG providers once more, an upper bound of 40 rpm is selected for the maximum gimbal rate in an ideal implementation. From the lower torque limit of 2 Nm, corresponding maximum gimbal rates can be calculated for aluminum, steel, brass, and tungsten flywheels using Equation 1.3 and Table 2.3.

The results are listed in Table 2.5.

Table 2.5: **Gimbal Rate Bounds to Achieve 2 Nm Torques**

Material	Lower Bound for $\dot{\phi}_{max}$ (rpm)	Upper Bound for $\dot{\phi}_{max}$ (rpm)
Aluminum	9.17	118
Steel	4.02	40.6
Brass	4.24	37.4
Tungsten	7.39	16.3

Clearly, the minimum inertias defined from only volume and mass arguments require high gimbal rates in order to achieve the 2 Nm torque identified as the minimum target for MAJIC CMG units. In the case of aluminum and steel, use of the minimum inertia results in required gimbal rates in excess of 40 rpm, the assumed practical limit for gimbal motor technology in this application. For these cases, a further restriction of inertia values is necessary to address the bounds selected for torque and gimbal rates.

Maximum torques that result from the use of the largest inertias identified in Table 2.3, a flywheel rate of 30 krpm and a gimbal rate of 40 rpm are listed in Table 2.6.

Table 2.6: **Maximum torques achievable by SWaP-compatible CMGs**

Material	Upper Bound for τ_{cmg} (Nm)
Aluminum	8.72
Steel	19.9
Brass	18.8
Tungsten	10.8

These values for maximum torque are ideal, though based on the practical limitations on motor technology as represented by the requirements for flywheel rate to remain at 30 krpm and gimbal rate to be restricted to 40 rpm. In a physical implementation, these upper bounds may in fact prove to be in excess of what may be reasonably engineered. From simulation data generated from sizing studies contained

in [3, 4], CMGs with a ratio of torque-to-angular momentum tend to avoid saturation and achieve long-term pointing accuracy in excess of higher torque-to-angular momentum designs; these higher torque-to-angular momentum designs are able to provide high pointing accuracy but only over the course of several mission actions before reaching saturation.

In order to make the largest, ideal CMG most practical to begin with, considerations for the torque-to-angular momentum ratio as well as ultimate power demands of the system motivate reducing the maximum gimbal rate to one that provides for a torque of equivalent numerical magnitude to the maximum identified angular momentum. That is, a torque of 4.75 N m is recommended to be matched with an angular momentum of 4.75 N m s; this implies a maximum gimbal rate of 1 rad s⁻¹ or 9.5 rpm.⁹ Of course, control gains for CMG actuation may be tuned to accommodate for torque-to-angular momentum ratios that differ from this 1:1 ratio, but this implementation is taken as a starting point for these future studies.

Table 2.7 lists the full variable parameterization for CMGs corresponding to this MAJIC study. Instead of listing the inertia values and gimbal rate values from Tables 2.3 and 2.5, the conditions from which these values are derived are included, namely CMG rotor radius, mass, maximum gimbal rate achievable, and minimum torque desired from a single CMG unit.

Table 2.7: **CMG Parameter Bounds for Sizing**

Parameter	Lower Bound	Upper Bound	Rationale
Radius	3 cm	5 cm	Volume Allowance from Table 2.1
Mass	-	4 kg	Mass Allowance from Table 2.1
ω_{rotor}	30,000 rpm	30,000 rpm	Assumed Engineering Limit
$\dot{\phi}_{max}$	Table 2.5	9.5 rpm	Engineering and τ_{cmg} / h_{rotor}
τ_{cmg}	2 Nm	Table 2.6	Human Factors [16]

⁹It should be noted that this recommendation is meant as a starting point for future trade analysis and is not rigorously shown to be optimal

2.3.4 Largest CMG Specification

From the above investigation of CMG parameterization, a largest-case CMG design is identified that has a maximum angular momentum and torque capacity while still maintaining the volume, mass, and engineering limitations described above. Table 2.8 contains specifications for this CMG unit design.

Table 2.8: Specifications for the largest-SWaP MAJIC CMG design

Largest CMG for MAJIC	
Material	Steel
Mass	4 kg
Radius	4.76 cm
I_{rotor}	$1.51 \times 10^{-3} \text{ kg m}^2$
ω_{rotor}	30,000 rpm
$\dot{\phi}_{max}$	9.5 rpm
h_{rotor}	4.75 N m s
τ_{cmg}	4.75 N m

2.3.5 Reducing CMG Size with a Monte Carlo Method

Now that a largest-case CMG size has been identified (Table 2.8) as well as parameters for CMG properties that correspond to SWaP and engineering limitations (Table 2.7), a Monte Carlo method can be used to find smaller CMG designs that satisfy the control needs of a given simulated mission. Executing this type of analysis requires repeated simulations of the same mission trajectory with different CMG designs selected from the within the parameter bounds identified.

A normal distribution is assumed for CMG material density, ρ , corresponding inertias, I_{rotor} , and maximum gimbal rate $\dot{\phi}_{max}$ for the purposes of this study. It should be noted that the mass properties of the MAJIC system are not altered in simulation even though the performance of CMG units is altered corresponding to a given CMG design's flywheel inertia, flywheel rate, and maximum gimbal rate. Because the flywheel rate has been set to 30,000 rpm, this reduces the total number of driving parameters for CMG performance to just two: CMG inertia I_{rotor} , and

gimbal rate $\dot{\phi}_{max}$ ¹⁰ A successful Monte Carlo analysis will sufficiently span the possible combinations of these variables. The material density is important as an impactor of the mass and volume that is required for a particular moment of inertia, as well as for the bound definition of the moment of inertia for CMG flywheel designs. As important as spanning the design space is a method of determining relative performance.

For each trial conducted in the Monte Carlo analysis, seven metrics were used to assess relative performance of different CMG designs. They include root-mean squared (RMS) attitude error¹¹, total fuel consumed, peak power required, total energy consumed, total time spent desaturating CMGs that have reached a singularity state, CMG flywheel radius and CMG flywheel mass. Collectively, these seven metrics represent the constraints of the optimization problem as defined by the following system goals: small attitude error, short time spent in desaturation, low system mass, small volume, and low power requirements. The seven metrics that are used are shown in Table 2.9 along with relevant units. Attitude error values used in the RMS calculation correspond to the smallest angle between the MAJIC body frame’s forward-pointing, x-axis and the desired pointing vector.

Table 2.9: Monte Carlo Sizing Performance Metrics

Metric	Units	Identifier
RMS Attitude Error	degrees (deg)	m_1
Fuel Consumed	kilograms (kg)	m_2
Peak Power	Watts (W)	m_3
Energy Consumed	Joules (J)	m_4
Time Desaturating CMGs	seconds (s)	m_5
CMG Rotor Mass	kilograms (kg)	m_6
CMG Rotor Radius	centimeters (cm)	m_7

After all the trials for a particular Monte Carlo simulation have been conducted, a cost function is used to evaluate the overall performance of each trial with respect

¹⁰A change in flywheel material density with constant inertia would simply change the size and mass of the rotor; while these values are important for determining an optimal CMG design, the effect on the MAJIC system’s mass properties and hence the effect on control performance deriving from system mass changes are not included in simulation.

¹¹The root-mean square of a quantity q over a time T with i intervals is: $q = \sqrt{\frac{1}{T} \sum_{i=1}^T |q_i|^2}$

to the others. For each trial j , the i^{th} performance metric $m_{i,j}$ for M metrics and N trials is normalized according to:

$$m_{i,j} = \frac{m_{i,j}}{\max\{m_i\}} \quad \forall \quad i = 1, 2, \dots, M; \quad \forall \quad j = 1, 2, \dots, N \quad (2.17)$$

In Equation 2.18, $\max\{m_i\}$ is the maximum value obtained for metric m_i across all N trials and $m_{i,j}$ is the value of metric m_i for trial j . The performance score J for a particular trial is computed by scaling each metric with a weighting vector W and then summing the scaled metrics. The optimal design will achieve the minimum performance J score. The equation for this process is written as:

$$J = \sum_{i=1}^M W_i m_i \quad (2.18)$$

For equal weighting of $M = 7$ metrics, $W = [1 \ 1 \ 1 \ 1 \ 1 \ 1 \ 1]$. Another weighting function may be employed should a designer wish to place more importance on one metric over another. For example, an optimization strategy that prioritizes attitude stability and CMG rotor mass over the other metrics might have a weighting vector $W = [3 \ 1 \ 1 \ 1 \ 1 \ 3 \ 1]$; for the resulting cost function, attitude stability and CMG rotor mass are three times more influential in the overall performance score than the other metrics. Still other weighting vectors corresponding to a different selection of performance metrics altogether are also possible and should be selected based on the overall objective of the optimization.

2.3.6 Sizing Mission Selection and Sizing Results

The Monte Carlo method described in Section 2.3.5 can be applied equally well to any simulated mission, though the optimal CMG for a specific simulation may not transfer equally well to other scenarios. For this reason, a mission that stresses the attitude control system more than any other mission is desired as a mission to serve as subject for the Monte Carlo analysis. A thruster-only Jetpack design with a thruster deadband of 2 degrees (full-width, corresponding to ± 1 degree error) and

that does not include CMGs is applied to the simulations described in Section 2.2.7 for this purpose. The total RMS attitude error for each mission is then calculated for comparison. Table 2.10 lists these attitude errors as well as the ΔV required for each mission to give an indication of the translation control effort required as well.

Table 2.10: **Simulated mission details** *Mission time, ΔV , RMS attitude errors for a thruster-only (2 degree deadband) Jetpack are listed for each simulated mission*

Sizing Mission	Mission Duration	ΔV	RMS Attitude Error
ISS Solar Array Inspection Inspection	50 min	3.57 m s^{-1}	4.19 deg
Asteroid Sampling I: Survey	50 min	6.25 m s^{-1}	13.92 deg
Asteroid Sampling II: Sample Action	8.2 min	0.80 m s^{-1}	1.11 deg
Crew Member Rescue	20 min	8.30 m s^{-1}	28.00 deg

It may be surprising that the Asteroid Sampling II: Sample Action mission has the lowest RMS attitude error performance; this may be explained by the fact that this mission entails a single translation along a straight-line path as well as sampling actions that are spaced-out in time from one another to allow the attitude control system time to return the system to a desired pointing vector before another action is simulated. In contrast, the other missions entail non-linear translations: the ISS Solar Array Inspection mission entails a 50 degree slew followed by translation in a planar geometry; the second asteroid sampling mission simulation including human actions involves a simple point-to-point translation; and the Crew Member Rescue mission involves translation in a plane that includes both the airlock and the incapacitated crew member (this mission makes the further assumption that the incapacitated crew member remains immobile with respect to the ISS LVLH frame of reference).

The reason for the higher attitude error of the Asteroid Sampling I: Survey mission as opposed to the ISS Solar Array Inspection mission may trace to the fact that the sampling mission trajectory involves three-dimensional translation tasks and long-distance travel that require large thruster impulses as compared with all other

simulated missions. The Crew Member Rescue mission involves a large change in mass properties mid-way through the mission as well as a slews to accommodate translation in a plane; for these reasons, it is expected that this mission has the highest calculated RMS attitude error.

A Monte Carlo simulation for the Asteroid Sampling Mission I (documented in [4]), Asteroid Sampling Mission II, and Crew Member Rescue Missions have been conducted with the parameter bounds and performance metric definitions described above. Results for these simulations in addition to the initial sizing studies documented in [3] as well as the largest CMG as identified in Section 2.3.4 are included in Table 2.11, side-by-side for comparison.

The reason that the Asteroid Sampling Mission II was also included in this Monte Carlo study despite the low RMS attitude error logged by a thruster-only implementation is the fact that this is the only mission simulated to include human motions corresponding to a high-precision task at a low gravity object; the large range of disturbance torques induced on the MAJIC system from these human motions were handled adequately by the thruster-only reaction control system, but this owes to the thruster reaction control system's specifications and torque-producing capacity. By running a Monte Carlo simulation on this mission, the size of CMGs required to maintain similar control can be investigated.

A Monte Carlo simulation of the Asteroid Sampling Mission I provides a comparative basis for other sizing studies conducted with this mission, including most notably the efforts concentrated on finding a small CMG as documented in [3]. Finally, simulation of the Crew Member Rescue mission provides knowledge of the size of CMGs required to maintain control during mission ops that require manipulation of large masses in a low gravity environment with the MAJIC system.

2.3.7 Monte Carlo Sizing Discussion

The sizing results presented in Table 2.11 illuminate the fact that smaller CMG designs have been identified that accomplish attitude control for the MAJIC system in the mission contexts of Asteroid Sampling I (long distance, high ΔV , 3-DoF trans-

Table 2.11: **Specifications for MAJIC CMG designs**

	Design from Largest SWaP Table 2.8	Design from 2015 [4]; based on Asteroid Sampling Mission I	Design from 2015; based on Asteroid Sampling Mission II	Design from 2015; based on Crew Member Rescue	Design from 2014 [3]; based on Asteroid Sampling Mission I
Material	Steel	Brass	Brass	Brass	Brass
Mass (kg)	4	2.35	1.83	1.87	0.98
Radius (cm)	4.76	3.89	3.57	3.60	2.90
I_{rotor} (kg m ²)	1.51×10^{-3}	5.92×10^{-4}	3.88×10^{-4}	4.02×10^{-4}	1.37×10^{-4}
ω_{rotor} (rpm)	30,000	30,000	30,000	30,000	25,000
$\dot{\phi}_{max}$ (rpm)	12.4	8.0	9.5	8.3	49.0
h_{rotor} (N m s)	4.75	1.86	1.22	1.26	0.36
τ_{cmg} (N m)	4.75	1.55	1.58	1.10	1.85

lations), Asteroid Sampling II (linear translation and attitude hold during human motions for sampling), and Crew Member Rescue (planar translation with large ΔV and mass offset). Although these results are promising, it must be stressed that these sizing missions only represent a fraction of what might be demanded from the MAJIC control system throughout a full EVA mission.

Surprisingly, the CMGs sized for the Asteroid Sampling Mission I most closely approach the the largest SWaP design; from this it may be concluded that the demands of repeated, long-distance, high ΔV maneuvers constrained neither to a line nor to a plane exceed the control demands of the other missions simulated. It may have been expected that the crew member rescue mission would result in the largest CMG size, both because of the large mass offset and large ΔV requirements. This does not appear to be the case for the particular mission simulated; perhaps results would have been different for a longer mission that required plane changes as in the Asteroid Sampling I mission.

Results from the Asteroid Sampling Mission II, which included human motions and disturbance torque profiles corresponding to these motions, also do not feature a CMG size larger than that of the Asteroid Sampling Mission I. Although the Asteroid Sampling Mission II lasts just 492 seconds and features one simple linear translation

followed by three human astronaut actions, those actions induce large and varied (though short-duration) disturbance torques on the MAJIC system. The reason that a larger CMG is not selected in this Monte Carlo simulation is most likely that the extra stability afforded by larger CMG designs does not outweigh the benefits from reduced size, weight and power consumed by the CMGs as calculated by the method described in Section 2.3.5.

2.4 MAJIC Utility Analysis

Assessing the relative utility of attitude control system options for the MAJIC system requires a comparative analysis of performance and cost. Because thrusters are already necessary for translation, the best argument for CMGs to be included in the Jetpack is one that focuses on the performance gains of the CMGs over using thrusters alone, as well as any added benefits that might be expected from the increased fuel economy of a MAJIC system as opposed to a Jetpack without CMGs.

Following actuator sizing, a utility assessment considers relative performance and costs of the combined control CMG+Thruster MAJIC system and thruster-only Jetpack. **Measurement of performance is achieved with a comparison of pointing accuracy** as evidenced by RMS attitude error across simulated mission actions or mission scenarios. **Measurement of cost is conducted with a comparison of consumable use**, i.e. the mass of thruster fuel consumed and battery energy used for CMG actuation. For this reason, further mention of cost analysis will refer exclusively to the mass-cost of a system. A mass-to-orbit cost projection follows this evaluation of EVA mass-cost that aims to illuminate long-term trends in consumption profiles and to contextualize the costs associated with the operational lifetime of MAJIC.

For the performance and utility analyses contained in this section, a CMG design identified with the Monte Carlo method described in Section 2.3.5 is used for evaluation. The selected CMG corresponds to a study of the Asteroid Sampling I mission, with specifications re-printed in Table 2.12 for convenience.

Table 2.12: **Specifications for the MAJIC CMG design evaluated for utility**

CMG Evaluated for Utility	
Material	Brass
Mass	2.35 kg
Radius	3.89 cm
I_{rotor}	$5.92 \times 10^{-4} \text{ kg m}^2$
ω_{rotor}	30,000 rpm
$\dot{\phi}_{max}$	8.0 rpm
h_{rotor}	1.86 N m s
τ_{cmg}	1.55 N m

A thruster-only Jetpack control system is used to simulate the same mission profiles that are simulated with use of the MAJIC system with CMGs described by Table 2.12. In this way, the comparison of pointing accuracy and consumable use between a thruster-only system and a MAJIC system can illuminate the relative utility of one system as compared with the other. In order to best represent potential capabilities of the thruster-only Jetpack, two deadbands are simulated: 0.5 degrees full width (± 0.25 degree error) and 2.0 degrees full width (± 1.0 degree error). The selection of these deadbands is motivated by the MMU and SAFER systems: the MMU was equipped with an adjustable deadband between 0.5-2.0 degrees [11], and the SAFER system currently features a fixed deadband of 2.0 degrees [14].

First, Jetpack utility is evaluated for the ISS Solar Array Inspection Mission, Asteroid Sampling Missions I and II, and the Crew Member Rescue Mission. Following single mission performance analysis, individual, simple mission tasks including straight-line translation and attitude hold during disturbance torques induced by human actions are considered. For all evaluations, use of CMGs is indicated by a label “Combined CMG+Thr” indicating the fact that CMG use for attitude control is implemented as a complementary control system to thrusters, which are required for translation.

2.4.1 Mission Scenario Performance and Mass-Cost

Table 2.13 lists the RMS attitude error, fuel use, and CMG energy and power demands for the mission scenarios considered in this study.

Table 2.13: Mission Scenario Performance Results

ACS Type	RMS Att Err	Fuel Used	Energy Used	Peak Power	% Time Sat
ISS Solar Array Inspection					
Thrusters (0.5 deg)	3.98 deg	1719.4 g	-	-	-
Thrusters (2.0 deg)	4.19 deg	265.9 g	-	-	-
Combined CMG+Thr	4.03 deg	288.5 g	1.85 kJ	3.85 W	0.0 %
Asteroid Sampling I (Survey Trajectory)					
Thrusters (0.5 deg)	11.71 deg	444.1 g	-	-	-
Thrusters (2.0 deg)	13.92 deg	430.1 g	-	-	-
Combined CMG+Thr	0.025 deg	391.2 g	1.79 kJ	5.17 W	0.0 %
Asteroid Sampling II (Sampling Operations)					
Thrusters (0.5 deg)	1.43 deg	76.7 g	-	-	-
Thrusters (2.0 deg)	1.11 deg	59.3 g	-	-	-
Combined CMGs+Thr	0.48 deg	35.2 g	346.8 J	4.66 W	0.0 %
Crew Member Rescue					
Thrusters (0.5 deg)	29.90 deg	680.0 g	-	-	-
Thrusters (2.0 deg)	28.00 deg	682.8 g	-	-	-
Combined CMG+Thr	30.38 deg	852.7 g	745.6 J	5.2 W	4.5 %

From these results alone, it may appear that a combined CMG-thruster system is only recommended for Asteroid Sampling Missions I and II; it is only for these missions that significant pointing accuracy gains are achieved, and it is also only for these missions that thruster fuel consumption is markedly reduced. In reality, though,

the results included in Table 2.13 obscure the time-dependence of performance - while CMGs do not achieve better *averaged* pointing accuracies for the ISS Solar Array Inspection Mission and the Crew Member Rescue Mission, CMGs do achieve better pointing accuracy during critical moments of these missions. This statement can be supported by analyzing attitude error plots in more detail.

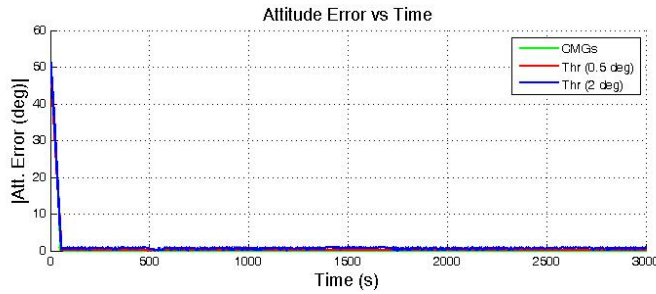
Before investigating the time-dependent attitude error profiles for each mission, conclusions can be drawn immediately from the use of consumables as evidenced by Table 2.13.

Performance Evaluation: ISS Solar Array Inspection Mission

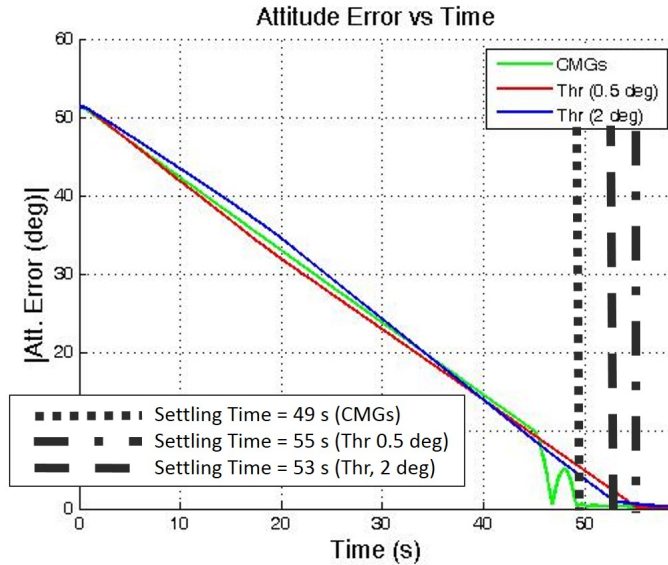
The ISS solar array inspection mission entails multiple sharp turns as can be seen in Figure 2-6. At mission start, there is a command for a 50% slew that corresponds to the large attitude error seen in Figure 2-12a. By the end of the mission, the newly-sized CMGs and the tight deadband thrusters achieve roughly equivalent pointing accuracy when averaged across the full mission time, though a zoomed image of the attitude error profile in Figure 2-12c reveals that for translation segments the CMGs significantly outperform thrusters in maintaining attitude control. Specifically, the green line in Figure 2-12b indicating absolute attitude error for CMGs does not exceed 0.1 degree following the initial slew maneuver. This is a large improvement over the absolute attitude error profiles for the tight and loose thruster deadband attitude control systems which hover around 0.25 degrees and 1.0 degrees, respectively, which correspond to half of the total allowable deadbands of 0.5 degrees and 2.0 degrees. Despite the overall RMS attitude results, CMGs clearly provide a higher level of stability and pointing precision for this mission as indicated by the zoomed image of attitude error in Figure 2-12b.

Mass-Cost Evaluation: ISS Solar Array Inspection Mission

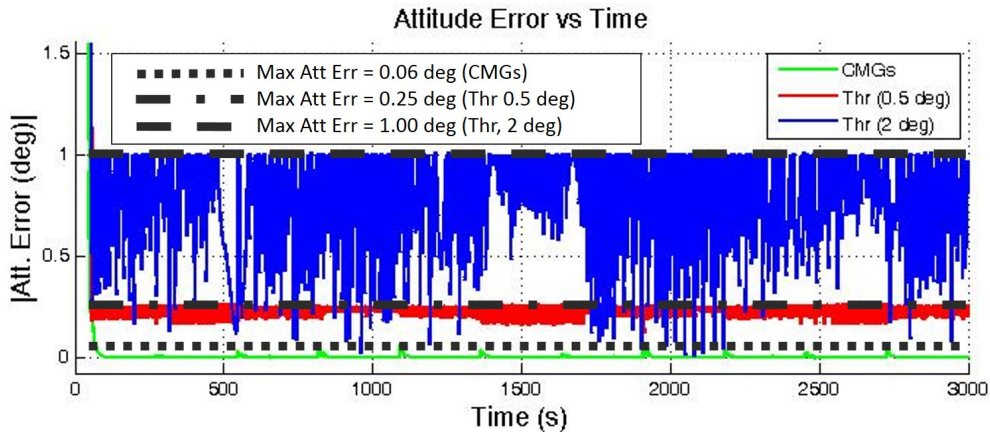
Thruster fuel mass required for the combined CMG+Thr attitude control system does not differ greatly from the loose deadband thruster control system as seen in Table 2.13, but both the combined system and the loose deadband thruster control



(a)



(b)



(c)

Figure 2-12: ISS Solar Array Inspection Mission Performance (a) Full attitude error profile for CMG+Thr combined control (green), the tight deadband thruster-only (red) and loose deadband thruster-only (blue); (b) Attitude error for a 50 degree slew maneuver at mission start. The slightly more negative slope of the tight deadband (red) profile results in an overall lower RMS attitude error for tight deadband thrusters, though CMGs ultimately reach the commanded attitude first; (c) A zoomed-in perspective of the attitude error profile over the whole mission, showing the CMG's superior performance for mission time 49s+.

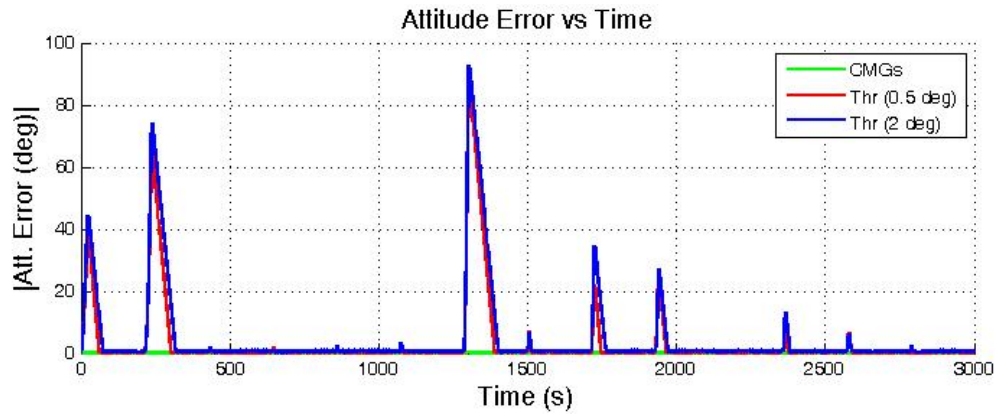
system depart considerably from the fuel consumption of the tight deadband thruster control system. Taken together, the simulation results indicate that a combined CMG and thruster system can provide the fuel economy of a loose deadband thruster-only system with pointing precision that exceeds a tight deadband thruster-only system for this proposed ISS solar array inspection EVA trajectory profile.

A total of 1.85 kJ of energy was required for use of CMGs in the 50 minute ISS Solar Array Mission. Assuming a central power source to be composed of Saft's VES 180 batteries (165 Wh/kg or 594 kJ/kg), the required battery mass is calculated to be just 3.1 grams. Even with a battery with lower specific energy, for instance 130 Wh/kg or 468 kJ/kg, the resulting battery mass for the Solar Array Inspection Mission is just 4.0 grams. Values for battery mass required for an hour of inspection activities can then be calculated to be 3.7 g/hr and 4.7 g/hr for a 165 Wh/kg and a 130 Wh/kg battery source, respectively.

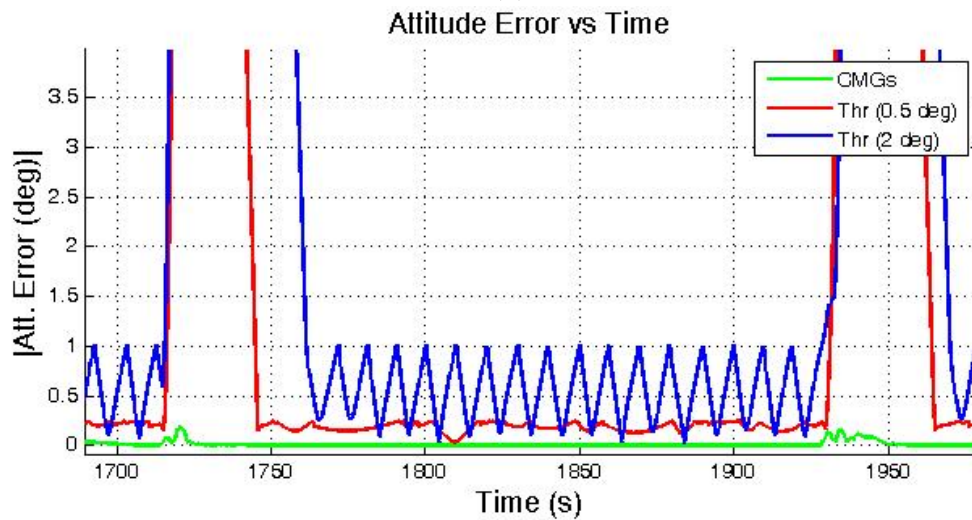
Performance Evaluation: Asteroid Sampling Mission I

Performance profiles for the first segment of the asteroid sampling mission, depicted in Figure 2-13 highlight the performance gains of a CMG+Thr control system indicated by the overall figures presented in Table 2.13. Once again, combined CMG+Thr results are plotted in green, tight deadband thruster-only control system results are plotted in red and loose deadband thruster-only control system results are plotted in blue.

As can be seen from Figure 2-13a, several locations in the mission trajectory overburden the thruster-only reaction control system. Instead of maintaining deadbands of 2.0 degrees and 0.5 degrees, the loose and tight deadband thrusters shown in blue and red, respectively, attitude errors in excess of 20 degrees occur a total of five times, with several smaller magnitude deviations from the desired deadband width. For visualization of comparable CMG performance during the same translation maneuvers, a zoomed perspective of the final two large (>20 degree attitude error) deviations at mission times 1725 seconds and 1950 seconds are shown in Figure 2-13b. In comparison to the thruster-only implementations, the CMGs are able to achieve attitude



(a)



(b)

Figure 2-13: **Asteroid Sampling Mission I Performance** (a) Attitude error profile for the newly-sized CMGs (green), the thruster-only 0.5 deadband ACS (full width, corresponding to ± 0.25 degrees) (red) and the thruster-only 2.0 deadband (full width, corresponding to ± 1.0 degrees) (blue); (b) A zoomed-in perspective of the attitude error profile, showing the CMG's superior performance for a majority of the mission; (c) Fuel consumption profile (color scheme same as in attitude error plots).

pointing throughout the mission. During large ΔV maneuvers that put stress on the attitude control system, attitude errors for MAJIC remain under 0.3 degrees.

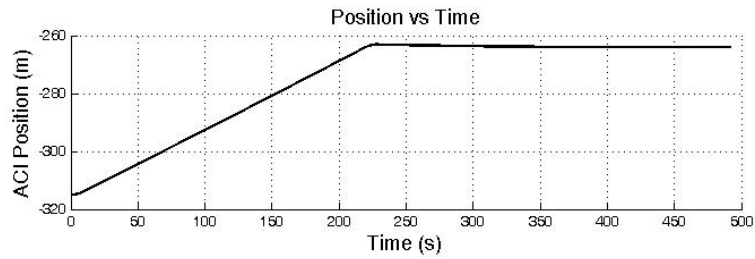
Mass-Cost Evaluation: Asteroid Sampling Mission I

In addition to improving the attitude control authority as evidenced by the RMS attitude error by multiple orders of magnitude over either thruster implementation, the use of CMGs for asteroid sampling also improved the thruster fuel economy (by 9% when compared with thrusters with a loose deadband and by 12% when compared with thrusters with a tight deadband). By referencing the total energy consumption of CMGs, the battery mass required to support the improved stability can be calculated. Assuming an EPS specific energy of 165 Wh/kg, a battery mass of 3.0 grams is required to support the 50 minute mission. For a more conservative estimate for specific energy of 130 Wh/kg for the MAJIC system EPS, a battery mass of 3.8 grams is required. For an hour of asteroid surveying activities, these values are projected to be 3.6 g/hr and 4.6 g/hr for a 165 Wh/kg and a 130 Wh/kg battery source, respectively.

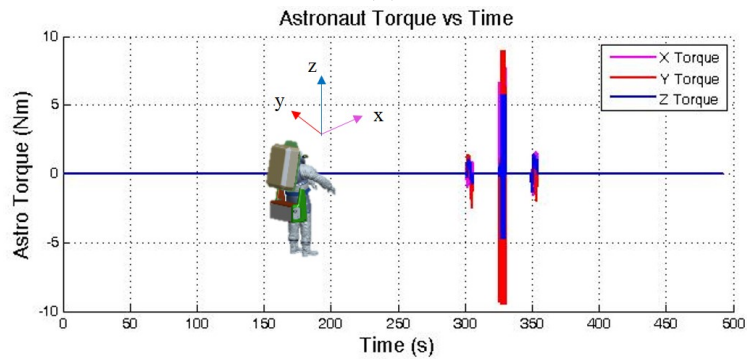
Performance Evaluation: Asteroid Sampling Mission II

Figure 2-14 depicts the attitude error profile of the three tested systems in the context of control system demands as evidenced by the translation profile and astronaut-induced torques arising from one set of sampling activities. Just as in the Asteroid Sampling Mission I: Survey mission, neither the tight nor the loose thruster deadband systems are capable of maintaining control during the acceleration and deceleration phases of translation as can be concluded by the large spikes in attitude errors at mission times 0 seconds and 220 seconds. Just as in Asteroid Mission I, the CMGs once again succeed in maintaining control before, during and after translation burns executed by thrusters.

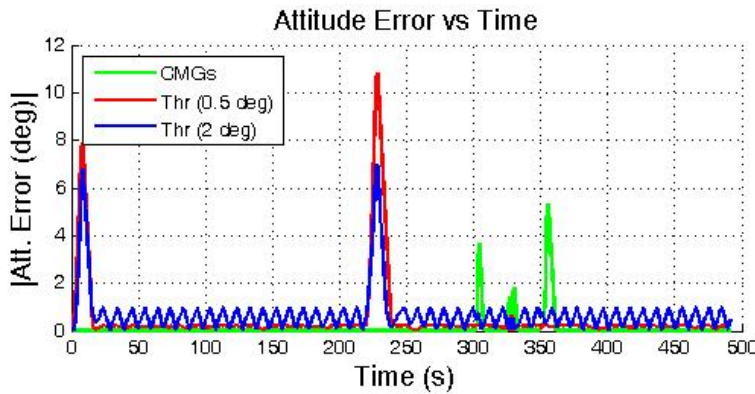
It is during the sampling activities that the CMGs do not maintain stiff control and instead allow for attitude errors up to 5 degrees. This is a result of the CMG subsystem's limited torque capacity: when disturbance torques such as these exceed



(a)



(b)



(c)

Figure 2-14: **Asteroid Sampling Mission II Performance** A translation of 85 meters is simulated beginning at mission time 0 s and ending at mission time 245 s; following this, a set of sampling maneuvers between mission time 300 s and 355 s is simulated as disturbance torques on the MAJIC system. (a) The translation profile in time for this mission segment; (b) The disturbance torque profile induced on the MAJIC system as a function of time; (c) Attitude error profile for the combined CMG-thruster MAJIC system (green), the thruster-only 0.5 deadband ACS (full width, corresponding to ± 0.25 degrees) (red) and the thruster-only 2.0 deadband (full width, corresponding to ± 1.0 degrees) (blue).

the torque capacity of the CMG array, the CMGs can only limit the accumulation of $\Delta\omega$ until disturbance torque magnitudes return to a value that can be controlled. This analysis reveals that larger CMGs may be necessary. In addition, modified Monte Carlo trials are warranted to analyze performance of specific maneuvers as opposed to averaged performance across an entire mission to provide a better estimate for CMG performance. An iterative process of evaluating expected torque magnitudes for EVA maneuvers and CMG sizing to account for these induced torques is recommended. A more detailed investigation of the capacity of CMGs to maintain control during human motions is included in Section 2.4.2.

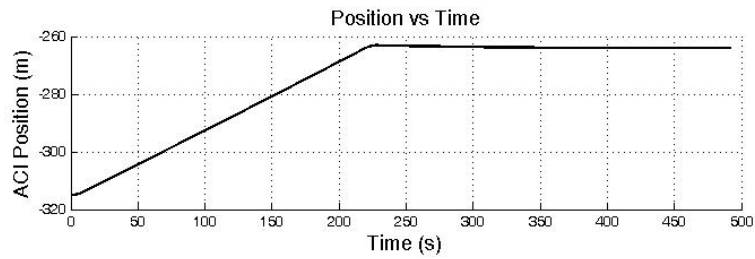
Mass-Cost Evaluation: Asteroid Sampling Mission II

Figure 2-15 depicts thruster fuel consumption profiles for the three systems evaluated. Both thruster-only systems require more fuel for the translation phase of the mission simulation, as well as the disturbance-rejection phase of the mission. As may be expected, CMGs do not require any thruster fuel to be consumed while rejecting astronaut-induced disturbance torques in the second half of the mission. In contrast, a characteristic step profile for thruster fuel consumption can be observed corresponding to this mission segment.

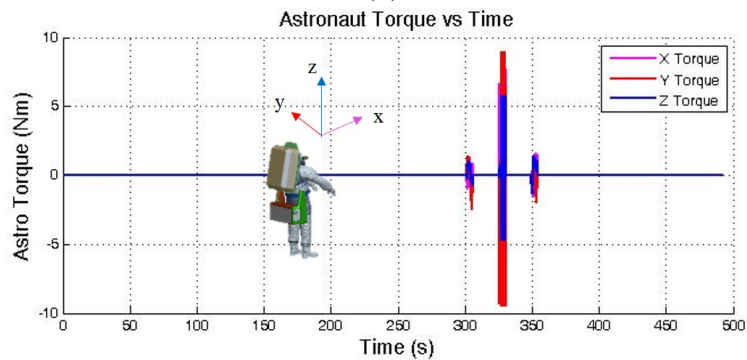
At the end of the Asteroid Sampling Mission II, a total of 346.8 Joules are consumed to support CMG operations. Assuming a battery specific energy of 165 Wh/kg, this consumption equates to a battery mass requirement of 0.58 grams; assuming a specific energy of 130 Wh/kg, this requirement increases to 0.74 grams. Projecting these figures to an hour of mission activities, these requirements become 4.3 g/hr and 5.4 g/hr.

Performance Evaluation: Crew Member Rescue Mission

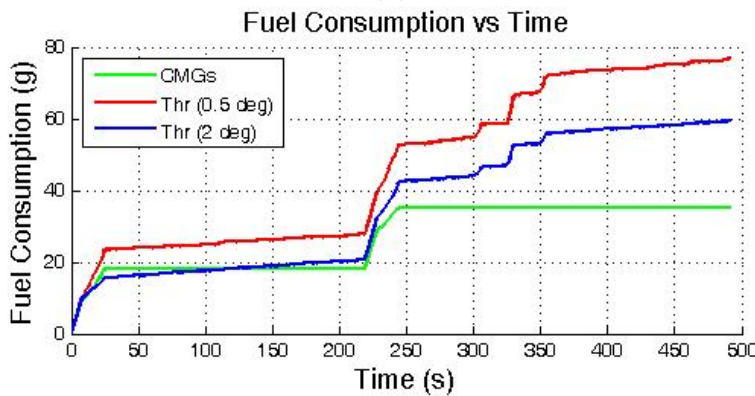
The Crew Member Rescue Mission poses the most significant challenge to the attitude control system of the MAJIC system. This mission simulation demands a high degree of control authority from systems that have been designed for less-demanding tasks and so identifies the consequences of using the MAJIC system for an



(a)



(b)



(c)

Figure 2-15: Asteroid Sampling Mission II Mass-Cost A translation of 85 meters is simulated beginning at mission time 0 s and ending at mission time 245 s; following this, a set of sampling maneuvers between mission time 300 s and 355 s is simulated as disturbance torques on the MAJIC system. (a) The translation profile in time for this mission segment; (b) The disturbance torque profile induced on the MAJIC system as a function of time; (c) Fuel consumption profile for the combined CMG-thruster MAJIC system (green), the thruster-only 0.5 deadband ACS (red) and the thruster-only 2.0 deadband (blue).

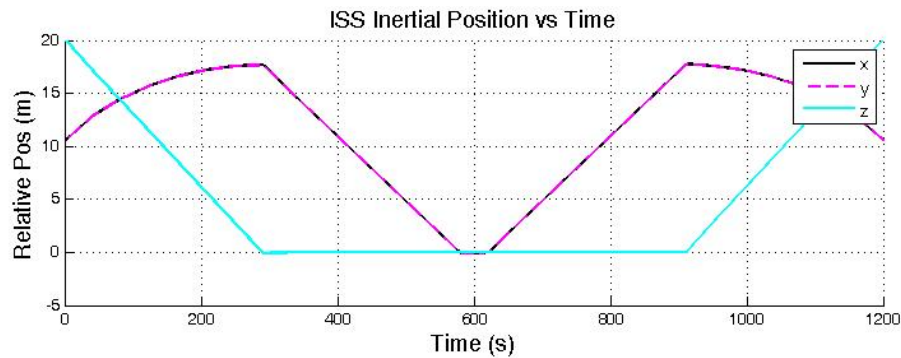
emergency task that asks more of the system than may otherwise be expected (recall, the optimal CMG selected from a Monte Carlo analysis of the Asteroid Sampling I: Survey mission is being used). The performance profiles for the combined CMG+Thr control system and thruster-only ACS implementations are shown in Figure 2-16.

The first plot (Figure 2-16a depicts the profile of the planar trajectory executed; ISS inertial coordinates are represented as centered on the incapacitated crew member's location. Jetpack mass properties are altered mid-way through the mission to reflect the tandem-astronaut configuration for the return journey to the airlock.

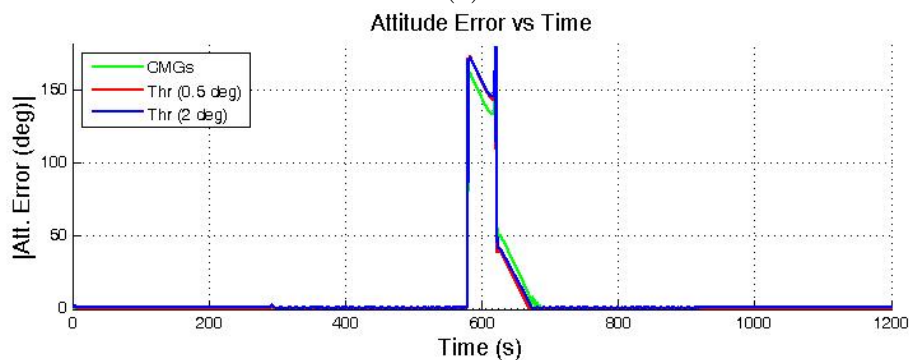
None of the system implementations can successfully maintain control when the rescuing astronaut initially reaches the incapacitated astronaut's position. This is as much an artifact of the mission simulation design as a reflection on the capabilities of each of the control systems tested; a more careful approach that maintains attitude control before grappling the incapacitated crew member may help prevent the nearly 180 degree spin undergone by the rescuing astronaut and incapacitated crew member pair upon initial grappling. A modified, slower return trajectory may limit the 360 degree spin that occurs during the first translational burn of the tandem pair, which also results in 22 seconds of saturation.

Despite these shortcomings in mission design, useful conclusions might be drawn from this simulation. Figure 2-16c depicts the latter half of the mission, when the astronaut tandem pair return to the ISS airlock. Because the center of mass of the system lies outside the active MAJIC system, linear translation without rotation requires an attitude control effort to counter induced torque on the system. During this segment of the mission, CMGs once again display their ability to maintain stiff attitude control throughout translation maneuvers. This stability is an important quality for an attitude control system to have during this type of rescue operation, since stability during the final approach and airlock encounter may mean precious seconds saved that could mean all the difference for an incapacitated crew member.

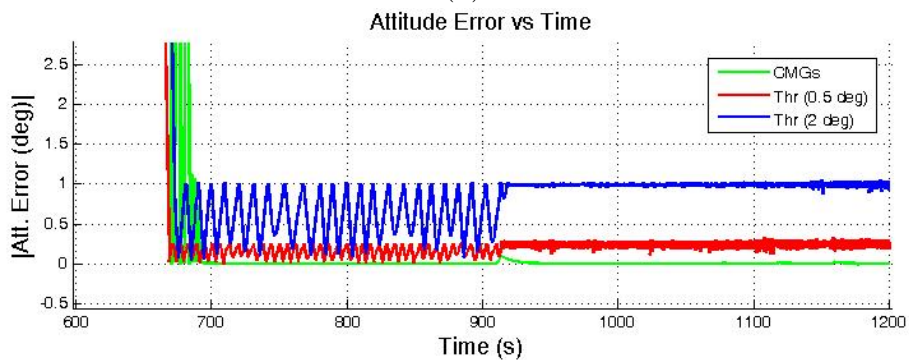
Given the fact that CMGs saturate in this simulation when the change in mass properties initially occurs, it may be advised to use thrusters for reaction control for the initial grappling of an incapacitated crew member and then switch to CMG



(a)



(b)



(c)

Figure 2-16: **Crew Member Rescue Mission Performance** (a) Trajectory profile; $(0,0,0)$ is taken to be the incapacitated crew member's location in the ISS inertial frame; (b) Attitude error profile for CMGs (green), the thruster-only 0.5 degree dead-band ACS (full width, corresponding to ± 0.25 degrees) (red) and the thruster-only 2.0 degree deadband (full width, corresponding to ± 1.0 degrees) (blue); (c) Attitude errors for the last 600 seconds of the mission, showing the CMG's superior performance for the critical mass-offset return phase of the mission.

attitude control for the delicate maneuvers necessary near the airlock to maximize the probability of a safe return to vehicle interior for both astronauts. If nothing else, simulations like this warrant further investigation of blending thruster and CMG control for the MAJIC system to avoid CMG saturation and maximize pointing precision and system stability.

Mass-Cost Evaluation: Crew Member Rescue Mission

The combined control system uses the most thruster fuel for the Crew Member Rescue Mission, while both the tight and loose deadband thruster-only systems use similar amounts of fuel. The reason for the increased fuel consumption for CMGs is desaturation; after desaturating CMGs, the fuel consumption rate for CMGs is reduced below the rates of either thruster implementation. but another is that increased fuel consumption also occurs later in the mission to accomplish the translation tasks required to return the tandem pair to the airlock. These trends can be seen in Figure 2-17. In the figure, the time period in which desaturation burns are executed is indicated by a pair of dotted vertical lines. Note the large rates of thruster-only fuel consumption (in blue and red lines) particularly at the end of the mission near the airlock as compared with the relatively lower rate of thruster fuel consumption for the combined CMG+Thr system (in green).

Over the course of this mission, CMGs use a total of 745.6 Joules of energy; once again using 165 Wh/kg and 130 Wh/kg as reference battery specific energies for the MAJIC system, battery masses of 1.3 grams and 1.6 grams are required for this 20 minute mission. Projecting these values to an hour, battery mass requirements per hour of rescue operational time may be predicted to be 3.9 g/hr and 4.8 g/hr for a 165 Wh/kg and a 130 Wh/kg energy source, respectively.

2.4.2 Simple Task Performance and Mass-Cost

In order to aid the assessment of relative utility for different attitude control implementations of a Jetpack, two types of discrete mission actions were simulated:

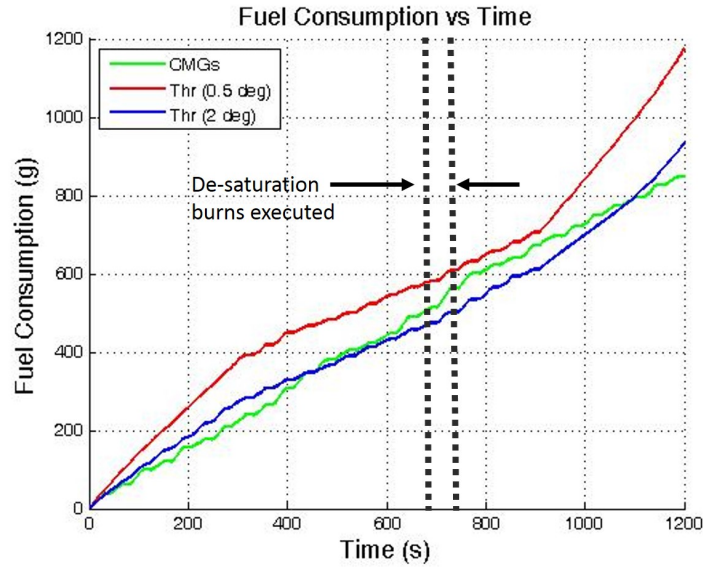


Figure 2-17: **Crew Member Rescue Mission Fuel Consumption.** *Fuel mass consumed over the course of the simulated crew member rescue mission is depicted for the tight deadband thrusters (red), loose deadband thrusters (blue) and the combined control Thr+CMGs (green). Note the smaller rate of fuel consumption for the combined control implementation for the majority of the mission as well as the increased fuel consumption for the same implementation during de-saturation procedures.*

first, a simple translation with and without a mass offset; and second, an attitude hold while disturbance torques are introduced from isolated human actions.

The first type of action is performed with a 10 meter translation for a mass offset corresponding to the change in mass properties developed for the crew member rescue mission. While this mass offset corresponds to the extreme case of transporting an incapacitated crew member, translation with a mass offset corresponds more generally to the situation that might occur should an astronaut need to transport a large or heavy object such as an experimental payload, a haul of samples or a heavy tool. The second type of mission action corresponds to the requirement of the Jetpack to provide a stiff work platform by rejecting astronaut-induced disturbance torques throughout an EVA mission.

In the subsections below the performance of the MAJIC system for each of these mission actions are compared both with graphical representations of attitude error and fuel consumption as well as tables that include the final results.

Translation Evaluation

The 10 meter translation task is simulated for thruster-only Jetpack systems with tight (0.5 degree) and loose (2.0 degree) deadbands as well as for the MAJIC system using combined-control with CMGs described by Table 2.12. Figure 2-18 shows the attitude error profile for the new CMGs and the thruster-only ACS implementations for both the solo and tandem (with crew member mass offset) translations. The plot at the top of the figure shows the distance traversed and indicates the two times at which thruster firings occur for to accomplish the 10 meter translation.

The graphical comparison of attitude error in Figure 2-18 shows that the thruster-only ACS implementations exhibit attitude errors of a few degrees at the beginning and end of translation as well as attitude errors corresponding to a 2.0 degree deadband or a 0.5 degree deadband. One reason the solo translation simulations result in larger attitude errors during the initial and final translation burns as compared with the tandem translation simulations is that the large mass offset of the tandem simulations results in immediate and sustained control effort to maintain attitude control; when there is no mass offset larger angular rates of the system are allowed to accumulate.

The MAJIC system using combined control with CMGs does not have perceptible attitude errors on this plot as seen by the flat green line at the bottom of the center plot. This of course corresponds to precise pointing during and after the translation maneuver, with or without a large mass offset. Because mass offset properties corresponding to the transport of an incapacitated crew member are used as opposed to less severe mass offset properties that might be realistic for the transport of an experimental payload, heavy tool, or haul of samples, the simulation results displayed in Figure 2-18 represent one of the more strenuous translation scenarios that are conceivable for EVA operations.

It should be noted that this mission profile is different from the crew member rescue mission in two ways: first, these translation simulations do not involve a change of mass properties mid-simulation as the crew member rescue simulation does; and

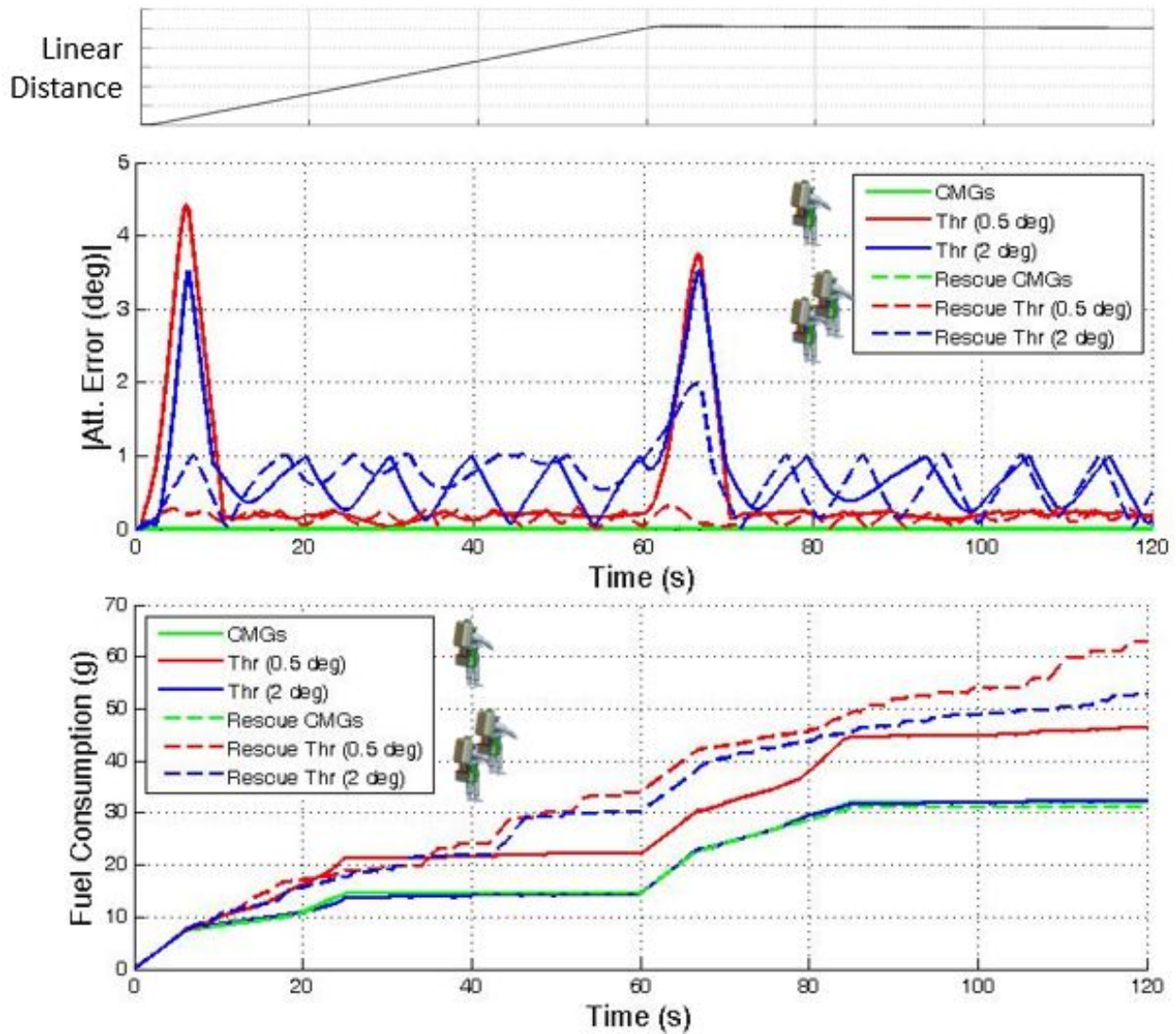


Figure 2-18: Attitude error and fuel consumption profiles for a 10 meter translation. Solid lines correspond to translation results with no mass offset and dotted lines correspond to results for translation with mass offset corresponding to the transport of an incapacitated crew member in a rescue scenario; distance traveled is indicated at the top of the figure.

second, these translations are composed of a single straight line as opposed to the curved profile of the crew member rescue mission depicted in Figure 2-10. In this way, the discrete action of a straight-line translation can be isolated and evaluated for the two cases of individual transport and transport with a large mass offset.

Table 2.14 lists the RMS attitude error and fuel consumption for CMG and thruster-only ACS implementations for the 10 meter translation task described in this section. In addition, total energy consumption and peak power requirements for the CMGs are included in the table to give an indication for battery mass required to support operations. Surprisingly, more energy is required from CMGs operating to maintain attitude control of the individual astronaut; this may be attributed to the fact that the tandem pair does not begin rotating as fast as for a single astronaut in response to the slight thrust vector pointing error involved with translation of the system simulated. This relationship varies as a function of the thruster impulse magnitude delivered to the system to execute a given translation; that is to say, for a higher ΔV maneuver needed for a quicker translation or for a longer distance translation, CMG energy consumption for the tandem pair may exceed that for the stand-alone astronaut. A translation distance of 10 meters over the course of 60 seconds (with another 60 seconds of no translation to allow for the control system to compensate for forces and torques induced with the deceleration burn) is intended to represent a standard translation task for low gravity astronaut EVAs.

For both the solo translation and translation with large mass offset, the CMGs selected for MAJIC significantly outperform thrusters in maintaining desired pointing throughout the simulated maneuver: while the RMS attitude error for the CMGs remains below 0.01 degrees, the RMS attitude error for thruster-only implementations ranges between 0.175 degrees and 0.974 degrees. In addition to improving the pointing accuracy of the Jetpack system, the use of CMGs also reduces the fuel consumed for a translation maneuver, most notably for the case of translation with a mass offset. Fuel consumption is increased by roughly 50% for thruster-only ACS implementations for the case of tandem translation with mass offset as compared with solo translation. In contrast, the fuel consumed with newly-sized CMGs remains constant for the two

Table 2.14: **10m Translation Performance**

ACS Type	RMS Att Err	Fuel Used	Energy Used	Peak Power
Translation Solo (No Mass Off-Set)				
Thrusters (0.5 deg)	0.968 deg	46.5 g	-	-
Thrusters (2.0 deg)	0.974 deg	32.4 g	-	-
Combined CMGs+Thr	0.004 deg	32.1 g	25.3 J	0.8 W
Translation with Incapacitated Crew Member				
Thrusters (0.5 deg)	0.175 deg	62.8 g	-	-
Thrusters (2.0 deg)	0.775 deg	52.7 g	-	-
Combined CMGs+Thr	0.001 deg	31.1 g	16.9 J	0.8 W

scenarios, highlighting the capability of CMGs to allow thrusters to function purely as translation actuators as opposed to also controlling for pointing.

By assuming platform stiffness is a priority for human exploration missions conducted with a Jetpack, consumption rates for fuel to be used in mass-to-orbit projections are taken with respect to tight deadband (0.5 degree full width, ± 0.25 degree error) thruster attitude control use. Table 2.15 lists the mass of consumables that are used during this 2 minute translation task as well as the consumption rates assumed for the mass-to-orbit projections. It should be emphasized here that most of the propellant used in the combined control case is during acceleration and deceleration phases of translation, and so extrapolating these values across an entire mission may considerably over-estimate fuel consumption rates for the MAJIC system. With this in mind, combined control fuel rates listed in Table 2.15 should be viewed as strictly conservative, over-estimates.

Table 2.15: 10m Translation Mass Cost

ACS Type	Fuel Used	Fuel Mass Rate	Energy Used	Battery Mass Rate (VES 180, 165 Wh/kg)	Battery Mass Mass Rate (Li-Ion, 130 Wh/kg)
Translation Solo (No Mass Off-Set)					
Thrusters (0.5 deg)	46.5 g	1.395 kg/hr	-	-	-
Thrusters (2.0 deg)	32.4 g	0.972 kg/hr	-	-	-
Combined CMGs+Thr	32.1 g	0.963 kg/hr	25.3 J	1.27×10^{-3} kg/hr	1.62×10^{-3} kg/hr
Translation with Incapacitated Crew Member					
Thrusters (0.5 deg)	62.8 g	1.884 kg/hr	-	-	-
Thrusters (2.0 deg)	52.7 g	1.581 kg/hr	-	-	-
Combined CMGs+Thr	31.1 g	0.933 kg/hr	16.9 J	8.54×10^{-4} kg/hr	1.08×10^{-3} kg/hr

Human Action Disturbance Torque Rejection

The astronaut actions included in the Asteroid Sampling Mission II are considered in more depth in this section. Table 2.16 lists these actions as well as the peak torque each action induced on the MAJIC system’s center of mass with respect to the MAJIC body’s reference frame. In addition to the originally simulated hammer blow, another hammer blow is simulated in which the torque disturbances are scaled down by a factor of five. The purpose of this is to identify how the different attitude control systems respond to a weaker hammer blow strike. For each of the actions, four seconds of activity by a large male astronaut (210 lbs, 6 ft 4 in) are assumed.

Figure 2-19 shows the torque profile and resulting attitude performance for the combined control CMG+Thruster MAJIC system as well as for thruster-only Jet-packs, one with a tight (0.5 degree full width) deadband and another with a loose (2.0 degree full width) deadband. The high-impact blow causes attitude errors for all implementations, but most of all for the CMG system. The limited torque of the CMGs means that the CMG subsystem only has a limited ability to counter distur-

Motion ID	Action Description	X (Nm)	Y (Nm)	Z (Nm)
1a	Hammer Blow (strong)	7.71	9.45	5.79
1b	Hammer Blow (weak)	1.51	1.85	1.13
2	Hip Reach	1.57	1.95	1.42
3	Overhead Reach	0.96	2.49	1.08

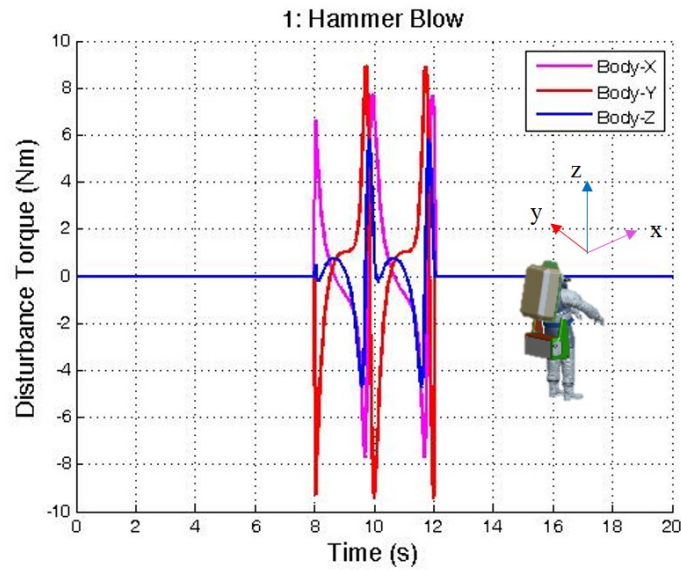
Table 2.16: **Astronaut Motions Simulated.** *Peak torques are listed and are measured in the MAJIC body coordinate frame acting on the MAJIC system’s center of mass.*

bance torques. Within a second after the hammer blow action, CMGs return the system to an attitude within 0.1 degrees of the desired pointing vector (see the green line in Figure 2-19b); this contrasts with the thruster-only attitude errors seen in red and blue, which are free to drift within their deadbands (0.5 degree full width deadband for red, 2 degree full width deadband for blue).

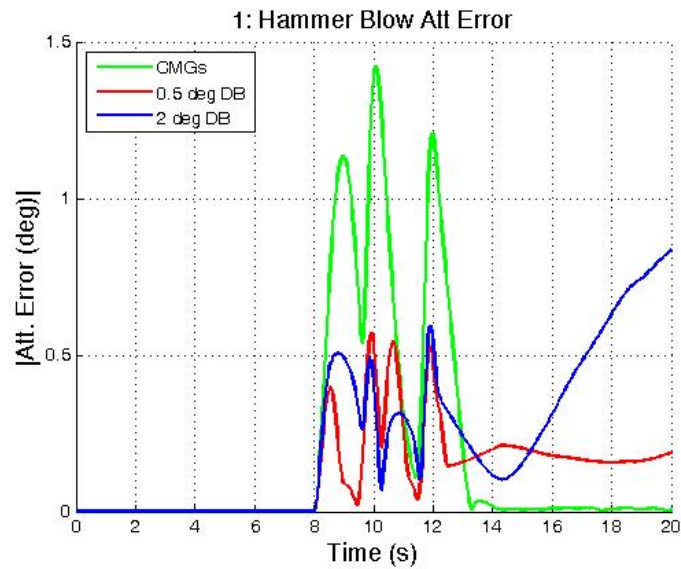
Figure 2-20 depicts the torque profile for a low-impact hammer blow with a disturbance torque profile scaled down from that described above (note the scale of Figure 2-20a). For the two thruster simulations, the motion of swinging the hammer leads to a drift in attitude error that is only corrected when exceeding the thruster deadband. This can be seen from the sharp points of the blue and red lines in Figure 2-20b around 14 seconds of simulation time at 1.0 degrees and 0.25 degrees attitude error, corresponding to the 2.0 degree and 0.5 degree deadband of the thrusters, respectively. Note that during these mission times there are no human actions conducted; rather the peaks in attitude error correspond solely to the thruster deadband. By contrast, after the four seconds of disturbance torques the CMGs return the MAJIC system to the desired pointing direction almost immediately.

A comparison between Figures 2-19b and 2-20b illustrates the fact that for small disturbance torques, CMGs exhibit superior performance to either thruster-only system. The ability of a CMG subsystem to respond to expected astronaut torques will likely determine the torque and angular momentum capacity that is ultimately selected as a target for a MAJIC system. This analysis shows that the small CMGs identified in Table 2.12 are not sufficient to maintain stiff attitude control for a hard hammer blow with disturbance torque peaks of 10 N m, while they are sufficient to ac-

commodate hammer blows with disturbance torques having peaks of 2 N m delivered to the MAJIC system.



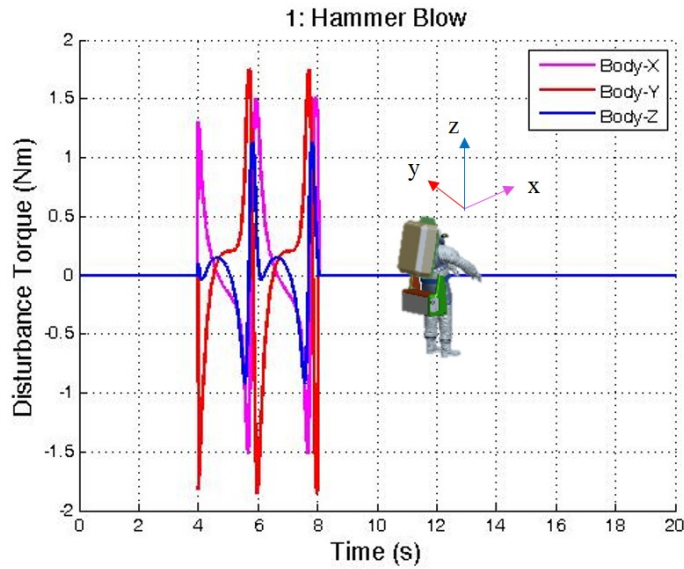
(a)



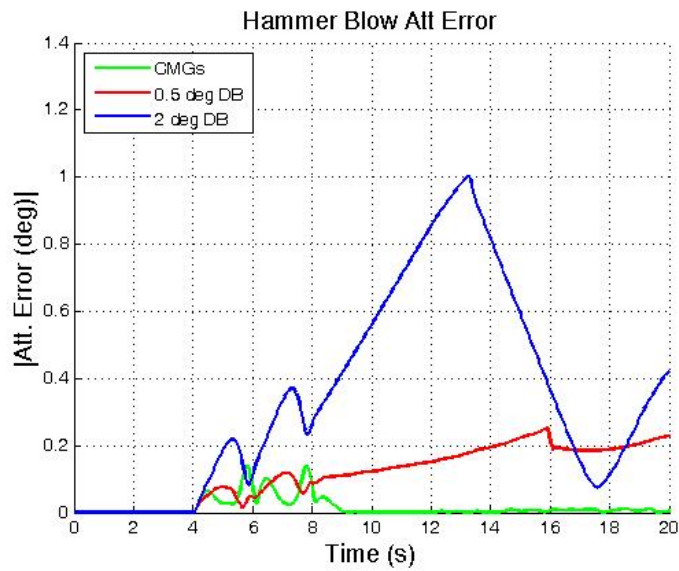
(b)

Figure 2-19: **Hammer Blow (strong- 10 Nm scale) Disturbance Torque Profile and Performance.** (a) Disturbance torque profile in the MAJIC body reference frame (x , y , z torques represented in magenta, red and blue respectively); (b) Absolute attitude error (CMGs in green, thrusters with 0.5 degree deadband in red, thrusters with 2.0 degree deadband in blue); (c) Fuel consumption (color scheme same as in attitude error plot).

The next two actions simulated are a hip reach and an overhead reach up, with



(a)



(b)

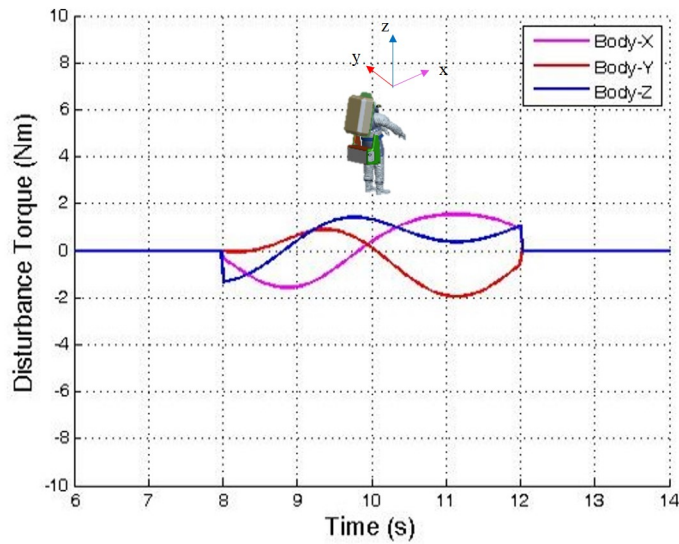
Figure 2-20: **Hammer Blow (weak- 2 Nm scale) Disturbance Torque Profile and Performance.** (a) Disturbance torque profile in the MAJIC body reference frame (x , y , z torques represented in magenta, red and blue respectively); (b) Absolute attitude error (CMGs in green, thrusters with 0.5 degree deadband in red, thrusters with 2.0 degree deadband in blue); (c) Fuel consumption (color scheme same as in attitude error plot).

associated torque profile and performance plots shown in Figures 2-21 and 2-22, respectively. For the hip reach, CMGs once again do not maintain platform stiffness, but instead allow for an error of nearly 1.5 degrees before returning the MAJIC system to a state of precise pointing (see Figure 2-21b). Because the disturbance torques for this maneuver all remain under 2 N m, this provides a good test of the system to see whether the good results from the 2 N m hammer blow test are universally applicable. Clearly, the hammer blow result does not apply here; whereas in the hammer blow disturbance torques were very short duration, the disturbance torque in Figure 2-21a include continuous torques over the course of 4 seconds, and induced torques of nearly 2 N m in all axes. The lesson that can be gained is that in order to determine the best CMG size for MAJIC, not only varied torque magnitudes but also varied torque durations must be applied to any proposed design before further development can continue.

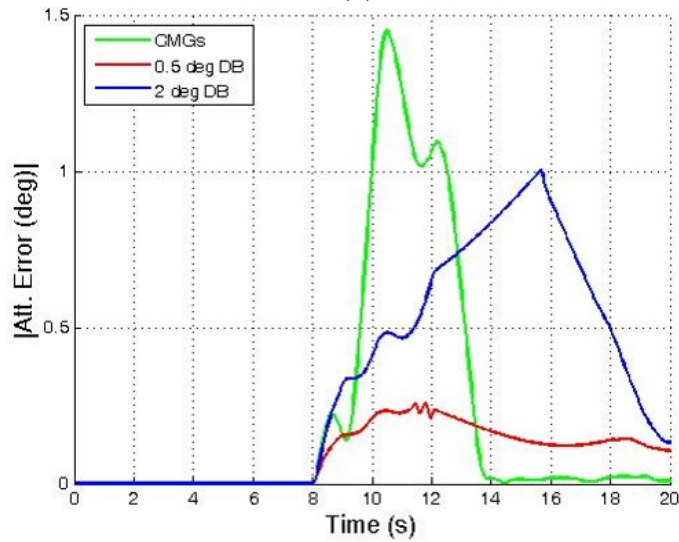
The final action simulated, the overhead reach, has a profile pictured in Figure 2-22a and corresponding system performances pictured in 2-22b. This time, only torque in the body-Y axis (corresponding to astronaut pitch) vary as considerably as those from the hip reach, while torques about the body-X axis (roll) and the body Z-axis (yaw) remain at or near 1 N m. For this action, CMGs successfully maintain control during the maneuver, though only with performance equivalent to the tight deadband thruster-only system. Of course, after the action is over the CMGs once again bring the system to a pointing vector that is far more accurate than what is possible with the thruster-only implementations.

Fuel consumption and CMG energy consumption along with corresponding mass-cost rate estimates for rejecting disturbances associated with the different human motions simulated are listed in Table 2.17. Only the strong hammer blow is included in this table to simplify mass-to-orbit estimation. As might be expected, since there is no translation and since CMGs do not saturate, no thruster fuel is consumed for the MAJIC system in the simulation for each action.

One important result from Tables 2.15 and 2.17 to note before a mass-to-orbit projection is described is the low energy consumption predicted for CMG operations.

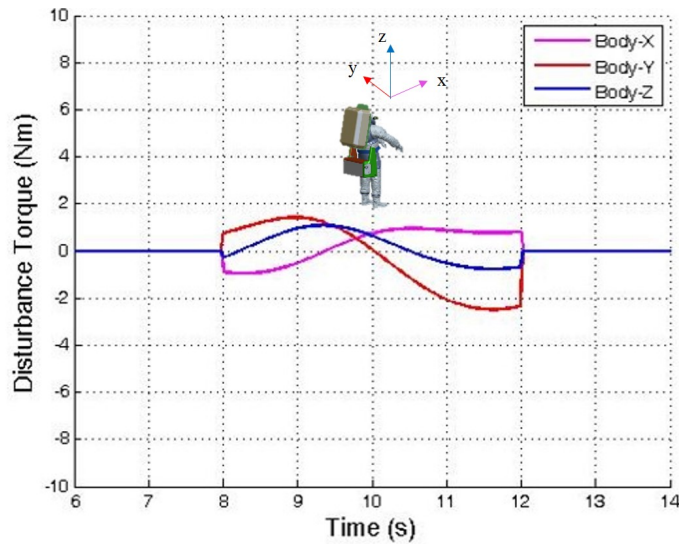


(a)

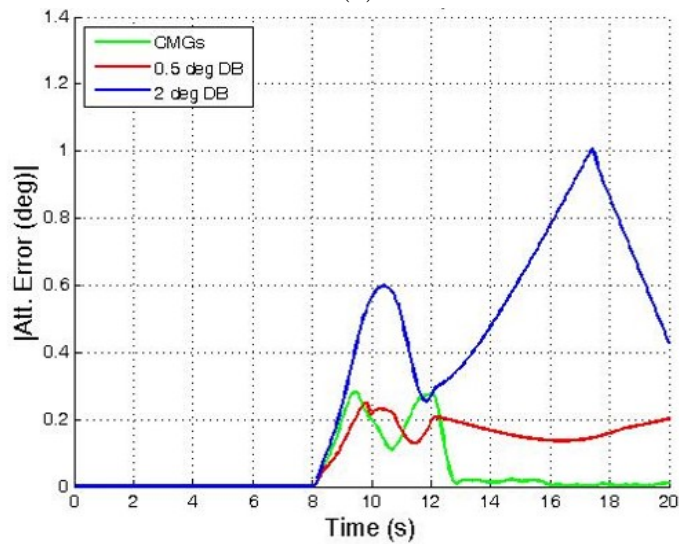


(b)

Figure 2-21: **Hip Reach Disturbance Torque Profile and Performance.** (a) Disturbance torque profile in the MAJIC body reference frame (x , y , z torques represented in magenta, red and blue respectively); (b) Absolute attitude error (CMGs in green, thrusters with 0.5 degree full width deadband in red, thrusters with 2.0 degree full width deadband in blue); (c) Fuel consumption (color scheme same as in attitude error plot).



(a)



(b)

Figure 2-22: **Overhead Reach Up Disturbance Torque Profile and Performance.** (a) Disturbance torque profile in the MAJIC body reference frame (x , y , z torques represented in magenta, red and blue respectively); (b) Absolute attitude error (CMGs in green, thrusters with 0.5 degree full width deadband in red, thrusters with 2.0 degree full width deadband in blue); (c) Fuel consumption (color scheme same as in attitude error plot).

Table 2.17: Human Action Mass Cost

ACS Type	Fuel Used	Fuel Mass Rate	Energy Used	Battery Mass Rate (VES 180, 165 Wh/kg)	Battery Mass Mass Rate (Li-Ion, 130 Wh/kg)
Hammer Blow (Strong)					
Thrusters (0.5 deg)	5.2 g	0.936 kg/hr	-	-	-
Thrusters (2.0 deg)	2.8 g	0.504 kg/hr	-	-	-
Combined CMGs+Thr	0.0 g	0.000 kg/hr	3.95 J	1.20×10^{-3} kg/hr	1.52×10^{-3} kg/hr
Hip Reach					
Thrusters (0.5 deg)	3.4 g	0.612 kg/hr	-	-	-
Thrusters (2.0 deg)	3.4 g	0.612 kg/hr	-	-	-
Combined CMGs+Thr	0.0 g	0.000 kg/hr	17.5 J	5.30×10^{-3} kg/hr	6.73×10^{-3} kg/hr
Overhead Reach					
Thrusters (0.5 deg)	5.2 g	0.936 kg/hr	-	-	-
Thrusters (2.0 deg)	2.8 g	0.504 kg/hr	-	-	-
Combined CMGs+Thr	0.0 g	0.000 kg/hr	12.1 J	3.67×10^{-3} kg/hr	4.65×10^{-3} kg/hr

Because the power consumption simulated is restricted to the gimbal motor functionality in an ideal setting (no friction losses or other engineering inefficiencies), this result indicates that a minimum power profile for CMGs is modest. With the addition of engineering losses as well as flywheel motor power consumption, these energy profiles will undoubtedly increase, but it is reassuring to know that the power required for the core functionality of the CMG subsystem is minimal.

2.4.3 Mass-to-Orbit Cost Projection

While the contrast in attitude error provides the best indication of relative control performance and system stability, the difference in thruster fuel consumption coupled with knowledge of CMG energy consumption can together be used to perform preliminary mass-to-orbit requirements analysis. Such an analysis is useful to identify at what point in the lifetime of the MAJIC system would the increased fuel economy of CMGs be sufficient to reduce the overall mass that must be brought to orbit. Thruster fuel use for human actions and for translation with and without mass offset to inform the mass-to-orbit projection. Values for CMG energy consumption and an assumption for battery selection will also be included in the mass-to-orbit calculation.

Mass-Cost Assumptions

Several assumptions are made for the purposes of this mass-to-orbit cost projection. First, a single mission is assumed to consist of three EVAs, each 6 hours in duration. Furthermore, it is assumed that two astronauts conduct each EVA, and that both astronauts are equipped with a Jetpack. Each mission is assumed to be 50% translation split 75%-25% between no mass off-set and a mass off-set; the other 50% of the mission is assumed to consist of attitude hold during astronaut motions. Astronaut motions are assumed to have equal contributions from hammer blows, hip reaches and overhead reaches. In reality, nearly 100% of an EVA would require some sort of low-amplitude torque disturbance rejection actuation as the astronaut moves his or her limbs and interacts with low gravity objects.



# of Missions	Mass to Orbit (Fuel) 	Mass to Orbit (Fuel+CMGs) 	Mass-to-Orbit Savings (kg)	Cost Savings (\$10k/kg to LEO)
1	42.2 kg	57.3 kg	-15.1 kg	-\$151k
2	84.4 kg	74.6 kg	9.8 kg	\$98k
3	126.6kg	91.9 kg	34.7 kg	\$347k
10	422.1 kg	213.0 kg	209.2 kg	\$2.1M

Figure 2-23: **Mass-to-Orbit Projections for a Jetpack with and without CMGs.** *Combined control with MAJIC requires thruster fuel, a CMG actuator suite and associated extra battery mass dedicated to CMGs to be sent to orbit; simple thruster-only control with a Jetpack only requires thruster fuel, but with more aggressive cargo delivery given the poorer fuel economy of a thruster-only system.*

The overall CMG system mass including CMG actuators, control electronics and structures is assumed to have a mass of 20 kg per MAJIC system. The EPS of the MAJIC system is assumed to have a specific energy capacity of 130 Wh/kg; both thruster fuel and required battery mass are included in the mass calculation. Additionally, a 100 gram per hour desaturation budget for each astronaut is added to CMG figures.

Finally, the tight deadband thruster (0.5 degree full width deadband) is assumed to be used. Mass-cost rates for tight deadband thrusters and CMGs with Li-ion, 130 Wh/kg specific capacity batteries are taken from values presented in Tables 2.15 and 2.17.

Projection Results and Discussion

Figure 2-23 depicts the results of the mass-to-orbit projection conducted for MAJIC. For just one mission, roughly 15 kg of extra mass is required to be sent to orbit; since the CMG subsystem is assumed to have a mass of 20 kg, there are clearly significant gains to fuel economy over the course of a single mission.¹² After just two

¹²Recall that one mission here is equivalent to three EVAs of 6 hrs with two MAJIC units in operation simultaneously. Further assumptions are found in Section 2.4.3

missions, the CMGs already pay for their own weight; if the MAJIC system is utilized for as many as 10 missions, this mass-cost projection predicts mass-to-orbit savings of over 200 kg. While the rate of occurrence for disturbance torques are conservative in this projection, the assumption that a tight deadband thruster implementation would always be used for a thruster-only Jetpack is more aggressive.

Even with the uncertainties inherent in designing a system without well-defined requirements, it is possible to design the next generation back-mounted Jetpack for astronaut EVAs around low gravity objects. The analysis contained in this chapter demonstrates the potential of a CMG-integrated Jetpack system to provide a stable and responsive work platform that enables precise EVA tasks that include asteroid sampling and scientific equipment installation or maintenance.

Chapter 3

CMGs for SPHERES: CDIO and Utility Analysis¹

The MIT SPHERES facility² provides an excellent testbed for combined control of spacecraft in low gravity with thrusters and CMGs. This chapter describes the concept, design, integration and operations (CDIO) of the SPH-Halo-CMG configuration of SPHERES at MIT's Space Systems Laboratory.

The primary CMG-related research goal of the SPHERES hardware demonstration effort is to address the question: **How does the use of CMGs for attitude control compare with the use of thrusters for attitude control of SPHERES?** In order to address this research question, the SPH-Halo-CMG system must have CMGs of the proper SWaP to make integration possible and to make research goals associated with demonstrating precision pointing and disturbance rejection possible.

¹This chapter includes contributions by a team of graduate students including the author of this thesis, Sam Schriener, Tim Setterfield and Morris Vanegas; these contributions satisfied partial requirements for the Fall 2013 16.851 MIT course on Space Systems Engineering, advised by Prof. Jeffrey A. Hoffman [1].

²For background on SPHERES, see Section 1.4

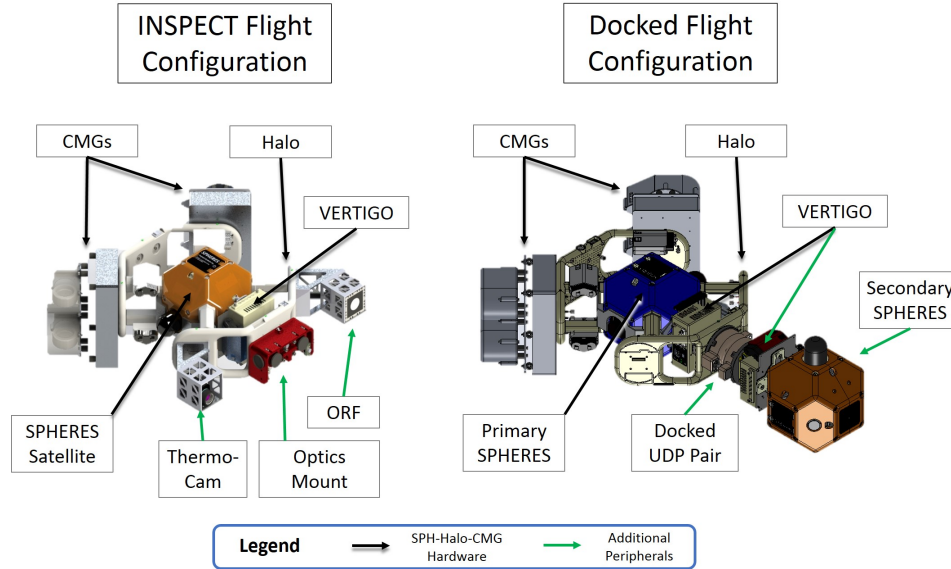


Figure 3-1: **SPH-Halo-CMG Flight Configurations** *The SPH-Halo-CMG configuration is used to host two different configurations used for flight testing aboard NASA’s Reduced Gravity Aircraft. The INSPECT configuration has an optical range-finder (ORF), stereoscopic cameras (Optics Mount), and a thermographic camera (ThermoCam); the Docked configuration has a Universal Docking Port used to dock to a Secondary SPHERES satellite.*

3.1 SPH-Halo-CMG Concept

The concept for a SPH-Halo-CMG configuration of the SPHERES facility involves interfacing commercially available CMGs to a central SPHERES satellite through the Halo expansion. This configuration allows for combined control of both thrusters and CMGs by the central SPHERES satellite. As such, the SPH-Halo-CMG system would enable controls research related to the MAJIC system described in Chapter 2 as well as proposed future spacecraft including (but not limited to) robotic refueling, assembly, maintenance or EVA inspection spacecraft.

Two system configurations explored in more depth with hardware demonstrations are pictured in Figure 3-1. SPH-Halo-CMG hardware components are identified with black arrows and peripherals added to the system are identified with green arrows. The INSPECT configuration is intended as a hardware simulation of future EVA inspection and diagnostic spacecraft. This configuration was flown aboard the August 2014 Reduced Gravity flight experiment with NASA’s Reduced Gravity Aircraft

[22]. The Docked configuration is intended as a simulation of both robotic servicing and assembly spacecraft (the UDP pair can be un-docked, leaving a single Universal Docking Port attached to Halo) as well as the MAJIC system described in Chapter 2. Just as an astronaut or an assembly or servicing spacecraft may grapple large objects during an mission, the central SPH-Halo-CMG configuration can grapple the extended mass of the Secondary SPHERES satellite. This second configuration is currently under further investigation at the Space Systems Laboratory in preparation for the upcoming August 2015 Re-Flight Opportunity following the previous August 2014 Flight Opportunity.

Just like the study for CMG integration in a low gravity astronaut EVA astronaut Jetpack described in Chapter 2, a problem with sizing CMGs for the SPHERES application is the variable nature of control demands that will be requested of CMGs in the SPHERES facility. Unlike MAJIC, the SPHERES facility is already at a high level of maturity and so mass properties are well known for certain components expected to be used during testing. Variability in expected control demands derives instead from the fact that the SPH-Halo-CMG system is intended as a controls research and development testbed to be used for any one of a number of configurations that are enabled with three SPHERES, docking ports, and peripheral sensors and actuators, some of which are in early stages of development. For instance, while SPHERES Universal Docking Ports and several peripherals such as the optics mount (stereoscopic camera pair) are already utilized in SPHERES testing and have well-defined properties, actuators such as robotic arms for SPHERES are in an immature state of development.

At the conception of this project, a particular scenario was envisioned in [1] for the SPH-Halo-CMG system to test CMG control authority. This scenario is the rotation and translation of a docked SPH-Halo-CMG + SPHERES configuration (seen on the right in Figure 3-1 in which only thrusters on the Primary SPHERES satellite in the SPH-Halo-CMG configuration are used for translation and only CMGs are used for rotation. By requiring the SPH-Halo-CMG system to control the large external and inert mass of a second, docked SPHERES satellite, controls research is enabled that

is applicable to MAJIC (specifically the scenario of crew member rescue and large mass manipulation) and proposed servicing spacecraft. The final selection of CMGs and their expected performance after implementation is described further in Section 3.2.

The system is conceived to operate in the MIT Space System Laboratory’s air-bearing table, flat floor and 3-DoF rotation air-bearing spike test facilities for initial integration and operations research. Following this initial integration and testing, microgravity operations aboard NASA’s reduced gravity aircraft (RGA) are used to identify 6-DoF dynamics and advance the state of control algorithms developed for the combined thruster-CMG actuators toward the goal of demonstrating expected CMG performance. Ultimately, the SPH-Halo-CMG configuration may operate aboard the ISS in order to further explore these research topics in a long-duration microgravity environment.

3.1.1 SPH-Halo-CMG System Requirements

Top-level system requirements for the SPH-Halo-CMG system are listed in Table 3.1. In addition to ensuring that CMGs are provided with adequate structural, power and data interfaces to operate in the proposed testing environments (Mission Requirement), integration of a CMG actuator suite must not interfere with critical SPHERES functionality including state estimation involving the use of ultrasound (US) receivers on the surface of SPHERES, communication, propulsion and IMU logging (Integration Requirement). In this way, the CMG subsystem will be restricted to a modular and non-essential addition to the overall system. Modifications to the original SPHERES system should be restricted to changes committed to communication and propulsion processes that can be turned on or off to enable CMGs to share control authority with the CO₂ thrusters on SPHERES. By adhering to this requirement, the integrity of the SPHERES system is preserved, and hardware demonstrations can directly compare system performance when functioning in a combined thruster+CMG mode as opposed to a t-only mode of operation.

In order to be most useful as a testbed for MAJIC and future manipulator and

Table 3.1: **Top-Level System Requirements.** *Table includes requirement statements, implications on project goals for each requirement, and the verification method necessary for each requirement.*

Requirement Type	Statement	Rationale	Verification
Mission	4-CMG array shall interface with Halo; controllable for 2-DoF trans + 1-DoF rot, 3-DoF rot or 6-DoF test scenarios	Advanced programmatic, experimental goal	Simulation, design, analysis and testing
Integration	4-CMG array integration shall maintain SPHERES functionality	SPHERES functions such as state estimation, communication and propulsion must remain operational to achieve SPH-Halo-CMG goals	Simulation, design, analysis and testing
Performance	Sufficient torque and ang. momentum shall be provided to rotate SPH-Halo-CMG + SPH docked configuration at min. rate of 1 deg/s	Programmatic, experimental goal	Simulation, design and analysis
Safety	SPH-Halo-CMG system shall not pose a danger to human operators or other assets in laboratory, RGA or ISS environments	Programmatic, experimental goal	Design and analysis

inspector spacecraft, sufficient attitude control from CMGs must at the very least be capable of rotating the SPH-Halo-CMG + SPH docked configuration at a rate of 1 deg/s (Performance requirement). This requirement for sizing not only allows for an eventual simulation of MAJIC EVA scenarios such as the rescue of an incapacitated crew member or the manipulation of heavy objects and large tools, but also will provide attitude control authority for a future SPH-Halo-CMG system augmented with heavy peripheral sensors or a manipulator arm that can grasp heavy objects.

Finally, the CMG actuator suite should not pose a threat to human operators or other valued assets in the laboratory, in a Reduced Gravity Aircraft or aboard

the International Space Station. This involves both mechanical and electrical design that ensures that CMGs remain physically isolated from the rest of the SPH-Halo-CMG system and are provided with the proper electromagnetic environment to ensure flywheel and gimbal motors and sensors fail in a safe manner.

It should be noted that requirements related specifically to normal SPHERES operations including state estimation, data logging and throughput requirements have not been explicitly included in this report; rather, we have chosen to identify only those system requirements that are unique to the SPH-Halo-CMG system considered in this chapter.

3.2 SPH-Halo-CMG Design

This section includes a description of the design activities conducted to select CMG actuators for the SPH-Halo-CMG system and to identify the structures, electronics and software necessary to interface CMGs with SPHERES to function as attitude actuators. The designs included in this section were developed as part of the Fall 2013 MIT 16.851 course and are documented in [1].

3.2.1 CMG Sizing for SPHERES

When the design efforts for the SPH-Halo-CMG system began in Fall 2013, few manufacturers of miniature CMGs existed. Furthermore, limited available funding meant the selection of CMGs was even more restricted. Honeybee Robotics Spacecraft Mechanisms Corporation (Honeybee Robotics) was one company that stood out as a primary option for a vendor. Not only do they have a long and successful history as mechanisms manufacturers for spaceflight programs including NASA's Mars Curiosity Rover [36], Honeybee Robotics also recently developed two miniature CMGs: the CMG-E-120-002 (CMG-120), an engineering unit; and the TORC-H86, a flight unit [37]. Ultimately, a working relationship among MIT, Draper Laboratory, and Honeybee Robotics was developed and the CMG-120s were chosen over the TORC-H86 CMGs primarily for cost reasons. Specifications for the selected actuators are

Table 3.2: **Angular momentum and torque specifications for the Honeybee Robotics CMG-120 actuator.** *Nominal values correspond to a flywheel rate of 6 krpm while the peak values correspond to a flywheel rate of 8 krpm.*

Mass	
Single CMG	700 g
Control electronics (for 4 CMGs)	500 g
Power	
Single CMG, steady state	< 1.0 W
Single CMG, peak torque	< 2.0 W
4 CMG Array, steady state	< 7.0 W
4 CMG Array, peak torque	< 11.0 W
Single CMG, spin-up	10 W peak, < 10 second spin-up
Angular Momentum	
Nominal, per CMG	0.120 N m s
Peak, per CMG	0.160 N m s
Torque	
Nominal	0.120 N m
Peak	0.160 N m
Flywheel Rate	
Nominal	6000 rpm
Commandable	8000 rpm
Interface	
	RS422 12 VDC Torque Triplets or Gimbal Rates

shown in Table 3.2.

For a sizing study, the cases of an astronaut moving a 50 kg mass (110 lbs) and an astronaut performing a quick hip-flexion motion were scaled down to the SPHERES using the same angular acceleration for the two cases. Table 3.3 shows a condensed and updated version of the scaling analysis performed for the purposes of the Fall 2013 MIT course 16.851 [38]. As can be seen in the table, the torque for the most extreme analogue case, hip flexion, cannot be counteracted when the inertia of Halo is included. This is acceptable since this represents a very difficult and rare case given the fact that most human actions during EVAs involve only the upper torso. With these reservations, the inability to accommodate for this hip flexion case does not preclude interesting demonstrations with the CMGs.

Because of a desire to minimize the mass and power of the CMG subsystem, only

Table 3.3: **SPH-Halo-CMG System Properties with CMG-120 Actuators** *An outline of the scaling analysis. Performance of the CMG-120 in pyramid and Box-90 configurations are considered. * The maximum pyramid configuration torque is equal to $(4\tau_{cmg} \times \sin(\beta))$ where $\beta = 54.74^\circ$ is the skew angle; † The maximum Box-90 configuration torque is not symmetric; maximums along principal axes ($2h_0$ and $4h_0$) and at 45° ($2\sqrt{2}h_0$) are shown.*

Mass	12.6 kg
Inertia (approx.)	0.237 kg m ²
Acceleration of 50 kg scenario	$\alpha \approx 0.8 \text{ rad/s}^2$, $\tau \approx 0.190 \text{ N m}$
Hip flexion scenario	$\alpha \approx 2.6 \text{ rad/s}^2$, $\tau \approx 0.616 \text{ N m}$
CMG torque delivered CMG-120	0.120 N m (max. single) 0.392 N m (max. pyramidal*) 0.24 N m, 0.48 N m, or 0.34 N m (max. Box-90†)

configurations with the minimum number of CMGs to enable redundant 3-DoF control were considered. Two options that meet this requirement are the pyramid and the Box-90 configuration [8, 25]. The pyramid configuration was previously introduced in Sections 1.5.2 and 2.1.2 as the preferred option for a CMG array for MAJIC, primarily because of the limited number of actuators and the spherical symmetry of the momentum envelope afforded (refer to Figure 1-11, re-printed below as Figure 3-2 for convenience).

A Box-90 configuration is equivalent to a pyramid configuration except for the fact that the skew angle is raised to $\beta = 90^\circ$ from the pyramid configuration's $\beta = 54.74^\circ$. Recall that the four-CMG pyramid configuration described in Section 2.1.2 has maximum collective angular momentum values, H_{cmg} , in the spacecraft body frame equal to $(3.15 \ h_{rotor} \times 3.15 \ h_{rotor} \times 3.26 \ h_{rotor})$ respectively, where $h_{rotor} = |\mathbf{h}_{rotor}|$ is equal to the angular momentum stored in a single CMG flywheel rotor. In contrast, the Box-90 configuration has maximum collective angular momentum values of $(4 \ h_{rotor} \times 4 \ h_{rotor} \times 2 \ h_{rotor})$.

The Box-90 configuration is considered in addition to the pyramid configuration primarily because the Honeybee CMG-120 actuators come hard-wired with a steering algorithm for the Box-90 configuration. By designing the mechanical interface for SPHERES to accommodate both the pyramid and Box-90 array geometries, immedi-

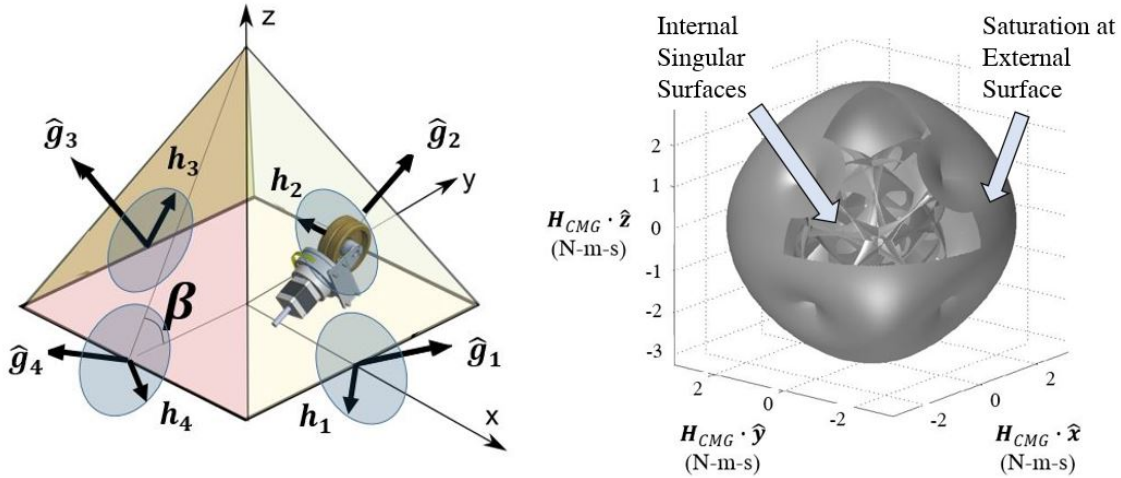


Figure 3-2: **CMG pyramid configuration and angular momentum envelope depicting singular surfaces.** *Left: A 4-CMG pyramid configuration, pyramid angle $\beta = 54.74^\circ$; a Box-90 configuration is equivalent to a pyramid configuration with a pyramid angle $\beta = 90^\circ$. Right: The pyramid array's nearly spherically symmetric momentum envelope has dimensions $3.15 h_{rotor} \times 3.15 h_{rotor} \times 3.26 h_{rotor}$ (pictured); by comparison, a Box-90 momentum envelope has dimensions $4 h_{rotor} \times 4 h_{rotor} \times 2 h_{rotor}$; images modified from [7] and [8]*

ate testing with the Honeybee Robotics steering law can be achieved, and long-term testing with a MAJIC-like pyramid steering law can follow.

3.2.2 Structural Design

The geometry of Halo includes three sets of two parallel faces for mounting components. All faces that are not parallel are either perpendicular or at a 45° angle to each other. Given the square base reference present in both the pyramid and Box-90 configuration, the perpendicular faces of Halo presented the opportunity to position four CMGs in either the pyramid or the Box-90 configuration. As mentioned in Section 3.2.1, a design that allows for both configurations was adopted so that immediate operations with a Box-90 configuration could proceed before attempting to implement pyramid steering logic simulated for the MAJIC system. An extra advantage of providing both options in a hardware demonstration is the extra controls research that is enabled - perhaps lessons from practical operation of both configurations will inform design decisions for the MAJIC program as well as for other spacecraft systems that

could benefit from including CMGs in their trade space for attitude control actuators.

The final conceptual mechanical design from [1] is shown together with SPHERES and Halo in Figure 3-3. The design occupies two Halo ports, with two CMGs at each port. Additionally, the top assembly includes the Honeybee Robotics CMG-120 control board mounted between the CMG actuator pair and the Halo structure. The two port design was chosen so as to keep the central port free for use as a docking port or as a support for another peripheral sensor or actuator for SPHERES.

As shown in Figures 3-3b and 3-3c, each CMG can be attached in two orientations (by rotating the CMGs 35.26° from each other) to achieve either the Box-90 (Figure 3-3b) or pyramid configuration (Figure 3-3c). The change between the two configurations is performed by unscrewing four captive screws on the mounting plates, rotating the CMG sub-assemblies, and reattaching the four captive screws (see Figures 3-3d and 3-3e). During this operation the CMGs are restrained by the retainers, which will prevent the CMG sub-assembly from floating away in microgravity.

The CMG system attaches to Halo's male mechanical interface with four screws. The interface is female on the CMG side, with four threaded holes on the electronics enclosure (Figure 3-3d) and the interface plate (Figure 3-3e). For the top CMG assembly, an electrical connection is made using the Halo connector (Figure 3-3d). This connection provides the power for the CMGs and signals for communication between SPHERES/VERTIGO and the CMG control board. A custom connector printed circuit board (PCB) is necessary to translate the USB signals from Halo to the RS-422 signals required by the CMG control board. The connector PCB will also attach to and redirect the four control board-to-CMG connections so that they exit at the connector breakouts (Figure 3-3d). The Honeybee LEO control board is placed upside-down to facilitate attachment to the connector PCB and create a design that only occupies two Halo ports. The mounting plates feature an elevated platform to support the CMGs. This elevated platform was included to add safety margin to the default floor clearance on the CMG-120 CMGs.

As Honeybee Robotics does not provide enclosures for the CMG-120 actuators, custom covers were designed in order to contain the actuators (Figures 3-3d and 3-3e).

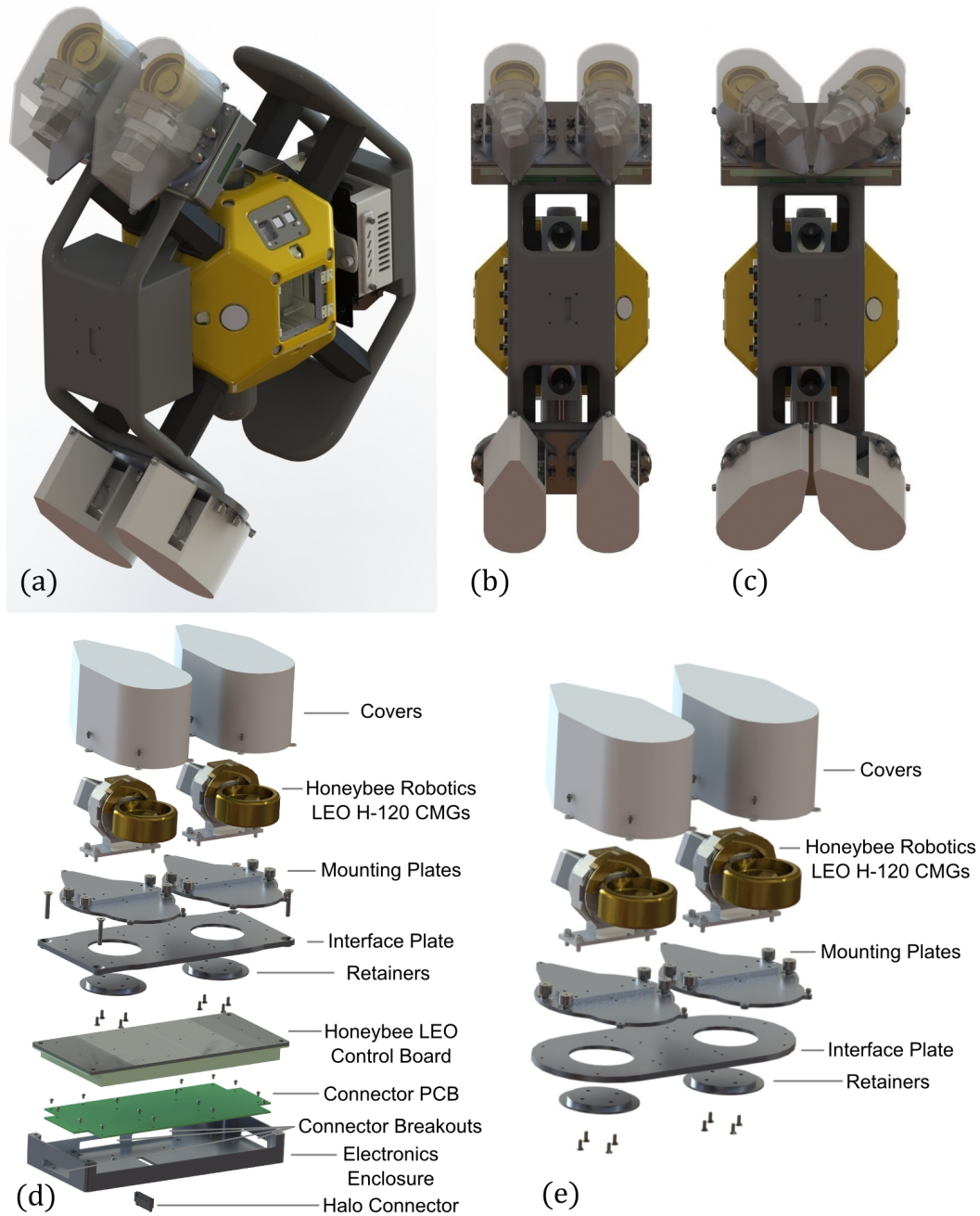


Figure 3-3: Mechanical design for SPH-Halo-CMG. (a) and (b) The CMGs attached to Halo in the Box-90 configuration. (c) The CMGs attached to Halo in the pyramid configuration. (d) An exploded view of the top CMG assembly. (e) An exploded view of the bottom CMG assembly. Image credit: Tim Setterfield [1].

The tapered shape at the rear of the covers and mounting plates is to accommodate a slip ring that will protrude from the back of the gimbal motors allowing for full 360° rotation of the gimbal.

The wires connecting components are not shown in Figure 3-3. Four connectors will exit the control board enclosure at the connector breakouts (Figure 3-3e); two of these will go to the CMGs located directly above and thus will only require short cables. The other two will need to pass to the other side of Halo. Cable mesh is used in practice. The connection to each CMG is achieved through a slot in the covers, visible on the bottom CMGs in Figures 3-3a, 3-3b, and 3-3c. Since the CMGs transfer significant torques to the SPHERES, structural rigidity is required, and so aluminum is used as opposed to printed plastic.

The masses of all major components are given in Table 3.4. The total mass of the designed system is 5.04 kg, not including the mass of the electronic components that will be required on the connector PCB or the mass of the wires connecting the control board to the CMGs.

Table 3.4: Mass budget for SPH-Halo-CMG system. *The masses of all major components excluding the electronic components on the connector PCB and the wires connecting the control board to the CMGs.*

Item	Material	Mass ea. (g)	Qty.	Tot. (g)
CMG-120 Actuators	Various	700.00	4	2800.00
LEO control board	Various	500.00	1	500.00
Mounting plates	Aluminum	122.81	4	491.24
Interface plate (control board side)	Aluminum	248.41	1	248.41
Plastic CMG covers	ABS	62.01	4	248.04
Interface plate (other side)	Aluminum	222.43	1	222.43
Electronics enclosure	Aluminum	217.88	1	217.88
Fasteners	Stainless Steel	Various	52	121.99
Retainers	Aluminum	28.52	4	114.08
Connector PCB (board only)	PTFE	74.31	1	74.31
Total				5038.38

The CMG system was carefully positioned so as to avoid obstructing the thrusters or ultrasonic receivers. Obstructing the thrusters would have the undesired effect of changing the direction of CO₂ flow and thus thrusting direction, which would influence

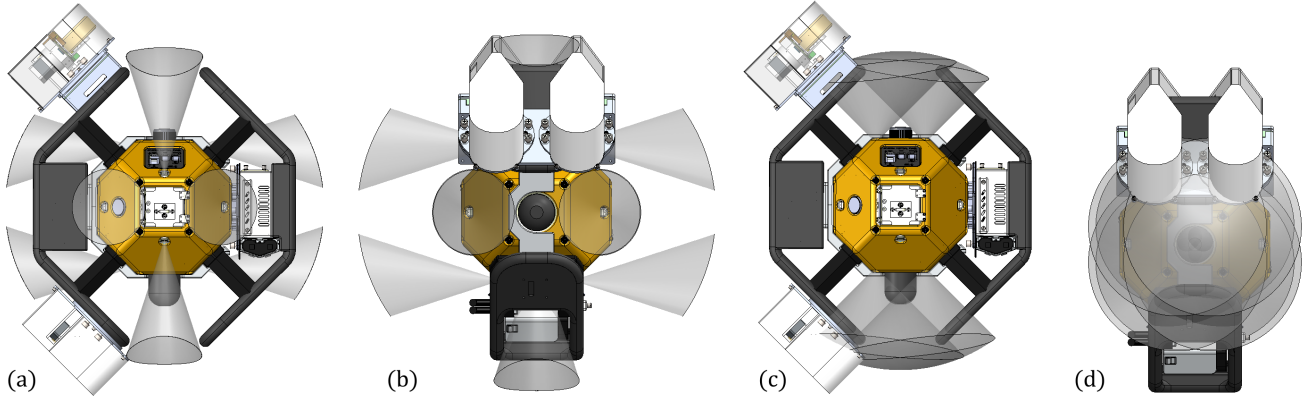


Figure 3-4: **SPHERES keep-out zones.** *Relevant keep-out zones for the Halo expansion are shown with the CMG system in its Box-90 configuration. (a) Right view of thruster keepout zones. (b) Bottom view of thruster keepout zones. (c) Right view of ultrasonic keepout zones. (d) Bottom view of ultrasonic keepout zones.*

control. Obstructing the ultrasonic receivers would decrease the accuracy of global metrology (external state estimation), which relies on ultrasonic ranging for position determination.

The keep-out zones are shown as cones in Figure 3-4. For the thrusters, these cones represent the volume over which the expansion of CO_2 occurs. For the ultrasonic sensors, these cones represent the ultrasonic “field of view”. The CMGs are shown in their Box-90 configuration as the CMGs are most likely to interfere with the keepout zones in this configuration. Figure 3-4a and b show that the proposed design does not obstruct the thrusters. As can be seen in Figure 3-4c and d, the ultrasonic field of view is already largely obstructed by Halo. The addition of CMGs thus does not add significant interference with the keep-out zones.

The attached SPHERES scenario was further analyzed to see how long the CMGs could stabilize full thrusting of the active SPHERE in a direction perpendicular to the attachment arm (Figure 3-5). The inertia of the passive SPHERE offsets the center of mass of the system; when the thrusters fire, this center of mass offset creates an adverse moment (an induced torque) which needs to be compensated by the CMGs. Because of the finite magnitude of angular momentum that the CMGs can provide, there is a limit to how long this maneuver can be performed. A summary of the performance of the studied CMG arrays in this scenario is included in Table 3.5.

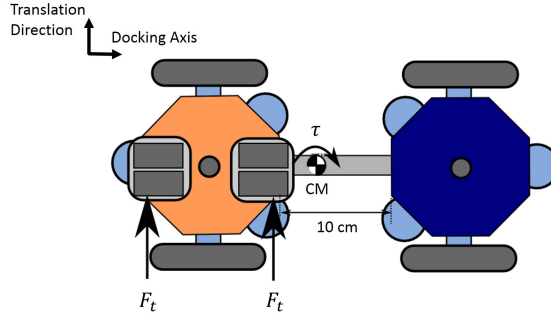


Figure 3-5: **A top view of two SPHERES satellites with Halo and on air carriages, attached 0.1 m apart.** *Two thrusters exert on the active SPHERE a force F_t , creating both an acceleration and an adverse moment τ .* Image adapted from [1]

Note the superior performance of the Box-90 configuration; this can be attributed to the asymmetric nature of the configuration: the array is oriented such that the spin axis controlled is aligned with one of the two more capable axes.

In addition to translation, a pure rotation demonstration is analyzed for the SPH-Halo-CMG + SPH system. The first environment in which this scenario would be demonstrated is on the air-bearing table, so an estimated inertia of the air carriages is included as in Table 3.5. For the Box-90 configuration, the two attached SPHERES can achieve a maximum angular velocity of $21^\circ/\text{s}$. For the pyramid configuration, the two attached SPHERES can achieve a maximum angular velocity of $24^\circ/\text{s}$. These angular rates significantly exceed the target of $1^\circ/\text{s}$ set in the requirements described in Table 3.1, representing the fact that the Honeybee CMG-120 actuators are properly (if not over-) sized. The extra capability afforded by these large actuators relative to the SPHERES facility ensures that a broad range of demonstrations may be executed corresponding to MAJIC research goals as well as research goals pertaining to manipulator or inspection spacecraft.

3.2.3 Electrical Design

This section contains the electrical design as envisioned in [1]. The schematic in Figure 3-6 shows the electrical path from SPHERES to the CMGs. Since the output of Halo is USB and the expected input of the CMG controller is RS-422 protocol,

Table 3.5: **Details of the SPH-Halo-CMG + SPH scenario (Figure 3-5)** Table includes expected performance of both the pyramid and Box-90 CMG arrays using the Honeybee Robotics CMG-120. Analysis credit: Tim Setterfield [1].

Variable	Value
Mass of system	26.7 kg
Inertia about new center of mass (z-axis)	0.94497 kg m ²
Center of mass (x-axis, primary sphere)	+0.15634 m
Duty cycle	40%
Thruster force F_t	0.098 N
Net force ($2 \times F_t \times 0.4$)	0.0784 N
Duration of compensation	47.0 s (pyramid) 40.7 s (Box-90)
Distance of travel	3.24 m (pyramid) 2.43 m (Box-90)
End velocity	0.138 m/s (pyramid) 0.120 m/s (Box-90)

an adapter has to be incorporated to ensure the communication protocols of the two serial interfaces are compatible. The interface protocol will change from RS-232 between SPHERES and VERTIGO to USB as a Halo output to RS-422 as a controller input. The schematic also shows that the CMGs will be powered by the four external Li-ion Nikon batteries located on Halo (Nikon model EN-EL4a) that provides 11.1V and 2500 mAh of power each.

SPHERES Expansion

The SPHERES expansion port is composed of an expansion PCB with a mating connector and a mounting plate. For protection, the assembly also includes a PCB board carrier and an expansion cover used to cover the electronics when the satellite is not in use. The SPHERES expansion port mounting plate can be seen in Figure 3-7 along with a 50-pin connector. The expansion port mounting plate is an aluminum plate with four captive thumbscrews. The thumbscrews are used to quickly attach payloads to a SPHERES satellite in a microgravity or ground laboratory environment.

The SPHERES Expansion Port has the capability to transmit multiple General

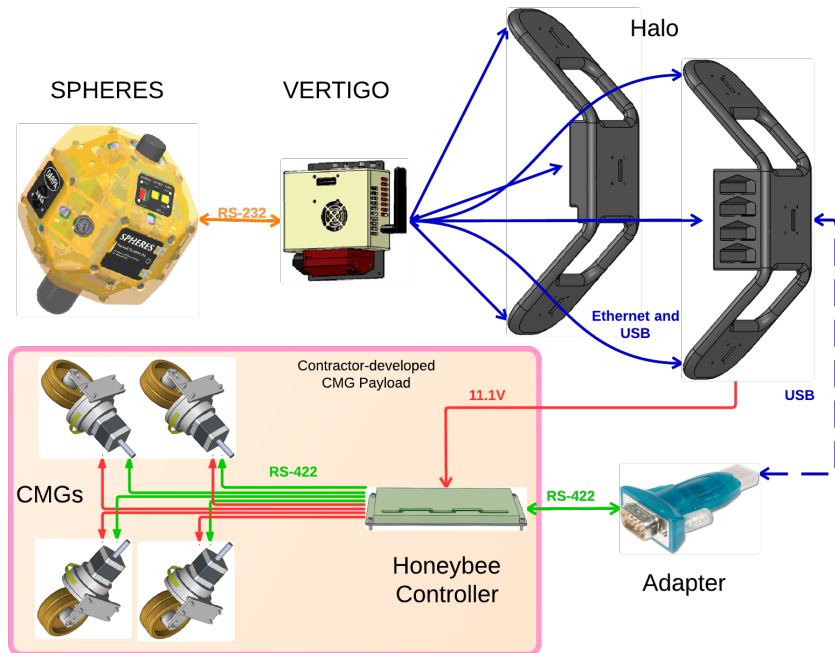


Figure 3-6: **Electrical interface schematic for SPH-Halo-CMG system.** *The path of information and power from SPHERES to CMGs is depicted. Image credit: Morris Vanegas, [1].*

Purpose Input/Output lines (GPIO), SPHERES reset signals, infrared (IR) and ultrasound (US) bypasses for both sensors on SPHERES and those sensors on the payload, RS-232 and RS-422 Universal Asynchronous Receive/Transmit (UART) signals, and power (Figure 3-8). There are also five pins that are not currently used to allow for the interfacing with future technology. For the SPH-Halo-CMG configuration, the following pins in the SPHERES Expansion Port will be utilized:

- +5VDC and Ground (pins 42, 44, and 30, 40, or 50)
- Basic UART RS-232 serial port (pins 14 and 16)

The 16 AA batteries inside SPHERES are capable of providing ± 15 VDC, +5VDC, regulated +3.3VDC, and ground connections. The maximum current limit is 0.5 amps, leading the team to use the Li-ion batteries on Halo to power the CMGs rather than the SPHERES batteries. Using +5VDC and ground for handshaking from SPHERES ensures and simplifies compatibility with USB further down the communication pathway.

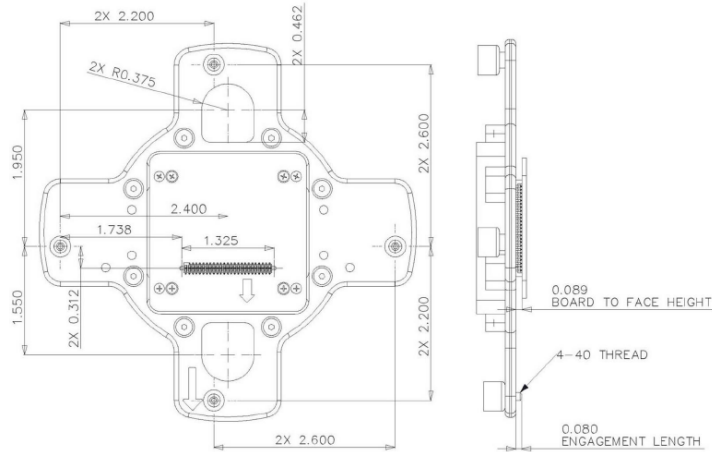


Figure 3-7: **SPHERES expansion port schematic.** *Expansion port aluminum plate dimensions and the 50-pin connector used to interface to the SPHERES satellite.*

This particular implementation takes advantage of the RS-232 serial communication capability on SPHERES. Rather than sending streams of bytes, UART converts bytes into a serial stream of bits (0s and 1s) with organization that includes a stop and start byte in each packet of data sent.

VERTIGO Expansion

The VERTIGO avionics stack is attached to the SPHERES expansion port with 4 threaded holes on the VERTIGO internal side that match the expansion port thumb-screw pattern on SPHERES. In order to accommodate the Halo expansion as well as other external payloads if Halo is not used, VERTIGO has an electrical and mechanical interface similar to the SPHERES expansion opposite the SPHERES connection. Because VERTIGO covers IR and US sensors, the sensors had to be replicated via pass-throughs. Figure 3-9 provides an illustration of the configuration on the external side of the VERTIGO stack.

The VERTIGO expansion port has the capability to transmit in Ethernet and USB protocol, can receive in RS-232 and RS-422, can transmit bypass signals for sensors on its payload, forwards SPHERES commands, and can transmit power from an external battery. For the SPH-Halo-CMG configuration, the following items in the VERTIGO expansion port will be utilized:

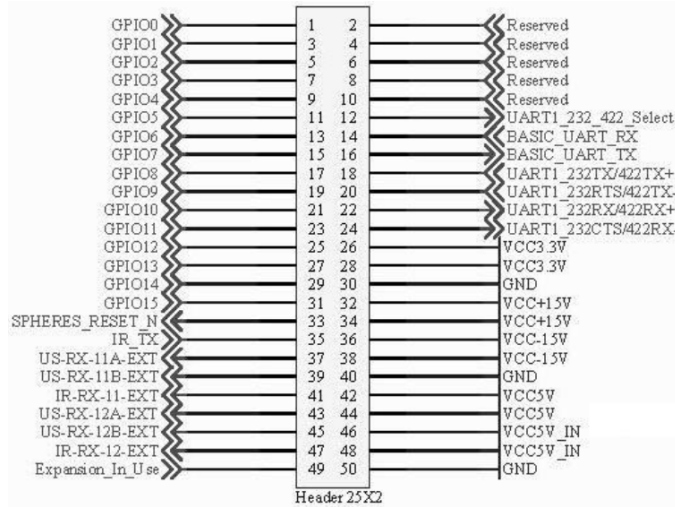


Figure 3-8: Pin layout for the expansion port. *SPHERES* expansion port electrical interface pin assignments.

- +5VDC and ground (any of the associated pins)
- Message input from SPHERES (pin 28)
- IR and US bypass sensor pins (pins 23, 25, 27, 29, 31, 33, 35)
- USB TX and RX (pins 16 and 18)

The VERTIGO avionics stack is powered through an external Nikon battery, as described at the beginning of this section. USB communication will take advantage of the +5VDC and ground from this single battery, as well as one of the four possible USB pair connections coming from the VERTIGO expansion port (Figure 3-10).

Commands from SPHERES into VERTIGO will utilize the RS-232 protocol, which VERTIGO is configured to accept. As is the case with SPHERES, VERTIGO will use the IR and US bypass sensors lines because the hardware covers the "keep-out zones" on the expansion side of SPHERES (Figure 3-4).

Halo Expansion

The Halo system attaches directly to the four threaded holes on the external side of the VERTIGO avionics stack. In order to provide maximum compatibility with current payloads, each of the 6 expansion ports of Halo also have the same physical

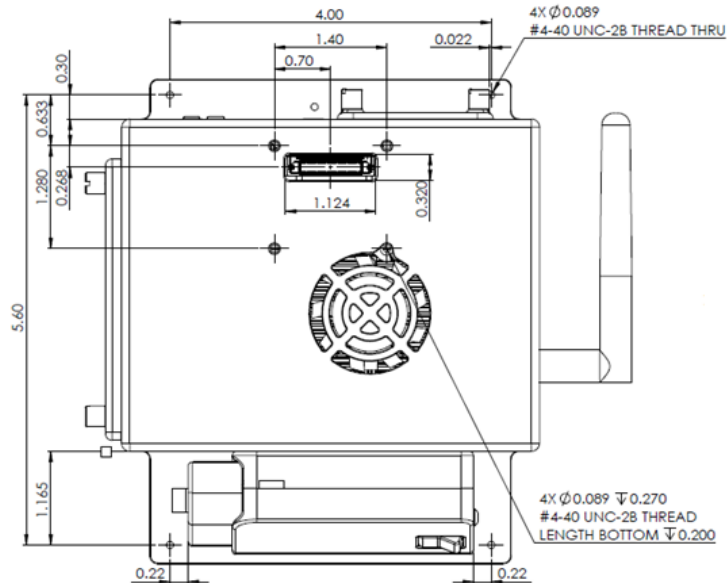


Figure 3-9: **VERTIGO expansion port.** *Expansion side of the VERTIGO avionics stack showing four threaded holes for captive thumbscrews and a 50-pin connector.*

external configuration as VERTIGO (Figure 3-11). Thus, Halo has four threaded holes in the same pattern as the VERTIGO expansion side to interface with payloads that have previously been attached to VERTIGO. In addition, each expansion port of Halo also has four captive thumbscrews on each face, making it modular for both male and female payload connections.

Halo increases the number of expansion ports of VERTIGO from 1 to 6. In doing so, the information from SPHERES sent to VERTIGO must be relayed to all faces of Halo. Since the commands are only being relayed, the pin layout for Halo is very similar to the pin layout for VERTIGO shown in Figure 3-10. The exception is that, rather than accepting RS-232 serial commands, the same pins on Halo accept USB commands because VERTIGO does not provide RS-232 output.

In addition, Halo houses four batteries on one of its two halves (see the left side of Figure 1-8). While the single battery on VERTIGO is used to power the VERTIGO computer, the four batteries housed in the Halo structure are used to power the CMGs.

Data transfer through Halo with USB rather than Ethernet has been selected. Although an Ethernet communication provides faster speeds than USB, implementa-

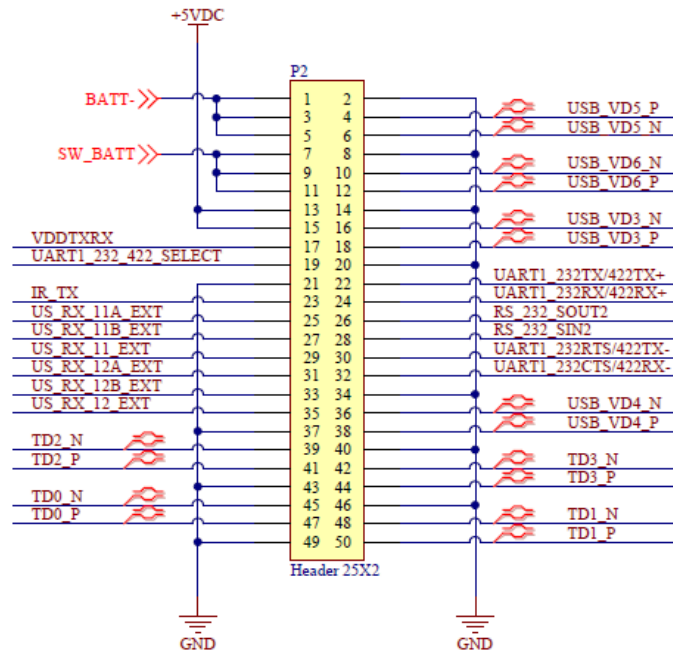


Figure 3-10: **VERTIGO expansion port electrical interface pin assignments.**

tion is more difficult. An Ethernet-to-serial connection requires large hardware that needs its own external power. The extra bandwidth is not worth the complexity of creating an adapter between two different communication protocols. A USB-to-RS-422 connection is simpler and requires smaller hardware. This USB communication is slower than Ethernet, but faster than RS-422, which is the limiting speed in the SPHERES-to-CMG communication path. It should be stated that USB has unknown latency issues. While the 16.851 team did not expect this latency to affect communication significantly, future testing was recommended (that has yet to be completed) to determine exactly how much latency is present with this adapter. Despite this, since the CMGs require a serial RS-422 protocol, the decision to use USB protocol as the output from Halo was made due to the similarity in protocols along with the simplicity and small hardware necessary for implementation.

USB Adapter

Since the output of Halo will be USB, an adapter needs to be included in order to convert the information into an RS-422 protocol for the CMG controller board. For the ground test, this will be accomplished with a commercial-off-the-shelf USB-to-

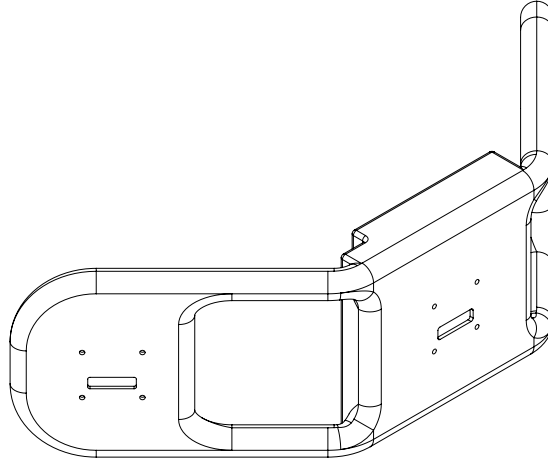


Figure 3-11: **Halo expansion mechanical interface.** *Diagram of one of two halves of the Halo expansion; each half hosts three total expansion ports to interface external payloads or actuators to the central SPHERES satellite.*

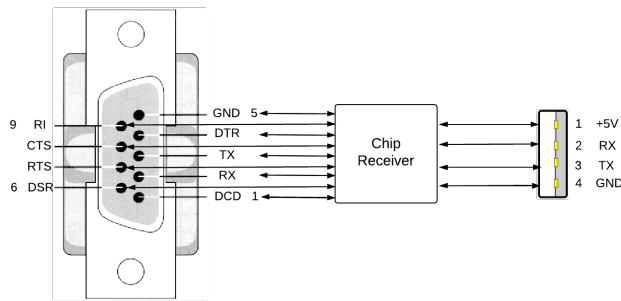


Figure 3-12: **USB to serial adapter pin assignments.**

DB9 adapter. The chip receiver associates the four USB inputs into output pins with the ability to respond to CTS (clear to send) and RTS (request to send) flow control signals necessary for both RS-232 and RS-422 handshaking communication. These 9 pin outputs will then be hardwired to the CMG controller board (Figure 3-12). The CMG controller board can accept either torque triplets for a Box-90 configuration or gimbal rates for any other configuration.

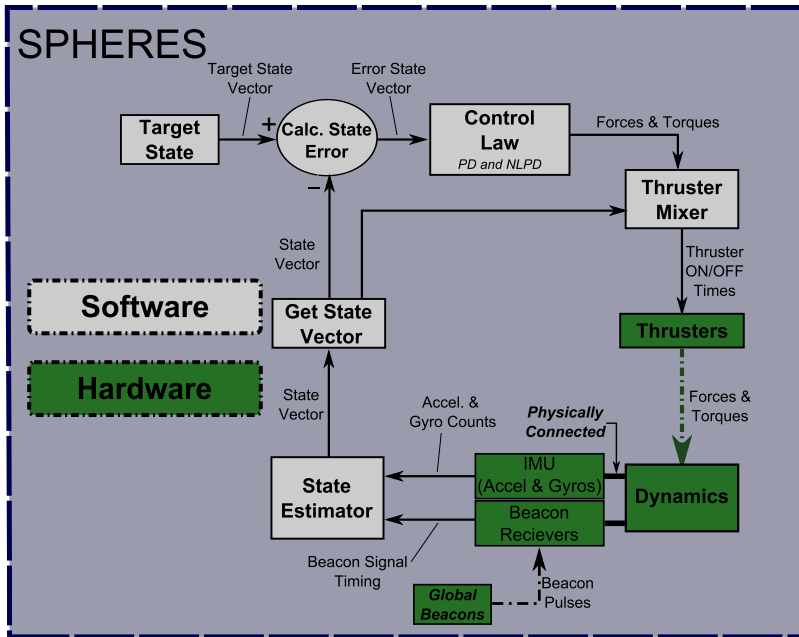


Figure 3-13: **SPHERES control loop.** A simplified depiction of the control loop on the SPHERES satellite including only key elements. Additionally, the type of data exchanged between each block is shown. The blocks in grey are implemented in the controller software, while the green blocks are hardware components that had to be simulated. Image credit: Sam Schreiner [1].

3.2.4 Flight Software Design

SPHERES Software Background

Towards the goal of using CMGs in closed-loop testing of SPHERES control algorithms, flight software must be written as part of a real-time embedded system. That is, communication with CMGs must be performed on a scheduled basis so that timing can be maintained for other functions vital to SPHERES control. As a controls research testbed, every aspect of the SPHERES satellites' control algorithm can be re-programmed. Initial software design had a goal of limiting complexity, and so CMG software was designed to work effectively within the existing priority-based multi-threaded environment. A simplified version of the SPHERES controller (which is replicated in the simulation) is depicted in Figure 3-13.

Beginning in the top left of Figure 3-13 and going clockwise, the satellite's internal estimate of its state (linear and angular position and velocity) is compared to the

target state. The difference is fed to the control law which calculates the force and torque vectors required to bring the satellite to the target state. There are a wide variety of control laws that may be implemented, including Proportional-Differential (PD) linear control laws, Proportional-Integral-Differential (PID) control laws and Non-Linear PD (NLPD) attitude control laws [39]. Initial simulations were conducted using a NLPD controller, though current research activities with the SPH-Halo-CMG system in preparation for the August 2015 flight opportunity involve PID control law development.

The force and torque vectors from the control law are fed to the mixer, which determines how to fire the thruster array to achieve the desired forces and torques. The thrusters then actuate, producing a net force and torque (not necessarily equal to those commanded by the control law due to thruster noise) which act upon the satellite body. The dynamics block represents the change in state of the satellite body, which is measured by the SPHERES IMU, which contains accelerometers and gyroscopes. SPHERES also has external state estimation or global metrology sensors that receive beacon pulses from externally-mounted transmitters (beacons) and function in a manner similar to GPS [19]. Finally, the state estimator utilizes the sensor inputs (using an extended-Kalman filter [39]) to create a new estimate of the satellite's state. The loop then repeats.

In Figure 3-13, the grey blocks are implemented in the control code (in C) on-board the SPHERES satellite and as such, when the controller code is integrated into the Simulink model these functions are included into the simulation. The green blocks represent hardware components that had to be simulated in the Simulink model outside the controller software.

SPH-Halo-CMG Controller Design

Figure 3-14 illustrates the conceptual design used to extend the SPHERES controller software to command the CMG payload. The nominal controller logic was designed such that the CMGs are solely responsible for actuating attitude control and the thrusters are solely responsible for translation control. In the controller de-

sign, the mixer routes force commands to the thruster array and torque commands to the newly created CMG Payload actuator. This scheme was chosen due to its simplicity in implementation, as well as its utility as a stepping stone for expanding combined control research in the future, perhaps allowing for blended control implementations.

Changes made to reflect the addition of CMGs to the original control loop (shown in Figure 3-13) include the following: Starting at the Control Law block, the torque vector is now directed to the CMG actuators while the force vector is still directed to the thrusters; moving further around the control loop, the control torque vector feeds to a CMG mixer, which either commands a gimbal rate for each CMG (for the case of a custom steering-law) or a three-element torque vector (for the case of using the Honeybee Robotics Box-90 steering law built into the control board); the CMG payload receives the gimbal rate or torque commands and enacts a torque on the dynamics block. It should be noted that the thrusters still enact a torque on the dynamics block, due to residual torques from off-axis net forces. The elements discussed in Figure 3-13 then serve to close the control loop and provide control authority using the thrusters and CMG payload.

Because SPHERES utilizes a multi-threaded processing environment, it is somewhat incomplete to consider the controller from the simple control feedback loop described in Figure 3-13 or Figure 3-14. That is, the processing thread responsible for implementing the control loop (the control thread) operates in the manner described above, but several other processing threads are running concurrently with the control thread. In real-time controller design, the priority, data-access, and function of each thread must be considered to avoid potential data corruption or loss of real-time control. With this in mind, an expanded view of the control loop timing as it accesses data from and commands other threads is depicted in Figure 3-15.

In Figure 3-15, the control thread operates on a 5 Hz cycle, actively engaging with the metrology thread that logs IMU data at 20 Hz and Beacon data at approximately 5 Hz. To maintain the standard 1 Hz thruster control cycle on SPHERES while allowing CMGs to operate on a quicker cycle to maintain stability during translation tasks, the thrusters are only commanded every fifth cycle ($5 \text{ Hz} \div 5 = 1 \text{ Hz}$). Also,

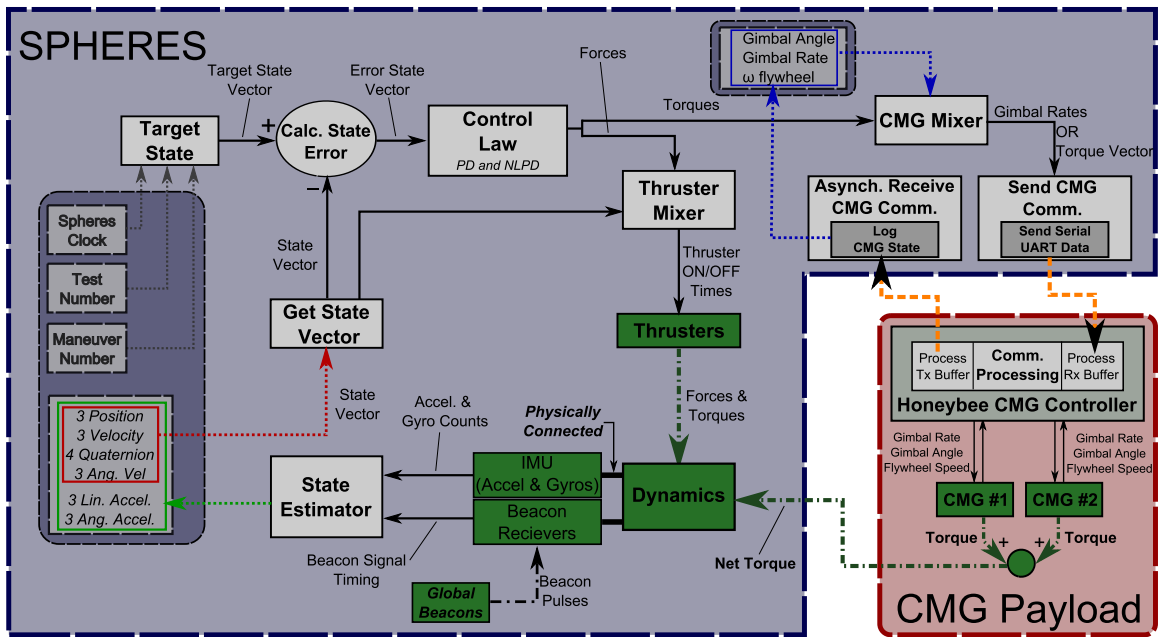


Figure 3-14: **SPHERES control loop with CMGs** *The conceptual illustration of the control loop on the SPHERES satellite, extended to command and interface with the CMG payload. This high-level design was used to guide the more detailed software design process. The blocks in grey are implemented in the controller software, while the green blocks are hardware components that had to be simulated. Image credit: Sam Schreiner, [1].*

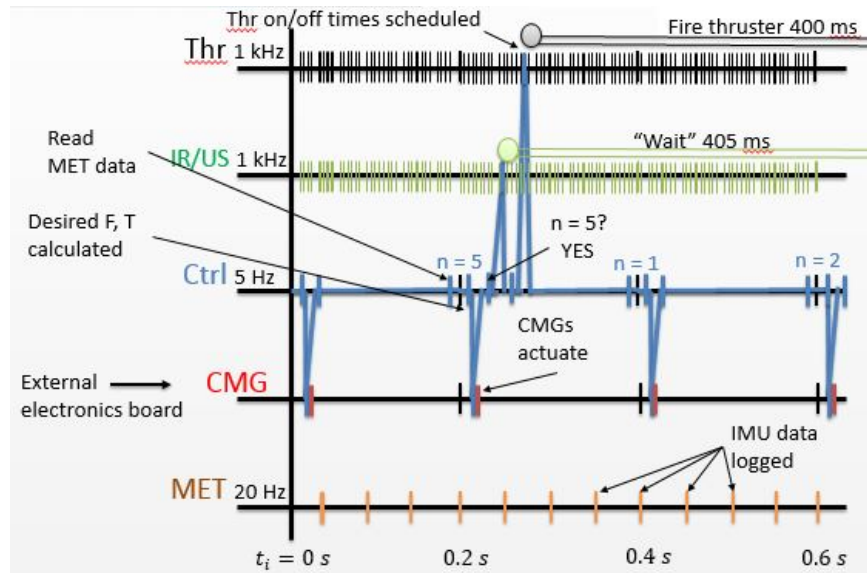


Figure 3-15: **Multithreaded scheduling for SPHERES control** *The action of a 5 Hz control thread (represented by a solid blue line) is traced; it first accesses data from the metrology thread, then commands the CMG thread (running on the CMG control board). On every fifth control cycle, the main 5 Hz control thread commands thrusters after first commanding the infrared/ultrasound (IR/US) thread to cease global metrology (used to locate the SPHERES within the experiment volume) in preparation for thruster actuation, which would interfere with US sensor operation.*

by maintaining thruster actuation at 1 Hz, adequate time can be provided for global metrology, which cannot function while the thrusters are firing due to the ultrasonic interference from the thruster noise [19]. The usual implementation of a 40% duty cycle (thrusters allowed to fire for 400 ms out of the 1 s control cycle time) for ground operations has been maintained for preliminary testing.

The control thread schedule as presented in Figure 3-15 is but one implementation method possible. In one of the cycles depicted, the controller first reads IMU data from the metrology thread and determines torque and force measurements to achieve the state commanded by the user. Following this, the controller commands CMGs to actuate and then checks to see if thrusters should be actuated to maintain a 5:1 ratio of CMG-to-thruster actuation (if the control cycle were instead chosen to be 10 Hz as mentioned above, this ratio would change accordingly). If thrusters are not to be fired in the cycle, nothing more is done; but if thrusters are to be fired, the command thread first commands the infrared/ultrasound thread to wait for a period of time

to ensure that thruster actuation doesn't interfere with global metrology. Following this, the controller provides thruster on and off times for the thruster thread, and then returns to await the beginning of the next cycle.

Alternate Controller Design for Attitude-Only Maneuvers

A different controller implementation has been envisioned for the upcoming Re-Flight Opportunity with NASA's Reduced Gravity Aircraft in August 2015. In this next flight opportunity, the pointing stability of thrusters only as compared with the use of CMGs will be tested. Because the time in microgravity is so limited on an RGA (usually 15-20 seconds per parabola), use of 1 Hz thruster firings with a 40% duty cycle may not result in distinct IMU readings for direct comparison with CMGs. That is, in order to best compare the performance of CMGs and thrusters in the limited time available during each microgravity parabola, the control authority of thrusters should be maximized.

Usually, global metrology provides information about the system's position in three-dimensional space. Since no translations will be executed during the upcoming Re-Flight Opportunity, the disadvantages of using metrology (i.e. limiting the duty cycle of thrusters) outweighs the potential advantages (i.e. additional information about relative orientation to supplement gyroscope readings). In addition to allowing thrusters to fire at any time, the control cycle has been shortened to allow for 10 Hz operations. Of course, this change is also in line with maximizing control authority that may be demonstrated within the limited window of microgravity afforded by the RGA. Finally, in order to better support 10 Hz control, IMU logging rate is increased from 20 Hz to 100 Hz. Because IMU data is collected at 1 kHz, using averaged values at 100 Hz does not pose a problem. Because no translation will be commanded, either thrusters or CMGs will be commanded at 10 Hz for attitude control. Using this implementation, there would be a 10:1 ratio between state estimation and CMG or thruster-only actuation. Table 3.6 lists the differences in control frequencies outlined in this section.

While the values in Table 3.6 correspond to control frequencies used in a CMG

Table 3.6: **Control Frequencies.** *Initial design values are used in preliminary simulations while the attitude-only design is implemented for the August 2015 Reduced Gravity Re-Flight Opportunity. Values correspond to CMG attitude control; for thruster-only attitude control, thrusters would fire at the frequency listed for CMG Command.*

Initial Design, for Position and CMG Attitude Control	
IMU Logging	20 Hz
Global Metrology	1 Hz
Thruster Command	1 Hz
Thruster Duty Cycle	40%
CMG Command	5 Hz
Alternate Design, for CMG Attitude-Only Control	
IMU Logging	100 Hz
Global Metrology	None
Thruster Command	None
Thruster Duty Cycle	100%
CMG Command	10 Hz

attitude control configuration, it is also necessary to test the system using thrusters only for attitude control to compare performance of the two system implementations. For the case that thrusters are used for attitude control, command frequencies for thruster attitude control would be equal to those listed for CMG control. That is, for the Initial Design, thruster commands would execute at 5 Hz as opposed to 1 Hz and CMGs would not be commanded; similarly for the Alternate Design, thruster commands would execute at 10 Hz as opposed to not firing at all, and CMGs would not be commanded.

3.2.5 SPH-Halo-CMG Simulation

A simulation was developed to design and test software in parallel with hardware. The simulation is built from an existing simulation of the SPHERES satellites (using thrusters only) previously developed by the SPHERES team for use in verifying test session flight software and in analyzing expected results from the ground laboratory, reduced gravity aircraft and the ISS. This simulation uses flight software written to run on the SPHERES processor (in C) and integrates that software into the Simulink simulation. This allows users to test flight software in its unaltered form in a high-

fidelity environment. Existing SPHERES software was extended to operate the CMGs as an additional actuator in the control loop. The implementation is based on the combined control concept of utilizing existing thrusters on SPHERES for translational control and CMGs for attitude control.

There were several high-level software objectives. The first objective of flight software for the SPH-Halo-CMG system is to create a simulation of the system by integrating a CMG actuator dynamics model within the existing SPHERES simulation. The simulation had to be flexible to enable the testing of multiple control schemes and allow users to implement operational flight software that may not include CMGs. After simulating a SPH-Halo-CMG system to demonstrate operation principles and to predict system performance, the primary objective became implementing flight software compatible with SPHERES, VERTIGO, Halo, and Honeybee CMG electronics to physically demonstrate the system's operation (for further information on this latter software objective, see Section 3.3.3 below).

Although the ultimate programmatic goal is to construct a system that uses CMGs to control all three rotational degrees of freedom, the initial software design focused on operating on the SPHERES air-bearing table test facility, to be later extended to simulating functionality of the SPH-Halo-CMG system in different testing environments and configurations. One reason for beginning with a simulation involving the air-bearing table test facility is that operations on the air-bearing table entail the control of only one rotational degree of freedom around the upward-pointing SPHERES-frame z-axis, rather than all three axes. Testing the software in this simpler configuration allowed for straightforward debugging and provided an avenue to directly test the software that will be used on the air-bearing table tests. It should be noted that although updated simulations are being developed for the August 2015 Reduced Gravity Re-Flight Opportunity, only preliminary simulations are described here.

The SPHERES simulation generates an animation of the satellite maneuvers to aid users in qualitatively evaluating the performance of their controller. Furthermore, the simulation logs several variables throughout the simulation, including the satellite

state vector, propellant usage, and thruster firing times. These variables allow users to quantitatively assess their control algorithm.

CMG Payload Simulation Design

The simulation was designed to replicate realistic communication interactions between the payload and the SPHERES controller. For instance, the simulation does not simply send a set of three numbers to the payload as a torque triplet command. Instead, the SPHERES controller converts the three values of the torque triplet to serial byte data and appends the appropriate communication protocols at the beginning and end of the message before sending the data across a simulated data bus. This includes adding the correct start byte, message ID, and message length identifier to the beginning of the message in order to accurately simulate the communications of CMG payload. This significantly reduced integration time required to establish serial communications with the physical hardware and served to improve the fidelity of the simulation at the same time.

A library of communication functions was written for the SPHERES simulation (mirroring communications software development for implementation on VERTIGO for physical demonstration) that allows a simulation user to send commands to CMGs corresponding to the following: requesting telemetry information from CMGs, enabling flywheel and gimbal motors, spinning up the flywheels, setting gimbal motor modes, gimbal angle and rate commands, sending torque commands, and setting a direction cosine matrix to inform the on-board Box-90 control law of the relative orientation of CMGs with respect to the laboratory frame. Given torque triplets or gimbal rate commands, the simulated CMG payload tracks the gimbal angle movement for a 2 CMG scissor pair. Gimbal angle prediction was not included on the SPHERES controller due to safety reasons. The appropriate manner to update the SPHERES' internal estimate of the CMG payload state is from feedback from the CMG payload (rather than predictive functions). Attempting to predict the state of an actuator works well under normal operating conditions, but can often lead to dangerous situations when the controller's model and the real state of the actuator

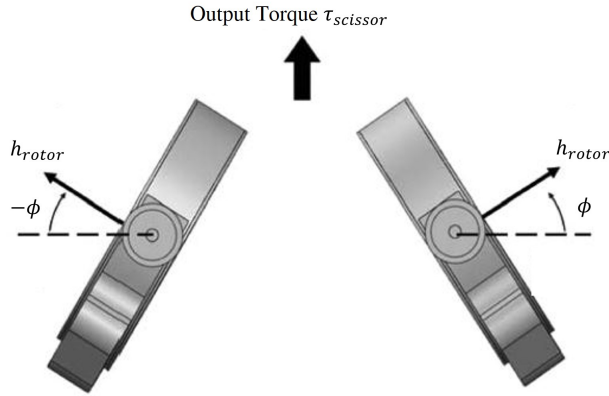


Figure 3-16: **Scissor pair diagram** A scissor pair CMG configuration generates torque $\tau_{scissor}$ about a single axis by constraining gimbal angles ϕ of the pair to be equal and opposite at all times, usually by mechanical means. Image modified from [9]

become significantly different [40].

A simple scissor pair array was chosen for the simulation primarily because of its simplicity and because of the transferability of information that might be gained from simulating this design. A scissor pair is composed of two CMGs with gimbal mechanisms tied to one another, usually mechanically [41]. In a scissor pair, CMGs are oriented such that the collective angular momentum of the pair is constrained to vary along a single line such that generated torques are constrained to a single axis. The maximum angular momentum and torque achievable by a scissor pair is $2h_{rotor}$ and $2\tau_{cmg}$, respectively; these values are less than the maximum angular momentum and torque achievable by both the pyramid array and the Box-90 array assuming the same CMG units are used to construct each type of array (though they are equivalent to the maximum values for the small axis on the Box-90 array - see Table 3.3). For more information about scissor pairs, see [6] or [9].

While simulating the pyramid configuration or the Box-90 configuration is ultimately desired to accurately estimate SPH-Halo-CMG performance, the decision to hold off on simulating them in detail within the context of SPHERES was made for several reasons. First, the Honeybee Robotics CMG electronics come hard-wired with a Box-90 control law that is proprietary; simulating the specifics of this control law to determine when singularities are approached, for instance, is thus not possible.

Second, a scissor-pair implementation is simple, and represents a lower limit of performance for a four-CMG array since the collective angular momentum and torque are less than the angular momentum and torque achievable with either the pyramid or Box-90 arrays about a single axis.

Furthermore, at the time that this first simulation was developed, Honeybee Robotics had offered to loan two TORC-H86 CMGs (similar to the CMG-120, except these are flight-quality with maximum angular momentum of 0.112 N m s and torque of 0.224 N m), lending more reason to simulate a scissor pair. With these considerations taken into account, a simulation utilizing a scissor pair composed of two TORC-H86 CMGs for single axis torque testing represents a useful first iteration of system simulation.

Numerous safety controls (pre-programmed onto the CMG controller by the contractor) were simulated as well. For instance, the payload will not generate a torque beyond 0.224 N m for each TORC-H86 CMG. For two TORC-H86 CMGs in a scissor pair, this means that the maximum torque generated by the payload was limited to $0.224\text{N m} \times 2 = 0.448\text{N m}$. Furthermore, the gimbal rates were limited to ≤ 2 rad/sec corresponding to TORC-H86 specifications [36]. The most important safety control to implement was the gimbal angle limits, which prevented the controller from actuating the gimbals into any null zones corresponding to singular surfaces. This was extremely important because the controller logic will normally generate extremely large, dynamically unstable oscillating gimbal rate commands near the null zones.

Simulation Results

After successfully modifying the existing SPHERES simulation to include CMGs, two different sets of maneuvers were simulated and analyzed. These simulations were used to compare the performance of the Sph-Halo-CMG system to that of the SPHERES system alone. It should be noted that the purpose of presenting these simulations is not to say they are perfect representations of their real-world analogues, but rather that they demonstrate how the simulation can be used to analyze the possible performance improvements from adding CMGs to a cold gas thruster system. The

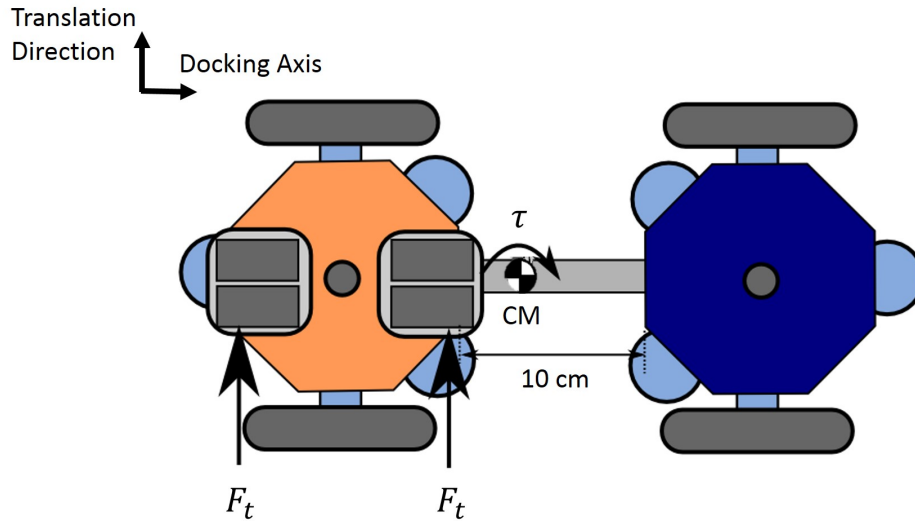


Figure 3-17: **Docked SPHERES configuration** *The active SPHERES satellite is to the left; when a translation burn is executed, a reaction torque is executed on the system since the system center of mass (CM) is off-set from the active SPHERES' thruster envelope. Force vectors corresponding to the active SPHERES' thruster locations are labeled to highlight this phenomenon. Image adapted from [1].*

first simulation represents the performance of the Sph-Halo-CMG system conducting a simple translation when a large external mass – in the form of a docked SPHERE satellite – is fixed to the system; the second simulation represents the performance of the Sph-Halo-CMG system alone conducting multiple maneuvers.

Docked SPHERES Maneuver The first considered scenario simulates the situation in which an active Sph-Halo-CMG system is docked to an inactive SPHERE satellite on the MIT SSL air-bearing table. This docked system, pictured in Figure 3-17, is commanded to translate in a direction perpendicular to the docking axis a distance of 0.5 m from the starting position. Because the center of mass of the system lies outside the active SPHERE satellite, linear translation without rotation requires an attitude control effort to counter induced torque on the system.

In order to compare the performance of combined CMG and thruster actuation as opposed to thruster-only actuation, the same maneuver is completed for both modes of operation, just as in the analysis conducted for the MAJIC system in Chapter 2. Quantitative values of interest are calculated and plotted by a MATLAB routine to

aid analysis. In particular, linear and angular position as well as linear and angular velocity as functions of time are plotted in addition to propellant usage and CMG gimbal angles for both modes of operation in the same test scenario. To supplement plotting results for trade analysis purposes, the same routine provides a preliminary indication of performance gains characterized by increased EVA times and mass savings that are enabled with CMG operation of a scaled system.

Not surprisingly, if the nominal position and attitude control algorithms are implemented with this new configuration, the thruster-only mode of operation fails to perform the maneuver as commanded and instead allows for the SPH-Halo-CMG system to enter into a spin resulting from the induced torque caused by the new center of mass of the system; the combined control mode of operation, by comparison, successfully performs the maneuver. By increasing the positional and especially the attitude controller algorithm gains for the thruster-only mode of operation, performance can be improved at the expense of fuel consumption, enabling a successful maneuver. Importantly, though, there is a limit to the increase in performance possible tracing back to the limited duty cycle of the gas thrusters of SPHERES.

Figure 3-18 corresponds to the docked SPHERES configuration simulation trials in which an active SPH-Halo-CMG system docked to an inactive SPHERE is commanded to translate 0.5m along a line orthogonal to the docking axis. Each plot contains six subplots: from left to right, top to bottom: linear position, angular position, linear velocity, angular velocity, propellant usage, and gimbal angle (or CMG Usage) for the SPH-Halo-CMG system (blue dashed line) and the SPHERES thrusters-only system (red solid line) as functions of time.

The plots in Figure 3-18 correspond to the best performance attained in simulation by a jets-only operation as compared with the best performance of a combined (CMG+jets) mode of operation. A non-linear PD control law was implemented with gains varying from 1-300. While both achieved similar linear translation performance as can be seen by the plot in the top-left of Figure 3-18, the attitude error³ varies

³Recall that the attitude error for this SPHERES simulation is defined to be in the plane of rotation only.

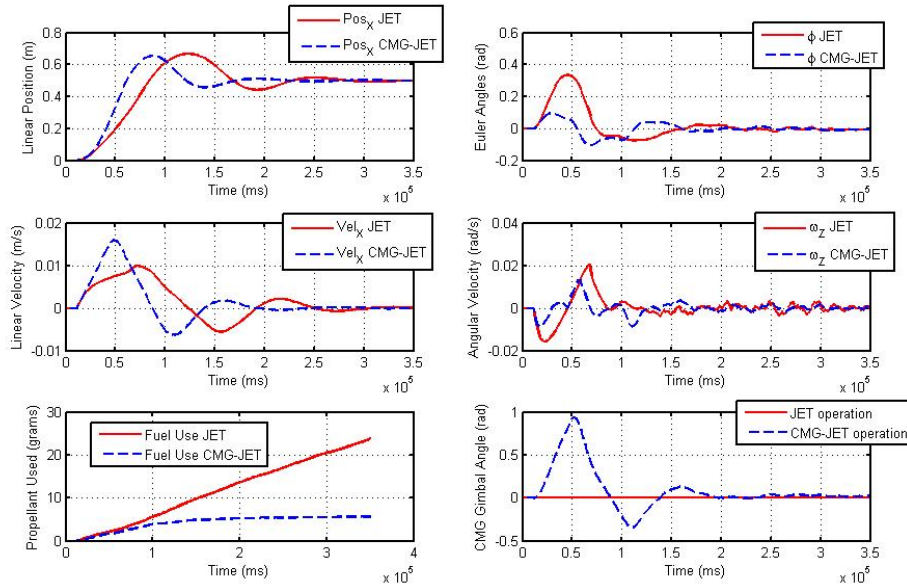


Figure 3-18: **Performance plots for Docked simulation.** *Top Left: Linear position (m); Top Right: Attitude error (rad); Mid Left: Linear velocity (m/s); Mid Right: Angular velocity (rad/s); Bottom Left: Fuel consumed (g); Bottom Right: Scissor pair gimbal angle (rad). Graphs from 16.851 final report [1].*

between the case of thruster-only operation and combined control indicating a clear performance increase for the case of combined control. In particular, at 0.5 seconds into the test during the translation burn, the thruster-only system accumulates an attitude error of 0.3 radians (17.2 degrees) while the CMG-integrated system accumulates only 0.1 radians (5.7 degrees), representing an improvement factor of 3 in attitude stability. This can be seen in the top-right of Figure 3-18. In addition to improving the attitude stability of the SPH-Halo-CMG + SPH docked system, the fuel consumption is reduced dramatically for the case of combined control as may be expected - in this case, by 76% (see the bottom left of Figure 3-18).

Astronaut EVA Maneuver The second set of planar maneuvers was intended to represent an astronaut conducting an EVA servicing mission to two different locations on the International Space Station. Figure 3-19 depicts the maneuver, in which the SPHERES satellite (the simulated astronaut) moves out to one node and conducts some maintenance activity that requires rotation (specifically, a rotation of 45 degrees

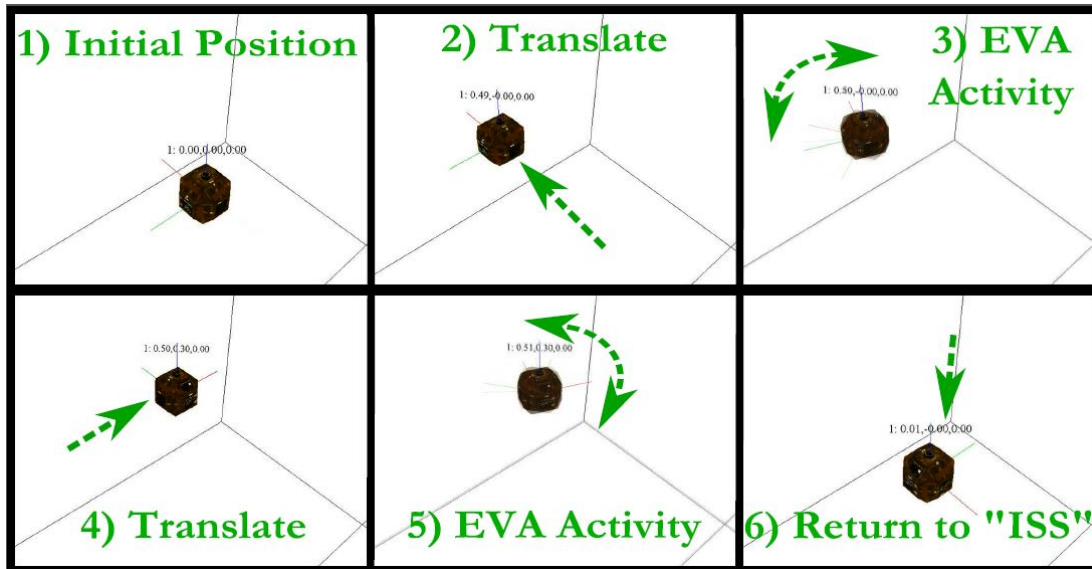


Figure 3-19: **Astronaut EVA maneuver with SPHERES** A series of screenshots depicting a maneuver designed to imitate an astronaut conducting EVA maintenance activity at two different locations. This animation is quantitatively assessed in Figure 3-20. Images from 16.851 final report [1].

in one direction followed by a rotation of 90 degrees in the other direction). Next, the astronaut moves to a second node and conducts the same rotation sequence. Finally, the astronaut returns to the airlock and turns 45 degrees to correctly orient him/herself to reenter.

As described above, a MATLAB routine was written to plot some of the quantitative data from the simulation, such as the linear and angular position, as well as the linear and angular velocity. To aid in the trade-off analysis, propellant usage and CMG gimbal angles are also plotted. These two metrics gave us insight into how much the controller was using the thrusters and CMGs. All of these variables were plotted for a combined control simulation as well as a simulation of a thruster-only control mode in Figure 3-20.

In Figure 3-20, the combined CMG-thruster system (*CMG-JET*) displays more precise performance in its angular position and velocity just as in the translation case. In addition, propellant savings achieved when using CMGs for attitude control are perhaps more clearly visible from the plots in Figure 3-20. In the case of this particular maneuver, a 39% reduction in fuel usage was observed.

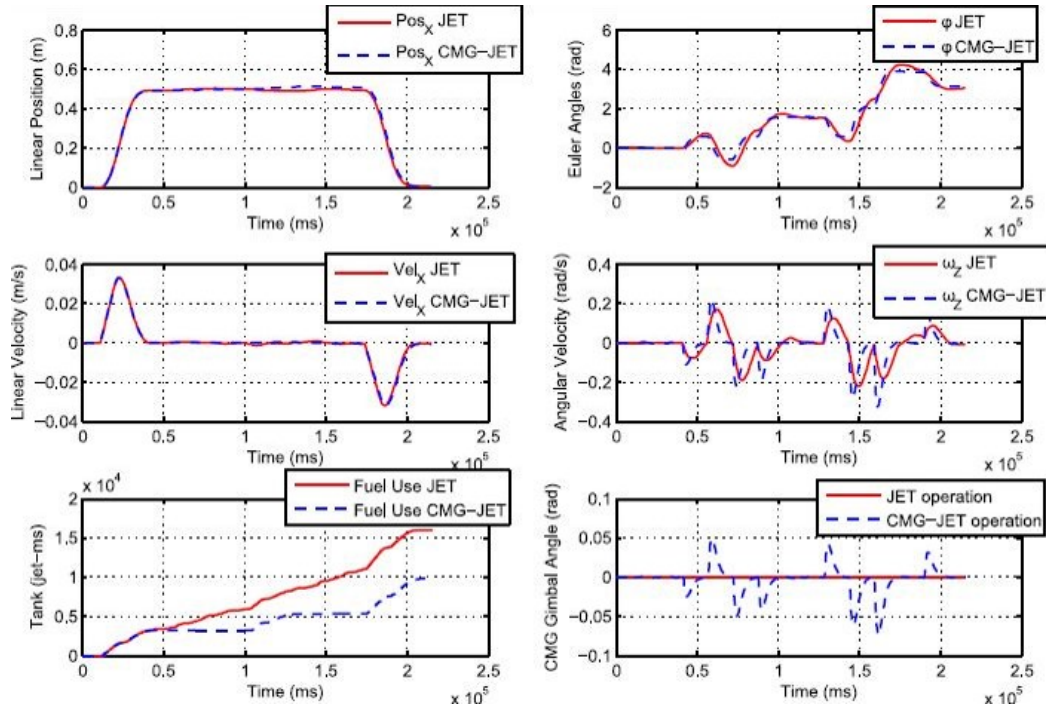


Figure 3-20: **Quantitative results for EVA astronaut maneuver with SPHERES** From left to right, top to bottom: Plots of the linear position, angular position, linear velocity, angular velocity, propellant usage, and scissor pair gimbal angle (or CMG Usage) for the combined control system (blue dashed line) and the thrusters-only system (red solid line). Graphs from 16.851 final report [1].

After conducting SPHERES simulations for both the Docked and Astronaut EVA scenarios, confidence was gained in the proposed system design. The following sections describe the integration and operations efforts leading to the physical demonstration of these mission scenarios. An updated simulation is under development that includes specifications for the CMG-120 actuators and 3-DoF rotation control (still with a scissor pair) for closed-loop operations with a flight configuration for the upcoming August 2015 Reduced Gravity Re-Flight Opportunity.

3.3 SPH-Halo-CMG Integration

This section includes details related to the mechanical, electrical and software integration efforts to realize the design outlined in Section 3.2. Several changes to proposed designs were necessary partly because of misinformation provided by Hon-

eybee Robotics (the CMG-120 was at the time of the project outset only a laboratory bench engineering model with poorly documented properties), and partly because of overlooked details of the system that only became readily apparent upon closer inspection. Integration activities described in this section were conducted by the author of this thesis along with the support of several undergraduate MIT students that took part in the Spring 2014 MIT 16.831 course and in MIT's Undergraduate Research Opportunity Program (UROP).⁴

3.3.1 Hardware Integration

Unforeseen Hardware Problems and Design Changes

Initial computer-aided design (CAD) models provided by Honeybee Robotics that were used for design studies included in [1]) and described in Section 3.2.2 did not completely match the physical CMG-120 actuators acquired. First, the initial CAD provided did not include a connector; we were informed of the connector's planned positioning but not of the specific dimensions. Second, the initial CAD included a protruding structure for what we were told was to be the slip-ring to enable full 360 degree rotation of the gimbal mechanism. Ultimately, this protruding structure was not included in the final design.

Despite the differences in the physical design of the CMG actuators, the enclosure design pictured in Figure 3-3 developed for the initial CAD model were found to be sufficient to enclose (without impeding) the physical actuator dimensions. To test this design, plastic enclosures were 3D printed and tested with the actuators. Although the covers indeed worked, there were several problems that were noticed quickly: first, there was no way to visibly check to see if the CMGs were oriented as telemetry suggested; second, the structure intended to hold the screws of the enclosure in place were found to be weak and prone to fracture. Finally, the spaces intended to allow

⁴James Krasner, Matthew Abel, and Nathan Miller provided support as CMG subsystem team members through the Spring 2014 16.831 course; Jose Gomez and Isaac Garza provided support as Summer 2014 UROPs in preparation for the August 2014 Reduced Gravity Flight Opportunity with NASA; Jose Gomez continued as a UROP for the CMG subsystem in the Fall of 2014 and Spring of 2015; Jacob Shearman provided subsidiary support for part of the Spring 2015 UROP period.

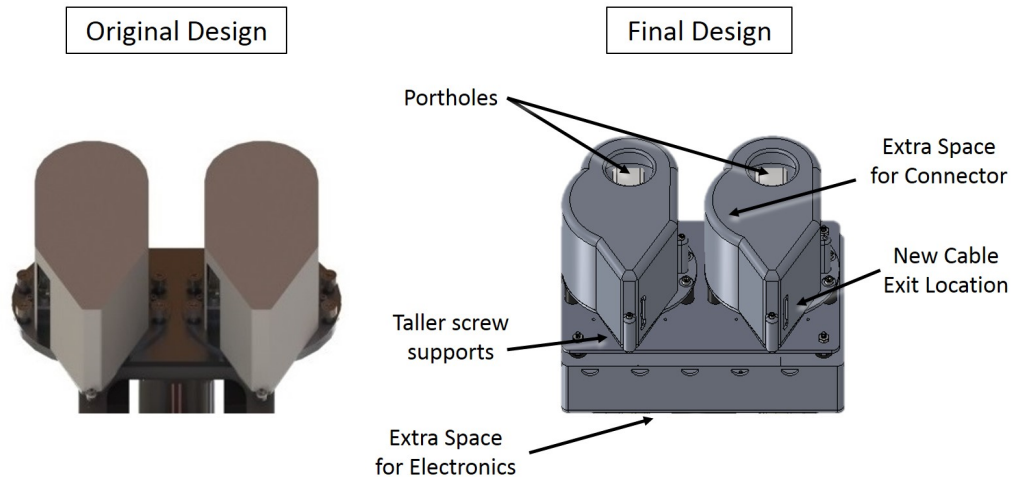


Figure 3-21: **Initial and updated designs for CMG enclosures and electronics housing.** *Left: The initial CAD model from Fall 2013 [1]; Right: The final, manufactured version.*

cables to enter the enclosure were not practical: they were very large which allowed for dust particles (or fingers) to enter the enclosure, and they were placed in such a way that the cables were strained unnecessarily.

Figure 3-21 depicts the original and final CMG enclosure and electronics housing designs. The enclosures were manufactured by ProtoLabs and funded by Draper Laboratory. The final version features a clear port-hole made of high-impact polycarbonate. Because the flywheel encoders (used to determine flywheel rates) are electrostatic discharge (ESD) sensitive and prone to complications with the introduction of dust, a priority for the enclosure was to minimize chance for dust to enter. In order to address this as well as the fact that the original placement of a cable pass-through caused excessive cable strain, the cable exit location was moved to the opposite side of the enclosure and made to be a small, grommet-fitted circular hole. The connector side was enlarged to enable the cable to have a large radius of curvature. Next, screw supports were made taller to eliminate the weakness identified in the original design. Finally, the electronics were given more space for cables to have ample room to ensure large radii of curvature to reduce strain, and also because a custom printed circuit board (PCB) was required to interface Halo with the Honeybee Robotics electronics. For more details about the PCB required, see Section 3.3.2.

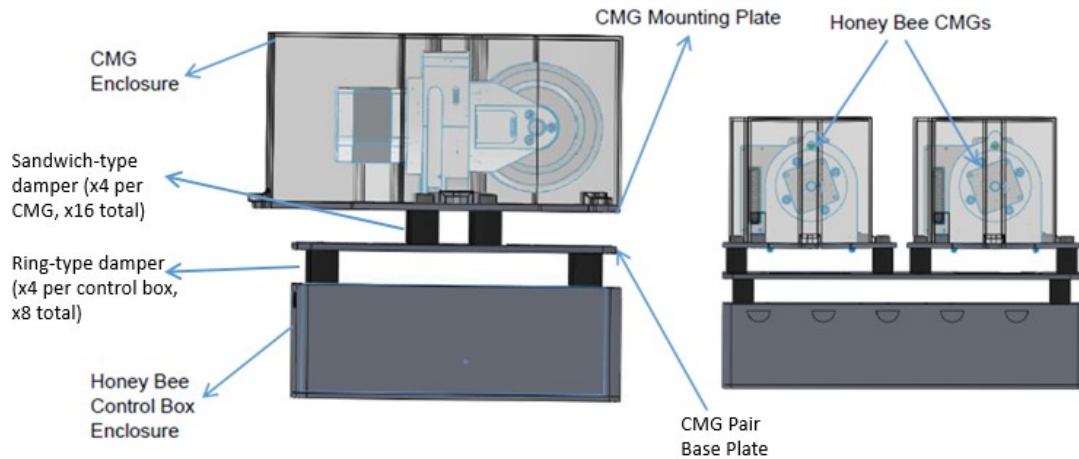


Figure 3-22: **Final damping solution for CMGs.** *A double-damping solution was arrived at as the preferred option for reducing vibrations induced on the Halo structure from improperly balanced CMGs. Ring-dampers were used to interface the control electronics box (and Halo) with a base plate; a set of sandwich-style dampers then separate the CMG enclosures from the base plate.*

In addition to these changes, one further change to the original mechanical design was deemed to be necessary after Hardware Acceptance testing with the CMG-120 actuators.⁵ Specifically, when first received from Honeybee Robotics, the CMGs exhibited significant vibrations while spinning at a nominal 6000 rpm. The vibrations were so large in magnitude and varied across the different CMG actuators that characterization testing with wireless accelerometers was conducted in order to report back to Honeybee. Because it was uncertain whether Honeybee Robotics might be able to eliminate the vibrations, a damping solution was determined to be necessary. After testing various options for including damping structural components to the mechanical assembly, a final implementation that resulted in the least amount of vibrations was settled upon as the final structural design. Figure 3-22 depicts the final design, which included the use of four sandwich-style rubber dampers to be used on each CMG actuator, with four additional loop-style rubber dampers to be mounted in between the CMG pair base plates and the electronics boxes.

⁵Hardware Acceptance testing involved operating all four CMGs with a Honeybee Robotics GUI in order to ensure that all functions of the CMGs were operable including mode-switching, flywheel and gimbal motor actuation.

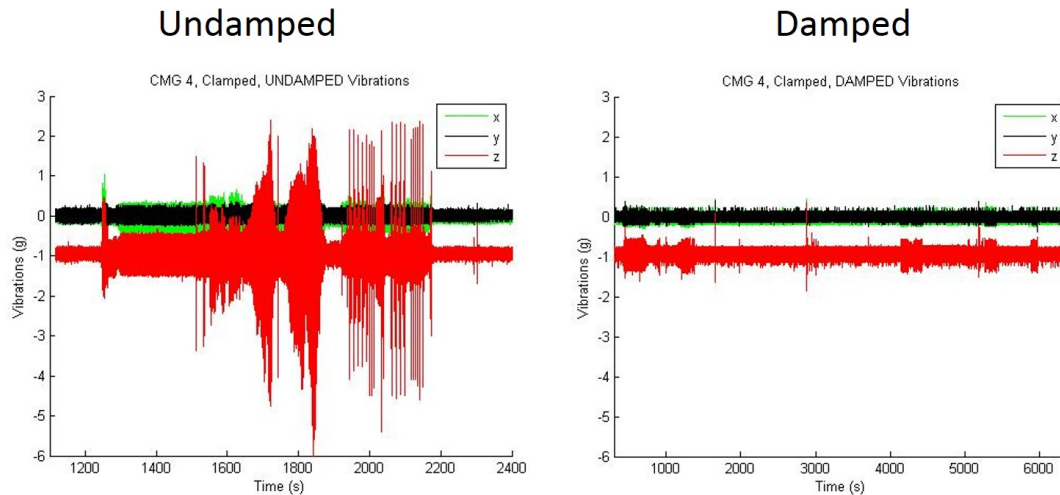


Figure 3-23: **Vibration profile for undamped and damped mechanical assemblies, worst case vibrations.** *Left: Accelerometer readings for the undamped, worst-case CMG-120. Right: Accelerometer readings for the same CMG-120 actuator stood-off with the damping solution depicted in Figure 3-22.*

Figure 3-23 depicts the vibration profile recorded with Axivity wireless 3-axis accelerometers [42]. During these tests, the wireless accelerometers were affixed to the lab bench worktable and so the measured accelerations of ± 4 Gs represents the shaking of the entire lab bench with an acceleration of more than four times the acceleration of gravity. Ultimately, other anomalies detected with flywheel rate tracking and gimbals rate telemetry logging, coupled with excessive vibrations caused the Draper and MIT team to return the CMG-120s to Honeybee for a refurbishment. Replaced hardware not only included new flywheels, but also upgrades to the electronics board and flywheel encoders.

Structural Analysis for Reduced Gravity Flight

⁶ A structural analysis was performed to ensure that a positive margin of safety is maintained on all load bearing components of the CMG array subassembly. The goal of the analysis was to verify positive safety margins with respect to the minimum required factor of safety of 2.0. All screws and fasteners were analyzed for tension and

⁶This structural analysis was conducted by Jose Gomez and Isaac Garza under the supervision of the author of this thesis in preparation for the August 2014 flight opportunity.

shear according to NASAs Preloaded Joint Analysis Methodology for Space Flight Systems Technical Memorandum (NASA-TM-106943) [43]. Maximum loading of 2 Gs is analyzed for the free-floating configuration and a maximum loading of 9 Gs in the aircraft forward direction is analyzed for the takeoff and landing configuration. This analysis was included in the Technical Equipment Data Package for both the August 2014 and upcoming August 2015 Flight Opportunities.

In addition to verifying all structural and fastener components meet the minimum safety margins, an analysis for the CMG enclosures was conducted in order to ensure that even in the worst failure event, Flyer safety would be maintained. The worst-case failure event assumed was a scenario in which a flywheel fractured and detached while spinning at the nominal 6000 rpm. If all the rotational kinetic energy stored in the flywheel's rotation were deposited in the enclosure wall during an impact event lasting 0.1 seconds across an area of $0.25 \text{ cm} \times 0.25 \text{ cm}$, analysis showed that a margin of safety was indeed maintained both for the aluminum and shatter-proof polycarbonate port-holes.

On-board the Reduced Gravity Aircraft, one CMG actuator enclosure was tested for integrity during a real failure event. Luckily, the previously-conducted analysis for safety was validated. One of the CMG-120 flywheels detached from its mechanical interface while spinning at 6000 rpm during the final flight. When this occurred, the enclosure contained the spinning flywheel for the remainder of the flight until the broken pieces could be removed after landing. It should be noted that the flywheel did not shatter as in the worst-case scenario used to inform enclosure design but instead only detached whole from its mechanical interface.

After the flywheel detachment event on the August 2014 Flight Opportunity, Honeybee Robotics updated the mechanical design of the CMG-120 actuators and returned refurbished units that were not only attached in a more robust manner but also more precisely machined for balancing (previous re-balancing efforts included attaching aluminum tape and small weights). Unfortunately, the units that were returned cannot operate at the previously nominal 6 krpm but instead operate at 5.4 krpm, most likely having to do with maintaining flywheel balance with a new mechan-

ical design⁷. Because the flywheel inertias have remained constant, this reduction in flywheel rate corresponds to a reduction in angular momentum capacity by 10% as well as a reduction in torque capacity by 10%.

3.3.2 Electrical Integration

Another difficulty encountered during integration involved power management and distribution through Halo expansion ports. Because Halo development ran parallel to CMG subsystem development, there were many opportunities for integration to go awry; luckily there were few problems except for one: the electrical design for interfacing PCBs between Halo and CMG electronics did not allow for enough current to flow out of a single Halo expansion port to power all CMGs; an update to the electrical system design was necessary to allow for power distribution through two Halo ports instead of just through one Halo port. In addition to the problem of providing power to the CMG electronics, there were issues encountered with the initial PCB design to convert between Halo USB signals and CMG RS-422 signals.

Over the course of the Fall of 2014 and the Spring of 2015, a new design was completed by Jose Gomez under the supervision of the author of this thesis and Danilo Roascio, the SPHERES lead scientist and resident post-doc. Figure 3-24 shows the updated schematic of the circuit board, with key components labeled. The 50-pin connector receives both power and USB data from Halo; for the primary PCB, power is directly passed to the voltage regulator, while for the secondary PCB (used only to get extra power from a second Halo expansion port), power is passed across four lines through the PCB-to-PCB connector to be delivered to the primary PCB's voltage regulator. The USB to UART RS-422 integrated chip (FT232R, chip U1 in Figure 3-24) converts the signal protocol between Halo's USB and the CMG control board's RS-422, and the Texas Instrument dual differential driver and receiver (SN65C1168E,

⁷This probable reason is one proposed by the author of this thesis and not by Honeybee Robotics; information provided from Honeybee only consisted of the fact that a new flywheels and a flywheel-to-motor mechanical interface was implemented, and that with the new set-up only 5400 rpm could be reliably maintained. Because of previous issues with a flywheel encoders required to measure flywheel rates for closed-loop flywheel rate control, the hardware update may not be the only factor in the flywheel rate reduction from 6000 rpm to 5400 rpm.

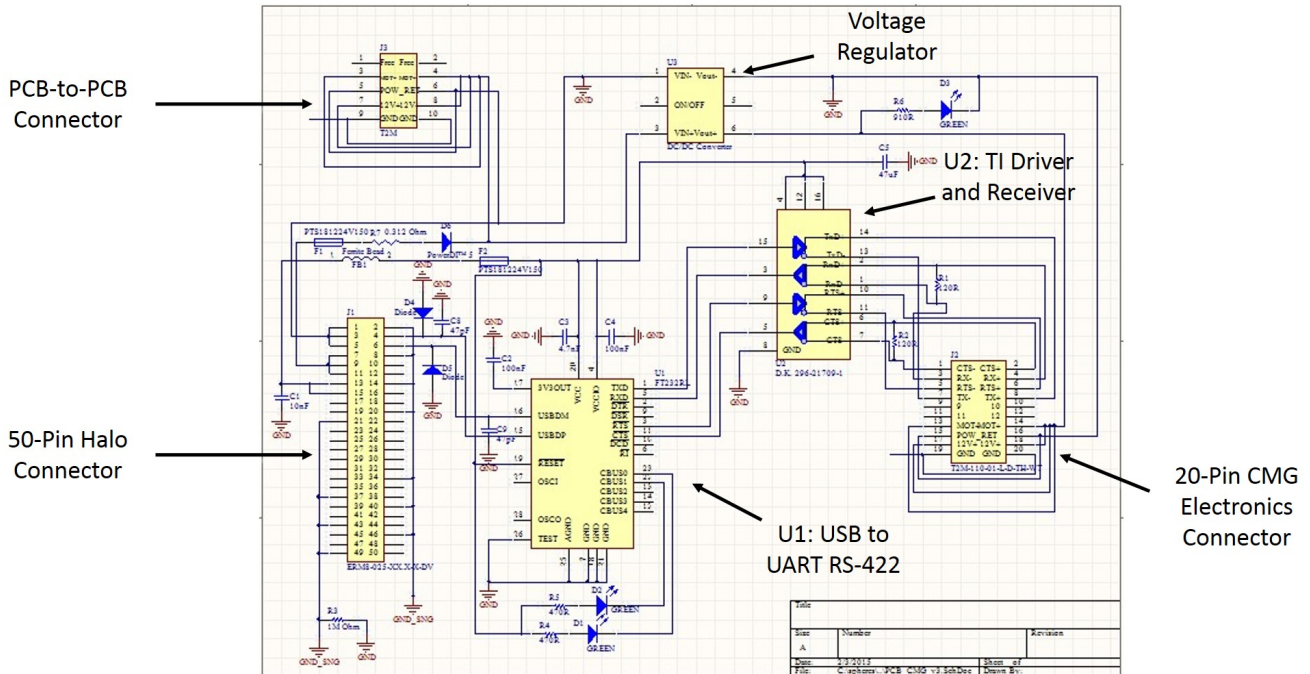


Figure 3-24: Schematic of the Halo-to-CMG printed circuit board. Major components have been labeled.

chip U2 in Figure 3-24) converts the voltage levels appropriately. Finally, the signal is passed to the CMG electronics through the 20-pin Samtec connector.

The newly-designed circuit board was then tested for power distribution using a dual laboratory power supply to ensure that the CMG electronics' 12 V could be maintained over a range of input voltages from Halo corresponding to low (10.0 V) to high (11.1 V) battery charge, and second when all four CMGs are connected and drawing maximum current (during spin-up and during maximum gimbal rate maneuvers). Data conversion was tested by attaching a USB cable to the signal lines that would normally be accepting USB lines from Halo, and the USB to UART RS-422 integrated chip (U1 in Figure 3-24) was tested with a loopback and the Windows program Realterm to ensure successful implementation. Following this, the dual differential driver and receiver (chip U2 in Figure 3-24) was tested with a loopback and Realterm to ensure that the addition of this IC did not interfere with signal conversion, and also with a voltmeter to ensure that this IC successfully converted USB voltages to RS-422 voltages.

3.3.3 Software Integration

Accomplishing the objectives of software integration includes deciding how to manage processing: should SPHERES conduct all control processes and handle all CMG commands while VERTIGO and Halo serve only as pass-throughs? Or should some of that responsibility be handled by the VERTIGO Avionics Stack? Because SPHERES has a well-established architecture to process IMU measurements and execute control algorithms, these processes were maintained on SPHERES (though of course with the changes to the mixer to accommodate combined control as discussed in Section 3.2.4 and pictured in Figure 3-14).

In the concept of operations for closed-loop control using Honeybee Robotic's Box-90 steering algorithm, then, SPHERES passes torque commands to VERTIGO, which then translates these commands into that which can be understood by the CMG control electronics. Honeybee's Box-90 steering law converts these torque commands into gimbal rate commands given knowledge of current gimbal angles and the assumed orientation of CMG actuators. Telemetry data is passed back to VERTIGO and stored for post-processing, while key information from that telemetry is passed back to SPHERES for display on a laptop GUI. Key telemetry data includes gimbal position and gimbal position command, gimbal rate and gimbal rate command, flywheel rate and flywheel rate command, gimbal mode, gimbal encoder status and flywheel velocity control loop status; the display of these values is intended to inform a human controller of the real-time state of CMGs in order to better assess anomalies should they occur during operations. This framework for software implementation is pictured in a block diagram in Figure 3-25.

In addition to the operations pictured in Figure 3-25, the VERTIGO Avionics Stack also provides commands to CMGs that mediate initialization procedures including gimbal homing (in order to initialize the gimbal position sensor encoder), flywheel spin-up, CMG orientation setting (with use of a direction cosine matrix) and initial CMG gimbal positioning (in order to afford a large controllability when operations commence). A library of functions for communications with the CMGs has

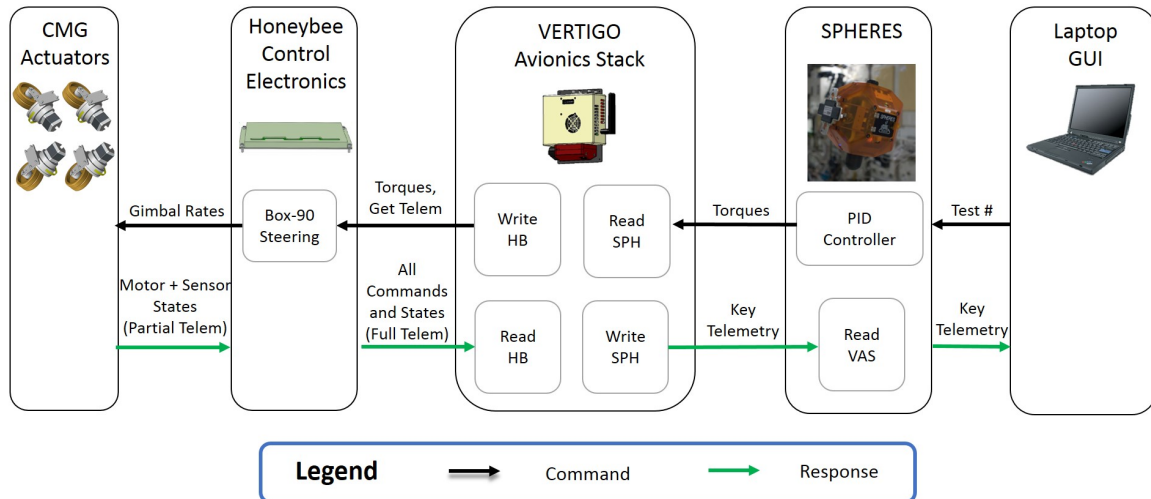


Figure 3-25: **Block diagram of software implementation.** *SPHERES* manages a control algorithm that determines requested forces and torques; forces are passed to thrusters (not shown) and torques are passed to *VERTIGO*, which converts the *SPHERES* torque command to a command the *CMG* electronics can interpret. Telemetry data from *CMGs* is stored on *VERTIGO* for post-processing, while key information such as flywheel rates, gimbal angles and gimbal rates are passed to *SPHERES* for display on the controller’s laptop *GUI*.

been implemented in *VERTIGO* software and integrated with existing Halo software written to operate peripherals attached to Halo ports.

3.4 SPH-Halo-CMG Operations

Thus far, SPH-Halo-CMG operations have been limited as the focus of research has been on fully integrating the system to a state in which closed-loop control operations is possible. Ultimately, the objective of executing torque maneuvers with *SPHERES* commands in a free-floating configuration was not achieved during the August 2014 Flight Opportunity. Even so, open-loop torques with a tethered configuration, commanded by a laptop were successfully conducted and slew rates of 1 deg/s to 49 deg/s were observed [22]. In addition to this past Flight Opportunity, operations of the *CMG* subsystem in the laboratory have yielded valuable results. Open loop torques on a fixed, 1-DoF rotation stand and on a fixed, 3-DoF rotation stand have established the functionality of *CMGs* in the context of *VERTIGO*-compatible

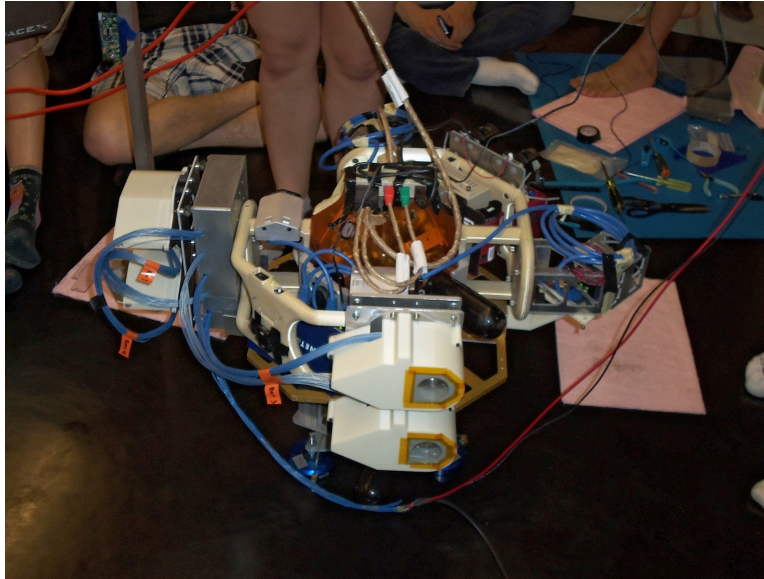


Figure 3-26: **The INSPECT configuration at the end of the undergraduate course 16.831 in the spring of 2014.** *Inspection operations on the MIT SSL's flatfloor facility were demonstrated with this partially-integrated INSPECT system; at the time of this photograph, CMGs are being commanded not by SPHERES but by an external laptop.*

driving software. Open loop torques executed on the 3-DoF stand have validated the direction cosine matrix used and provide confidence for future closed-loop trials on the glass table and on the upcoming August 2015 Re-Flight Opportunity. Full characterization of the array awaits demonstration of full integration with a central SPHERES satellite with inertial measurement unit logging in a microgravity environment.

As previously mentioned, NASA has granted the Draper-MIT SPHERES collaboration another opportunity to test the SPH-Halo-CMG configuration on-board their Reduced Gravity Aircraft. On-going testing in the Space Systems Lab will ultimately result in an operable system for this flight opportunity. This will hopefully result in the ability to draw concrete conclusions for a comparison between thruster-only control and combined thruster and CMG control for the SPHERES facility and for related research projects including MAJIC and proposed manipulator and inspection spacecraft.

3.5 SPH-Halo-CMG Utility Analysis for the SPHERES Simulation Results

As in the MAJIC study of Chapter 2, the question remains for the SPH-Halo-CMG system as to whether increased platform stability, a reduced risk of thruster gas impingement on sensitive work stations, and decreased propellant consumption outweigh the increased complexity and mass requirements incurred with the addition of CMGs. Although this trade study would most greatly benefit from hardware demonstration results of closed-loop operations expected to be conducted soon, a high-level, first-order trade study of the SPHERES facility with and without CMGs was conducted in [1] using the SPHERES simulation results described in Section 3.2.5.

3.5.1 Mission Duration Increase

The clearest, most transferable result from the simulation study presented in Section 3.2.5 is that a CMG integrated system uses less propellant than the thrusters-only system, though there is also quantifiable evidence for increased attitude stability afforded by the CMG integrated system. This further bolsters the findings of the MAJIC study described in Chapter 2, which concluded that a CMG integrated EVA maneuvering unit could feature improved fuel economy and attitude stability with the addition of CMGs. The analysis conducted here first assumes the same amount of SPHERES tanks are available at the ISS or in the laboratory and instead the variable that changes is the total test time that those tanks might afford; next, an investigation into the mass that might be conserved is conducted much like the MAJIC utility analysis that concerned mass cost estimates.

The mission duration capability $T_{mission}$ is calculated by determining how long the given maneuver could be repeatedly carried out before exhausting the SPHERES

propellant tank:

$$T_{mission} = \frac{\text{Tank Capacity (172g)}}{\text{Propellant for 1 maneuver}} \times T_{Maneuver} \quad (3.1)$$

where $T_{Maneuver}$ is the time to complete 1 maneuver. Comparing these calculations for the thrusters-only and combined CMG-thruster systems, the 16.851 team observed a 325% increase in mission duration from 0.7 hours to 3.0 hours for the Docked SPHERES maneuver and a 64% increase from 2.3 to 3.8 hours for the astronaut EVA maneuver (see Table 3.7). For both cases, batteries with large enough energy capacity are assumed to be used such that propellant limits mission time as opposed to CMG battery life.

3.5.2 Preliminary Mass Trade Analysis

In addition to the mission duration analysis, a preliminary mass trade-analysis was conducted. The first step was to calculate the mass of propellant saved by using CMGs rather than thrusters for rotational commands. Figure 3-27 shows the amount of propellant used in the analogue EVA maneuver simulation for the thrusters only (red solid line) and for the integrated thruster and CMG controller (blue dashed line). To calculate propellant used, the cumulative thruster-open time was multiplied by the mass flow rate of the thrusters. There are several mass flow rate numbers in the literature. Chen (2002) [44] empirically determined a mass flow rate of 0.378 grams/sec for a single thruster open, while a SPHERES technical document determined a value of 0.174 grams/sec (per thruster) with all 12 thrusters open. Because our trade study was first-order, we simply used the average of these two values for our final mass flow rate (0.276 grams/sec). The propellant mass saved for both the astronaut EVA maneuver and the SPHERES docked maneuver is listed in Table 3.7.

Additionally, if the system could be designed to carry less propellant due to the integrated CMGs, this would also lead to a reduction in tank mass. To estimate this mass savings, the effective tank mass used in the thrusters-only system was estimated as the original tank mass (440 grams) times the mass fraction of propellant

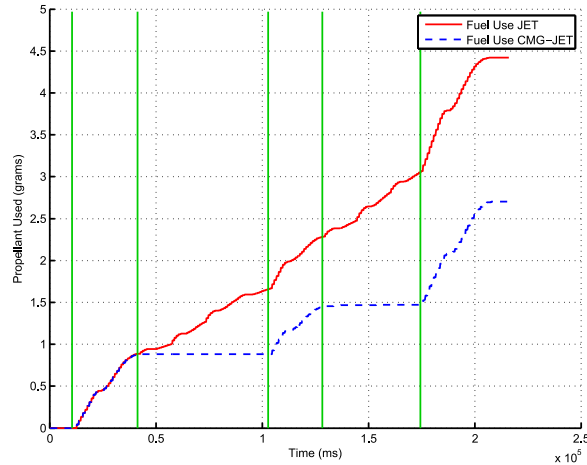


Figure 3-27: **Propellant consumption for the SPHERES-simulated astronaut EVA maneuver.** *The propellant used to conduct a simulated astronaut EVA maneuver using the SPHERES satellite with thrusters as the only actuator (red solid line) and with the combined thruster and CMG actuators (blue dashed line). This comparison clearly outlines the fuel saved by using CMGs to augment thruster actuation. The green vertical lines indicate the beginning and ending of maneuvers corresponding to Figure 3-19.*

used in the simulated maneuver (4.4 grams used/ 172 grams total for the astronaut EVA maneuver, 5.6 grams used/ 172 grams total for the docked maneuver). This resulted in a tank mass estimate of 11.3 grams needed for the thrusters-only actuated SPHERES to complete the astronaut EVA maneuver. The same calculations used on the combined CMG-thruster system resulted in a required tank mass of 6.9 grams. The propellant tank mass saved by adding CMGs is also listed in Table 3.7.

Each TORC-H86 CMG weighs 0.6 kg and the CMG controller board weighs 0.7 kg, for a total of 1.9 kg for the entire CMG scissor pair payload. As mentioned before, if this mass were simply compared to the propellant mass savings (a few grams), the trade-analysis would conclude that CMGs are not feasible. However, this comparison is not appropriate: in the EVA maneuver described in Figures 3-19 and 3-20, the CMG gimbal angle reached a maximum absolute value of 0.072 radians, which is 4.6% of its maximum value of $\pi/2$ radians. Similarly, the average absolute gimbal rate was 0.0037 rad/sec, which is 0.19% of its maximum value of 2.0 rad/sec. These two values show that the CMG payload is underutilized by a significant factor, thus explaining why the mass of the CMG payload considerably outweighs the propellant

mass savings.

For a fair comparison of the two options, the mass of the CMG payload was scaled down according to the gimbal angle usage to provide a better estimate of the true CMG payload required. That is, during the EVA maneuver the gimbal angle only reached 7.2% of its maximum value. This means that only 7.2% of the angular momentum envelope was utilized, so if the flywheel was 7.2% of its current mass, the CMG payload could have still performed adequately. The scaled-down mass is presented in Table 3.7.

Similarly, the CMG power usage had to be scaled down. Due to the complex nature of power consumption, we used the same scaling factor as described in the previous paragraph (momentum envelope utilization) as opposed to more sophisticated factors that would also account for average gimbal rate usage. This was done because this scaling factor was the most conservative measure. Scaling down CMG power resulted only 0.30W of the original 4W being ‘utilized’. This value was used as the average power consumption throughout the test session to generate the total energy used by the CMG payload (62.05 J). The total energy consumed by the CMG payload was used to calculate the battery mass needed using typical energy density values for Lithium-Ion batteries. Using a specific energy of 130 Wh/kg as in the MAJIC study, an additional battery mass of 0.13 grams is required to support the CMG payload for this maneuver.

To reiterate, these calculations are only intended to provide an extremely rough estimate of the mass and power trade-off between the thrusters-only system and the combined CMG-thruster system. The scaling factors include many assumptions that are likely only true as first-order estimates, if that.

As can be seen from Table 3.7, the mass trade analysis for a single mission may not support the addition of CMGs, but over the course of several missions, the greater fuel economy of the combined control system will ultimately save mass-cost. Equivalently, if the total amount of fuel consumed on a mission remains constant, the immediate benefit from improved fuel economy may be taken to be the increased mission duration that is afforded as evidenced by the mission duration figures included in Table 3.7.

Table 3.7: **Mass trade-off for simulated SPH-Halo-CMG system** *A summary of the mass trade-offs involved in adding a CMG payload to the SPHERES satellite testbed. These trade-offs are maneuver-dependent, and are thus presented for both the ‘EVA’ and ‘Docked’ maneuvers.*

CMG Payload Specs	EVA	Docked
Nominal Mass	1.9 kg	1.9 kg
Utilized Mass	136.3 g	1476.5 g
Nominal Power	4 W	4 W
Utilized Power	0.30 W	3.14 W
Add'l Batt Mass	0.10 g	1.68 g
CMG Added Mass	136.4 g	1478.2 g
Thruster Sys. Savings	EVA	Docked
Fuel Mass Saved	1.7 g (39%)	18.2 g (76%)
Tank Mass Saved	4.4 g	46.5 g
Thruster Mass Saved	6.1 g	64.8 g
Mission Duration	EVA	Docked
Thrusters-Only	2.3 hr	0.7 hr
Thrusters+CMGs	3.8 hr	3.0 hr
Duration Increase	1.5 hr (64%)	2.3 hr (325%)

Similarly, the CMG power usage had to be scaled down. Due to the complex nature of power consumption, the same scaling factor as used for mass scaling is used. This results in a reduction of the original 4 W simulated as being consumed to only 0.30 W power. This value was then used as the average power consumption throughout the test session to generate the total energy consumed by the CMG payload: 62.05 J. Using a specific energy of 130 Wh/kg for batteries as in the MAJIC study, an additional battery mass of 0.13 grams is required to support the CMG payload for this maneuver. To reiterate, these calculations are only intended to provide a rough estimate of the mass and power trade-off between a thruster-only and combined control system. The scaling factors include assumptions that may only be true as first-order estimates. The conclusions that may be drawn from this preliminary simulation study must be done with caution. When the SPH-Halo-CMG system is fully integrated and operational in a closed-loop implementation, a more realistic utility analysis can be conducted.

Chapter 4

Conclusion

This thesis details the research conducted between September 2013 and August 2015 at Draper Laboratory and MIT’s Space Systems Laboratory to explore the utility of control moment gyroscopes as attitude control actuators for a low gravity astronaut EVA Jetpack. In order to accomplish this goal, a double-pronged research effort was executed that involved:

1. Improving and utilizing an existing Draper and MIT simulation to explore the combined thruster and CMG control concept proposed for the Mobility Augmenting Jetpack with Integrated CMGs; and
2. Physically demonstrating this combined control concept in the context of the re-configurable SPHERES controls testbed facility at MIT’s SSL.

4.1 MAJIC Research Conclusions

The first research effort listed focused on addressing the question of what size, weight and power (SWaP) CMG would be appropriate for the Jetpack application and whether this size would provide the benefits of increased stability and fuel economy as identified in [2]. Since a previous study showed that CMGs small enough to “pay for their weight” in a single mission do not deliver sufficient performance gains to an astronaut user [3], it was unknown whether any CMG that could fit within the

physical envelope and power budget of a realistic Jetpack system could in fact provide the performance gains desired. Not only was a much larger CMG design identified with both SWaP and practical engineering constraints in mind (see Table 2.8), but an improved Monte Carlo sizing methodology was employed to identify smaller CMGs than this upper limit that could provide the performance gains desired from the MAJIC system (see Table 2.11).

Three mission scenarios in particular were considered for detailed simulation: ISS solar array inspection, asteroid survey and sampling and crew member rescue. Together, these missions span a broad range of potential EVA missions including translation with and without large mass off-sets corresponding to heavy tools, scientific payloads or other crew members; and attitude hold in the presence of disturbance torques arising from 6-DoF suited astronaut dynamics corresponding to limb articulation and tool use. Both the combined control MAJIC system and a thruster-only Jetpack were evaluated in the context of these missions. Two settings for deadbands were tested in the thruster-only implementation: a tight (0.5°) and a loose (2.0°) deadband, corresponding to settings previously used for back-mounted thruster mobility units for astronauts [11, 14].

Results for relative performance (attitude stability) and mass-cost (fuel and energy consumption) for MAJIC and for thruster-only implementations in these extended mission scenarios are described in Section 2.4.1. For most of these missions, the MAJIC system exhibited both better attitude stability and better fuel economy. For those missions in which thrusters demonstrated better mission-averaged attitude stability, analysis of the time-dependent attitude error reveals that CMGs indeed exhibit significant gains in pointing precision over thruster-only implementations for the vast majority of mission time, but slower settling times over the course of desaturation events and slewing resulted in misleading overall averages.

In order to better identify the utility of integrating CMGs into the Jetpack, discrete mission actions including a linear translation with and without a mass off-set as well as disturbance rejection of torques associated with astronaut limb motion and tool use were analyzed, isolated from the other mission actions. In this way, a basis

set of actions was analyzed that may be combined in any number of ways to construct a variety of missions. From this analysis, the CMGs that were selected from the sizing process were shown to be superior to thruster-only implementations in maintaining platform stability during translations, including both translations with no mass offset and translations with a mass offset corresponding to a crew member rescue scenario.

For cases in which the center of mass of the system moves considerably as in the Crew Member Rescue Mission, linear translation without rotation requires an attitude control effort to counter induced torque on the system. Just as transporting an incapacitated crew member causes a mass offset, so too does manipulating a large payload; for these scenarios, torques induced on the astronaut would cause additional jet firings for attitude control in a thruster-only system that wouldn't otherwise be necessary if CMGs were employed for attitude control.

The stability afforded by CMGs for the both the Crew Member Rescue Mission and linear translation trials highlights the fact that a CMG size considerably smaller than the maximum SWaP allowance¹ is still capable of maintaining stability for a demanding control task, enabling fuel to be saved and thrusters to be reserved for translational force delivery alone.

The same was not shown to be true in all cases for simulated human motions. Instead, for motions that involved high torques (≥ 1.5 N m) for sustained periods of time, CMGs performed equally or worse than thruster-only modes of operation. Even for larger CMGs, there will be a limit to the torque magnitude and duration that can be accommodated by a CMG subsystem, a fact which must be considered for EVA missions that involve MAJIC in the future.

In the end, both in the extended mission scenario simulations and in discrete mission action simulations, the combined control MAJIC system demonstrated performance gains in the form of improved pointing stability and fuel economy. Assumptions for an average EVA mission scenario were made and combined with mass-cost

¹Recall that an optimal CMG from Monte Carlo trials conducted on the Asteroid Sampling I: Survey mission resulted in a CMG with angular momentum and torque values of 1.86 N m s and 1.55 N m, respectively, as compared with the maximum SWaP CMG angular momentum and torque values of 4.75 N m s and 4.75 N m s, respectively.

estimates from the discrete action analysis to yield mass-to-orbit projections for the MAJIC system as compared with a tight-deadband thruster-only Jetpack. After the mass-cost savings from discrete mission actions were combined according to assumptions made for EVA duration and relative content of linear translation, mass off-set and disturbance rejection, it is projected that after only two missions composed of three 6-hour EVAs with two astronauts each, the MAJIC system saves total mass required to be sent to orbit; after 10 missions, over 200 kg of material is estimated to be saved with use of a MAJIC system over a thruster-only Jetpack. Of course, the improved fuel economy of the MAJIC system is only a symptom of the primary objective: the maintenance of superior pointing stability with use of CMGs for attitude control instead of thruster-only control.

4.2 SPHERES Research Conclusions

The research efforts described in this thesis concerning a physical demonstration of the combined control concept envisioned for MAJIC with the SPHERES facility has focused primarily on design, integration and testing efforts to establish a functional facility for controls testing. Several unforeseen engineering difficulties impeded the progress of this effort, though even with these obstacles, a CMG subsystem functionality (open loop torque execution) was successfully demonstrated in all three rotation axes (first in a 1-DoF rotation test stand and next in a 3-DoF rotation test stand) in the laboratory. Furthermore, CMG torques sufficient to induce angular rates in excess of 5 degrees per second of a SPH-Halo-CMG configuration augmented with optical, range-finding and infrared payloads (the INSPECT system) were demonstrated in microgravity aboard NASA's reduced gravity aircraft.

Notable lessons from the obstacles encountered in the integration and testing of the SPH-Halo-CMG system are: 1. CMGs tend to be noisy (in vibration) if not very precisely balanced and so damping of some sort is almost assuredly recommended for practical systems; and 2. Extensive power and data testing at each stage of integration are required to ensure full system operability. More lessons are sure to be

learned as soon as closed-loop operations begin.

Once again, as with MAJIC simulations, CMGs for SPHERES promise to not only improve system stability despite large variation in mass properties in the system or disturbance torques applied to the system, but also to increase the thruster fuel economy of the system. Unfortunately, these potential gains have not yet been demonstrated physically, though the SPH-Halo-CMG facility is nearly at a state of maturity that would afford detailed investigations into comparative closed-loop control.

4.3 Future Work

While the research described in this thesis has built a basis from which general conclusions about the utility of integrating CMGs into a low gravity astronaut Jet-pack or future manipulator and inspection spacecraft, the work described here is, in the author's opinion, merely a starting point. The promising results from MAJIC simulations should be explored in more depth; and after building a system in the SPHERES-Halo-CMG configuration that is capable of physically demonstrating combined control concepts, the proverbial stage has been set for useful, cutting-edge investigations of novel spacecraft control mechanisms that can potentially expand the possibilities for human and robotic exploration. The following sections describe recommended future work in more detail.

4.3.1 Future MAJIC Work

There are three major areas in which MAJIC research could most benefit from further investigation:

1. Control logic development
2. Sizing method refinement
3. Simulation realism

First, the development of more sophisticated control logic to command thruster and CMG actuation in MAJIC is recommended. For high torque maneuvers, for instance, improved performance may be expected from a system that combines thruster and CMG actuation to counter a given disturbance torque. Desaturation logic may also be changed to return CMGs to a state well within the angular momentum envelope of the array as opposed to merely returning the CMGs to a state close (9/10 the distance) to the momentum envelope edge, thus providing the array with more flexibility of control before another saturation event occurs. Adding CMGs as attitude actuators to a Jetpack is an exciting prospect, and the many ways in which they could be employed to the advantage of the astronaut pilot may yet be uncovered, a possibility that can only be addressed with continued controls research.

Next, the sizing methodology presented in Section 2.3.2 can yet be improved upon. The right balance between CMG unit angular momentum capacity and torque capacity is still not well defined, neither in literature nor in the present document. This thesis recommends maintaining a maximum gimbal rate of 1 radian per second or less in order to ensure that singularity encounters remain infrequent (recall, traversing the momentum envelope with quick gimbal motions leads with higher probability to the intersection of a singular surface, requiring an external torque to return CMGs to a fully controllable state once more). How can the best ratio of CMG angular momentum to torque be determined for an unknown set of mission trajectories and disturbance torques? If something might be said about the statistical distribution of trajectories or disturbance torques expected to be induced on the system, do conclusions concerning optimal angular momentum to torque ratios change? To begin to address questions like these it is advised that an even more systematic approach to sizing is initiated, in which various angular momentum to torque ratios are tested for an even broader range of mission scenarios than those that were tested in this research.

Finally, improving the realism of the simulation will only strengthen any conclusions that may be drawn. CMGs are modeled as perfect actuators, responding immediately to control requests; a delay in CMG response is the first change that

may be implemented. Next, the power consumption of CMGs has only been modeled in a rudimentary manner, by tracking the commanded individual CMG torques. CMG flywheel power consumption and assumptions for motor inefficiencies and friction losses may also be built into the simulation. Additionally, the sensors modeled in the simulation are assumed to be perfect. By adding sensor noise, more realistic closed-loop control performances may be observed.

In addition to these three major areas for improvement, the MAJIC simulation can be made easier to use; for instance, implementing human torques and mass property changes is cumbersome and process-intensive; helper functions to set mission parameters would help future sizing and utility analyses proceed at a faster rate and with greater repeatability.

4.3.2 Future SPHERES Work

The focus of future SPHERES work for CMG actuator utilization should be on closed-loop control research to determine the relative utility of using CMGs for attitude control in simulated contexts for MAJIC as well as other spacecraft such as robotic manipulator or inspection spacecraft.

A second reduced gravity flight opportunity was extended to the Draper and the MIT SPHERES team for the summer of 2015; in this flight, a SPH-Halo-CMG configuration is planned to fly with a secondary SPHERES satellite, and after initial characterization of CMG torque execution in microgravity, characterization of the closed loop control system in microgravity can commence to ensure that rise time, maximum overshoot and settling times have been set with proper gains. Following characterization activities, a closed loop slew maneuver (step-response) and known disturbance rejection (impulse-response) caused by SPHERES thruster firings can be analyzed for CMGs and for thrusters alone.

By testing each planned flight test on the ground on air-bearing table test facilities, confidence in the system can be gained and valuable data can be recorded for immediate use in application to the MAJIC research contained in this thesis. Ultimately, more tests that include multiple-SPHERES configurations and the use of a

robotic arm may be conducted with the SPH-Halo-CMG system to continue to collect data for combined control research with thrusters and CMGs. The opportunity to work with physical hardware is rare, and should be utilized to the maximum extent. Ultimately, preparations for CMG subsystem delivery to the ISS for extended combined controls research is planned as the long-term future work objective for the SPHERES research contained herein.

4.4 Closing Remarks

While specifics have not yet been solidified for the future of human or robotic exploration, there is a strong argument for the addition of a Mobility Augmenting Jetpack with Integrated CMGs to the technologies already used to facilitate low gravity operations. Such a system would improve EVA efficiency and expand astronaut mobility for complex EVA scenarios. This system would also improve EVA safety by providing a strengthened self-rescue capacity to an astronaut user as compared with the current SAFER unit, as well as providing an improved capability to rescue fellow crew members. Finally, a system utilizing a combined control concept would potentially provide long-term mass and cost savings.

The unique capacity of single-gimbal CMGs to provide a large range of torques suitable for stabilizing a suited astronaut conducting EVA activities with massive experimental payloads or equipment is an exciting avenue for continued research. An added benefit of pursuing a combined control concept for an Advanced Jetpack is that lessons learned can be directly applied to the research and development of robotic, autonomous systems for low-gravity servicing and assembly. Simulating the Mobility Augmenting Jetpack with Integrated CMGs and physically demonstrating the combined control concept on MIT's SPHERES satellite testbed provides an example of how a combined control research program can benefit the development of multiple spacecraft concepts sharing a common control problem.

The research described in this thesis builds on previous research at MIT and Draper and applies practical size, weight and power constraints as well as a new

method to identify CMG actuator designs applicable to the Jetpack application. In doing so, the feasibility of the combined CMG and thruster control of a Jetpack has been demonstrated. Identified improvements to attitude stability and fuel economy in simulated studies merit further investigation of CMG integration into the Jetpack. The actuator sizing method and utility assessment procedure contained in this thesis may be readily applied to these future design studies.

Furthermore, the integration of a control moment gyroscopes into the MIT SPHERES facility enables future combined control algorithm development at MIT and Draper for the purposes of both Advanced Jetpack and robotic service and assembly spacecraft research. Laboratory and reduced gravity testing of the CMG-integrated SPHERES facility with NASA's Reduced Gravity Flight Opportunities Program in August 2013 and August 2014 together provide the practical experience necessary to facilitate rapid development of physical demonstrations of combined control algorithms at MIT and Draper. The SPHERES facility's on-going presence at the International Space Station also provides a readily accessible avenue for future microgravity research on the combined control concept. Together, these accomplishments represent the first step toward realizing the concept of using control moment gyroscopes and thrusters together in human-operated and autonomous spacecraft to improve the flexibility and utility of future astronaut EVAs and robotic space missions.

Bibliography

- [1] Sam Schreiner, Timothy Setterfield, Todd Sheerin, and Morris Vanegas. “Design and Simulation of an Integrated CMG and Thruster Control System”. MIT Course 16.851 Final Report, December 2013.
- [2] Michele D. Carpenter, Kimberly Jackson, Babak Cohanin, Kevin R. Duda, Jared Rize, Celena Dopart, Jeffrey A. Hoffman, Pedro Curiel, Joseph Studak, Dina Poncia, and Jennifer Rochlis Zumbado. “Next-Generation Maneuvering System with Control-Moment Gyroscope for Extravehicular Activities Near Low-Gravity Objects”. In *Proceedings of the 43rd International Conference on Environmental Systems*, Vail, CO, July 2013. AIAA.
- [3] Michele D. Carpenter, Kimberly F. Jackson, Babak E. Cohanin, Kevin R. Duda, Celena H. Dopart, Jared P. Rize, Todd F. Sheerin, and Jeffrey A. Hoffman. “Operator Evaluation of a Mobility-Augmenting Jetpack with Integrated Control-Moment Gyroscopes”. In *Proceedings of the 36th IEEE Aerospace Conference*, Big Sky, MT, March 2015. AIAA IEEE.
- [4] Todd F. Sheerin, Michele D. Carpenter, and Jeffrey A. Hoffman. “Actuator Sizing and Utility Assessment of Control Moment Gyroscope for an Astronaut EVA Jetpack”. In *Proceedings of the 45th International Conference on Environmental Systems*, Bellevue, WA, July 2015. AIAA, AIChE, ASME and ICES.
- [5] T. B. Murtagh, C. E. Whitsett, M. A. Goodwin, and J. E. Greenlee. “Automatic Control of the Skylab Astronaut Maneuvering Research Vehicle”. *Journal of Spacecraft and Rockets*, 11(5):321–326, 1974.

- [6] Daniel Brown and Mason Peck. “Energetics of Control Moment Gyroscopes as Joint Actuators”. *Journal of Guidance, Control and Dynamics*, 32(6):1871–1883, November-December 2009.
- [7] V. J. Lappas. “A Control Moment Gyro (CMG) Based Attitude Control System (ACS) for Agile Small Satellites”. Ph.D. Thesis, University of Surrey, School of Electronics and Physical Sciences, October 2002.
- [8] H. Yoon. “Spacecraft Attitude and Power Control Using Variable Speed Control Moment Gyros”. Ph.D. Thesis, Georgia Institute of Technology, Atlanta, GA, 2004.
- [9] Laura L. Jones, Rodrigo A. Zeledon, and Mason A. Peck. “Generalized Framework for Linearly Constrained Control Moment Gyro Steering”. *Journal of Guidance, Control, and Dynamics*, 35(4):1094–1103, August 2012.
- [10] Kriss J. Kennedy, Leslie Alexander, Rob Landis and Diane Linne, Carole Mclemore, and Edgardo Santiago-Maldonado. Human Exploration Destination System Roadmap: Technology Area 07, April 2010. National Aeronautics and Space Administration.
- [11] J. A. Lenda. *NASA-CR-151864 Manned Maneuvering Unit: Users’ Guide*. Martin Marietta Corp., P.O. Box 179, Denver CO 80201, May 1978.
- [12] Jim Dumoulin. Mission 51-A. <http://science.ksc.nasa.gov/shuttle/missions/51-a/mission-51-a.html>, June 2001.
- [13] K. J. Grady. “The Dynamics of the Solar Maximum Mission Spacecraft Capture and Redeployment on STS 41-C”. In *Proceedings of the Eighth Annual Rocky Mountain Conference*, pages 495–510, Keystone, CO, February 1985. National Aeronautics and Space Administration.
- [14] EVA Systems Group. *USA Simplified Aid for EVA Rescue (SAFER) Operations Manual SAFER OPS 21002*. National Aeronautics and Space Administration, Lyndon B. Johnson Space Center, Houston TX, August 20 1998.

- [15] Jared Philip Rize. Simulation Development and Analysis of Attitude-Control System Architectures for an Astronaut Mobility Unit. SM Thesis, Massachusetts Institute of Technology, 77 Massachusetts Avenue, Cambridge MA 02139, June 2014.
- [16] Celena Dopart. Astronaut-centric analysis of a jetpack with integrated control-moment gyroscopes for enhanced extravehicular activity performance. SM Thesis, Massachusetts Institute of Technology, 77 Massachusetts Avenue, Cambridge MA 02139, June 2014.
- [17] H. Cheng, L. Obergefell, and A. Rizer. *Generator of Body Data (GEBOD) Manual*. General Dynamics Corporation, no. al/cf-tr-1994-0051 edition, March 1994.
- [18] Leia A. Stirling. *Development of Astronaut Reorientation Methods: A Computation and Experimental Study*. Ph.D. Thesis, Massachusetts Institute of Technology, 77 Massachusetts Avenue, Cambridge, MA 02139, 2008.
- [19] Alvar Saenz-Otero. *Design Principles for the Development of Space Technology Maturation Laboratories Aboard the International Space Station*. Ph.D. Thesis, Massachusetts Institute of Technology, Department of Aeronautics and Astronautics, 77 Massachusetts Avenue, Cambridge MA 02139, June 2005.
- [20] S. Chintalapati, C. A. Holicker, R. E. Schulman, B. D. Wise, G. D. Lapilli, H. M. Gutierrez, and D. R. Kirk. “Update on SPHERES-Slosh for acquisition of liquid slosh data aboard the ISS”. In *Proceedings of the 49th AIAA/ASME/SAE/ASEE Joint Propulsion Conference*, San Jose, CA, July 2013. AIAA/ASME/SAE/ASEE.
- [21] Jacob G. Katz. *Achieving Broad Access to Satellite Control Research with Zero Robotics*. Ph.D. Thesis, Massachusetts Institute of Technology, Department of Aeronautics and Astronautics, 77 Massachusetts Avenue, Cambridge MA 02139, June 2013.

- [22] David Sternberg, Todd F. Sheerin, and Gabriel Urbain. “INSPECT Sensor Suite for On-Orbit Inspection and Characterization with Extravehicular Activity Spacecraft”. In *Proceedings of the 45th International Conference on Environmental Systems*, Bellevue, WA, July 2015. AIAA, AICHe, ASME and ICES.
- [23] Jessica Gersh and Mason A. Peck. “Violet: A High-Agility Nanosatellite for Demonstrating Small Control-Moment Gyroscope Prototypes and Steering Laws”. In *Proceedings of the AIAA Guidance, Navigation, and Control Conference*. AIAA, 10-13 August 2009.
- [24] H. Kurokawa. “A Geometric Study of Single Gimbal Control Moment Gyros”. Report of Mechanical Engineering Laboratory 175, Ministry of International Trade and Industry, 1998.
- [25] Frederick A Leve. Development of the Spacecraft Orientation Buoyancy Experimental Kiosk. Master’s Thesis, University of Florida, 2008.
- [26] H. Kurokawa. “Survey of Theory and Steering Laws of Single-Gimbal Control Moment Gyros”. *Journal of Guidance, Control, and Dynamics*, 30(5):1331, 1340 2007.
- [27] J. R. Zumbado, P. H. Curiel, and S. Shreiner. ”Hands-Free Control Interfaces for an Extra Vehicular Jetpack. In *Proceedings of the 2013 IEEE Aerospace Conference*, 2-9 March 2013.
- [28] A. Fujiwara, J. Kawaguchi, D.K. Yeomans, M. Abe, T. Mukai, T. Okada, J. Saito, H. Yano, M. Yoshikawa, K.J. Scheeres, O. Barnourin-Jha, A.F. Cheng, H. Demura, R.W. Gaskell, N. Hirata, H. Ikeda, T. Kominato, H. Miyamoto, A.M. Nakamura, R. Nakamura, S. Sasaki, and K. Uesugi. “The Rubble-Pile Asteroid Itokawa as Observed by Hayabusa”. *Science*, 312:1330–1334, June 2006.
- [29] David L. Baker. “Warm Gas Pressurization of Propellant Tanks”. http://www.nasa.gov/centers/wstf/pdf/210567main_warm_gas_press_of_propellant_tanks.pdf.

- [30] B. S. Cohen and R. S. Legge. “Optimization of a Small Satellite Tridyne Propulsion System”. In *Proceedings of the 35th IEEE Aerospace Conference*, number 2036, Big Sky, MT, March 2014.
- [31] Nazareth S. Bedrossian, Joseph Paradiso, Edward V. Bergmann, and Derek Rowell. “Steering Law Design for Redundant Single-Gimbal Control Moment Gyroscopes”. *Journal of Guidance*, 13(6):1083–1089, Nov.-Dec. 1990.
- [32] Saft Batteries. “Saft batteries... powering outer space for half a century”. Online Brochure http://www.saftbatteries.com/force_download/1302_Saft-SpaceBrochure_8.5x11.pdf, April 2013.
- [33] R. Signorelli. *High Energy and Power Density Nanotube-Enhanced Ultracapacitor Design, Modeling, Testing and Predicted Performance*. Ph.D. Thesis, Massachusetts Institute of Technology, 77 Massachusetts Avenue, Cambridge MA 02139, June 2009.
- [34] V. J. Lappas, W. H. Steyn, and C. Underwood. “Design and Testing of a Control Moment Gyroscope for Small Satellites”. *Journal of Spacecraft*, 42(4):729–739, 2005.
- [35] D. J. Richie, V. J. Lappas, and P. L. Palmer. “Sizing/Optimization of a Small Satellite Energy Storage and Attitude Control System”. *Journal of Spacecraft and Rockets*, 44(4):940–952, 2007.
- [36] Honeybee Robotics. “Honeybee Robotics Planetary Exploration”. <http://www.honeybeerobotics.com/services/space/planetary-exploration>, July 2015.
- [37] Honeybee. “Microsat CMG Attitude Control Array”. <http://www.honeybeerobotics.com/wp-content/uploads/2014/03/Honeybee-Robotics-Microsat-CMGs.pdf>, July 2015.

- [38] Samuel Schreiner, Timothy Setterfield, Todd Sheerin, and Morris Vanegas. “Hardware Demonstration of an Integrated CMG and Thruster Control System”. MIT Course 16.851 Midterm Report, October 2013.
- [39] Katsuhiko Ogata. *Modern Control Engineering*. Prentice Hall, 5th edition edition, 2009.
- [40] Nancy Leveson. *Engineering a Safer World: Systems Thinking Applied to Safety*. MIT Press, 2011.
- [41] D. Brown and M. A. Peck. “Scissor Pair Control Moment Gyros: A Mechanical Constraint Saves Power”. *Journal of Guidance, Control and Dynamics*, 31(6):1823–1826, 2008.
- [42] Axivity. “Axivity AX3 Data Sheet”. http://axivity.com/files/resources/AX3_Data_Sheet.pdf, July 2015.
- [43] Jeffrey A. Chambers. “(NASA-TM-106943) Preloaded Joint Analysis Methodology for Space Flight Systems”. NASA Technical Memorandum (NASA-TM-106943) <http://ntrs.nasa.gov/archive/nasa/casi.ntrs.nasa.gov/19960012183.pdf>, December 1995.
- [44] Allen Chen. “Propulsion System Characterization for the SPHERES Formation Flight and Docking Testbed”. SM Thesis, Massachusetts Institute of Technology, Department of Aeronautics and Astronautics, 77 Massachusetts Avenue, Cambridge MA 02139, May 2002.